Physics – Uspekhi **62** (2) 131 – 165 (2019)

REVIEWS OF TOPICAL PROBLEMS PACS numbers: 47.70.Fw, 61.82.Bg, 66.30.Ny, 81.20.Ka, 81.20.Rg, **82.20. – w**

Ignition and combustion of titanium particles: experimental methods and results

O G Glotov

DOI: https://doi.org/10.3367/UFNe.2018.04.038349

Contents

1. **Introduction** **131**
2. **History and new challenges** **132**
3. **Regularities in titanium oxidation and ignition** **133**
4. **Combustion of titanium compact specimens. Convection and blow-off effects** **142**
5. **Specific reacting of pressed and poured specimens, aerogels, and aerosuspensions** **146**
6. **Burning of individual titanium particles** **149**
7. **Characteristics of oxide particles produced in titanium combustion** **156**
8. **Titanium combustion mechanism** **159**
9. **Conclusion** **161**

References **163**

Abstract. We have collected and systematized data on patterns and features of the ignition and combustion of titanium in the form of centimeter-sized samples and microparticles with dimensions ranging from several units to several hundred micrometers in the shape of individual particles, air suspensions, and poured and pressed samples. Factors have been identified that affect the temperature and time characteristics of ignition and burning, as well as the composition and dispersity of the formed condensed products, including those in the nanometer-sized range. We also present a modern paradigm of the mechanism of burning and formulate the issues to be resolved to gain a better understanding of how metal transforms into oxide.

Keywords: titanium, particle, ignition, combustion, burning time, fragmentation, dispersion of fragments, phase content, condensed combustion products, morphology, particle size distribution, nanoparticles, spherules, photocatalytic properties, dopants

1. Introduction

There is a variety of important topical issues related to the combustion of metals. Research activities may be divided here into three areas: *fire and explosion hazard, energetic combustion, and technological combustion*. The first area comprises the issues of safe structural and technological use of metals in gaseous oxidizing environments, including ignition conditions, combustion parameters, and methods for protecting against inadvertent fire (coating and adding dopants). It should be noted that at elevated oxygen pressures even those metals that do not ignite under normal conditions, such as steel, can catch fire [1]. In the case of dispersed materials, for example, powdery metals [2], fire hazard is related to the ignition, explosibility, and combustion of aerosuspensions. Concentration limits, minimum ignition energy, flame propagation and protection against flame, and combustion outcomes (maximal temperatures and pressures) are considered for those materials.

Energetic combustion involves the issues related to the capability of a metal to exothermically interact with an oxidizer. Using metal as a specific energetic material, a metallic fuel, has a number of characteristic features. First, of most interest are metals with high combustion heat (over 8 kJ g^{-1}) [3], such as Al, Mg, Be, Ti, Zr, Li, and some of their compounds (hydrides and alloys; for example, AlH_3 and Al/Mg) [3–6]. Second, to increase the reaction surface, metal microparticles are used whose characteristic size is about several units to several tens of micrometers [3]. Third, the goals and methods intended for practical use are very numerous, although all of them are based on a single key feature, i.e., the release of heat in combustion. Metallic fuels are used in (1) condensed systems, such as composite propellants, and plasma fuels [5–7]; pyrotechnic and explosive compositions [8–10]; (2) systems and devices based on the airdispersive combustion [6, 11–13], and (3) engines that operate using water as an oxidizer [14].

In *technological combustion*, metal performs the function of a reagent for manufacturing desired products with specified properties (oxides, nitrides, carbides, etc.) as part of compressed, bulk, gel-like, aerogel, and airdispersive systems [11, 15–18].

The combustion of metals comprises a set of interrelated physical and chemical processes and phenomena, the main

O G Glotov Voevodsky Institute of Chemical Kinetics and Combustion, Siberian Branch of the Russian Academy of Sciences, ul. Institutskaya 3, 630090 Novosibirsk, Russian Federation
E-mail: glotov@kinetics.nsc.ru

Received 9 January 2018, revised 23 March 2018
Uspekhi Fizicheskikh Nauk **189** (2) 135 – 171 (2019)
DOI: https://doi.org/10.3367/UFNr.2018.04.038349
Translated by M Zh Shmatikov; edited by A Radzig

Table 1. Physical properties of Ti and TiO_2.

Metal, oxide	Density, g cm^{-3}	Melting temperature, K	Boiling temperature, K	References
Ti	4.5 4.505 4.507	1950 1881 1941	3550 3560 3560	[19] [21] [22]
TiO_2	4.2 3.84	2128 2143	4100 3200	[19] [21]
Combustion heat is 19.68 kJ per gram of metal				[19]
Pilling–Bedworth coefficient is 1.73				[19]

ones being the transport of an oxidizer to a metal and chemical reactions between that metal and/or intermediate oxidation products with the oxidizer. Due to differences in the properties of metals and their oxides, there are no universal mechanisms of metal ignition and combustion. The specific features of the reactions are not similar to each other, and each metal is of interest for basic research. In applied research, study activities are determined by the importance and occurrence of practical applications. For example, inasmuch as Al is used in composite propellants, the ignition and combustion of Al particles have been actively studied in a number of countries for more than half a century [3, 6, 19, 20]. The focus of this review is titanium. The main physical properties of titanium and its highest oxide are displayed in Table 1. It is noteworthy that the numerical values depend on the literature source from which they are taken.

On the one hand, Ti is a light, high-strength, and corrosion-resistant structural material that is used in extreme environments (in rocket, space, and aviation engineering [23, 24], chemical reactors, etc.). Titanium is the fourth most widely used structural material after Al, Fe, and Mg, and its wider application is often limited by its comparatively high cost. On the other hand, Ti is a pyrophoric metallic fuel. Using Ti in this function as part of pyrotechnic compositions is explored in Refs [8, 9], and in technological combustion compositions in Refs [15, 25]. Under investigation is the use of Ti in composite propellants [26–28] and in industrial and technological explosives [29–31] as an energetic component and a combustion modifier of composite propellants [32].

Since Ti may be utilized for two different purposes (as a structural material and metallic fuel), Ti ignition and combustion are studied using both bulk specimens and microparticles. Titanium is a high-melting nonvolatile metal having a high-melting solvable oxide, and its combustion substantially differs from that of Al and Mg. Ti features a 'surface' combustion [5], while Al and Mg evaporate and react in a vapor-phase regime at some distance from the surface of the metal.

Generally speaking, to understand the ignition and combustion of metal particles, it is necessary to know critical ignition conditions; the timeframe of ignition and combustion at different gas temperatures and pressures; the temperature in the particle and its vicinity at different stages of the process, and the combustion product composition, degree of dispersion, and structure [33]. The listed characteristics cannot be immediately obtained in practice, thus necessitating the gathering of information.

We collect and systematize in this review data on Ti ignition and combustion and the development of condensed combustion products; our goal is to streamline the understanding of the mechanisms that operate in these processes. Some results have been obtained in experiments with bulk specimens; however, we had to attract them due to the lack of dedicated data for particles. Looking ahead, we may note that the currently available information is insufficient to develop a comprehensive physical paradigm of Ti combustion. The simulation of Ti combustion is currently at its initial stage, so we do not examine theoretical studies. We formulate in this review those questions whose lack of answers hinders the development of understanding of Ti combustion mechanisms and outline research priorities. Progress in the nearest feature will presumably be driven by experimental research; therefore, we pay special attention in this review to the technical details of experiments.

The specific features of the behavior of Ti incorporated into mixed gasifying compositions before entering to a gas phase (for example, particle agglomeration) are beyond the scope of this review and are barely considered here. Nor do we examine mixed SHS (self-propagating high-temperature synthesis) systems containing titanium. Airdispersive systems containing titanium particles will be discussed with a focus on the mechanisms of combustion and production of condensed compounds.

2. History and new challenges

Basic studies of Ti combustion as a structural material began when the introduction of this metal into aviation and space engineering commenced in the 1960s through 1980s. Research focused on determining the characteristics needed in practice (for example, dependence of the centimeter-sized specimen combustion rate on ambient conditions) and left virtually unexplored the combustion *mechanism*. The employment of powdery Ti in pyrotechnical systems does not need a detailed understanding of the particle combustion mechanism either. Numerous studies of the combustion mechanism in SHS systems containing Ti concentrated on particular issues. Studies of the Ti-particle combustion mechanism in a gaseous oxidizer, unlike studies of the Al combustion mechanism, were not driven by any practical need, so conducting corresponding experiments *de facto* halted in the 1960s. The situation changed in 2005 when it was proposed by Weiser et al. [34], seemingly for the first time, to use the combustion of Ti particles in air to create a cloud of photocatalytically active TiO_2 particles to deactivate harmful and hazardous substances that emerge in atmospheric air as a result of a human-made accident or terrorist attack. As a result, interest in the combustion of Ti particles has revived, as evidenced by new experimental studies currently being conducted in Germany, China, Portugal, Russia, the USA, Ukraine, France, and Japan. Explorations of Ti particle combustion mechanisms focused on practical issues with a goal to enhance the extent of metal combustion and attain a high yield of highly dispersed oxide with required parameters. It is apparent that, for the combustion process to be efficient, it must be arranged based on a combustion mechanism paradigm. It is necessary, in particular, to determine in what way the characteristics of the produced TiO_2 particles are related to the conditions of the combustion of mother Ti particles.

We present in this review the current state of studies of Ti particle combustion in air and the priority issues to be explored, taking into consideration a new challenge: the synthesis of nano-sized titanium dioxide particles.

3. Regularities in titanium oxidation and ignition

Oxidation of metals and the issues of ignitability and explosivity of metal powders are considered in monographs [2, 3, 6, 13, 35–39] and reviews [40–44]. The pyrophoric capacity of metals is believed to be proportional to combustion heat and inversely proportional to heat conductivity and specific heat capacity [38]. Publications [3, 6, 33, 37, 42] contain descriptions of the laboratory setups and techniques for determining some quantitative characteristics.

For example, the so-called minimum ignition temperature (MIT) T_{ign} is widely used; this is the temperature at which the specimen begins to rapidly heat up due to an exothermic process and eventually ignites [2]. To determine T_{ign} of a powder, a heated body is usually brought into contact with the powder, and, for simplicity, the temperature of the body, rather than that of the powder, is controlled. In the opinion of the authors of monograph [2], the accuracy with which T_{ign} is determined depends on the selected technique, and none of the techniques has any substantial advantages. Therefore, the authors of Ref. [2] recommend applying a technique that simulates the conditions under which the powder will be presumably used and yields the results that correspond to those conditions. In the absence of an accurate physical definition for T_{ign}, this parameter may serve as a handy and intuitively clear characteristic of the material. To study individual Ti particles, versions of a track technique are often applied, where particles are inserted into a transparent pipe containing a moving heated oxidizing gas. Environment parameters are usually fixed, and, in observing the behavior of particles, researcher can determine the timeframes of their inflammation and combustion.

Titanium and its alloys [24, 45–49] are utilized under extreme conditions; therefore, their inflammation behavior has been explored in depth as a function of ambient temperature and pressure, the geometry of specimens, and a number of other parameters. In the relevant experiments, so-called compact specimens (rods, wires, pipes, plates, and foils) are used, and the critical conditions for ignition are determined.

Table 2 displays some typical experimental setups, specimens, and parameters being determined; it also allows the

Table 2. Typical setups of experiments with titanium materials.

1	2	3	4	5
Material (grade)	Object under study and arrangement of the experiment	Environment, pressure of 0.1 MPa (unless specified otherwise)	Parameters being determined. Peculiarities of experiments	References
Refined Ti iodide. Impurities $< 0.01\%$. In the powder, the particle shape is close to spherical	Compact specimens, layer	Oxygen, air	Ignition temperature and time. Specimen is heated in an inert gas, then the environment is substituted with an oxidizing medium	[50]
	Suspension of 2-, 6-, and 15-μm diameter particles with a concentration of 0.5 kg m^{-3} in gas	N_2/O_2, Ar/O_2, and CO_2/O_2 mixtures	Oxygen concentration required for ignition	
Magnesiothermal Ti, TU (technical specifications) 10-0; magnesiothermal Ti, TU 7-77, electrolytic Ti PTSS TU 49-0561-2/0-80	Powder in gas permeable shell in muffle furnace; blow-off at a rate of 5–23 cm s^{-1}	Oxygen, air, nitrogen	Ignition temperature and time. Blow-off	[51]
Magnesiothermal powder, TU 10-0	Thermogravimetry (TG) with the specimen heating rate of 5 and 10 K min^{-1} at temperatures $T = 823-973$ K	Air	Oxidation kinetics	[51]
VT1-0, titanium fine powder (PTM in *Russ. abbr.*))	Differential thermal analysis (DTA)/TG with a linear heating rate of 10 K min^{-1}. Isothermal oxidation at $T = 873-1073$ K	Air	Photomicrographs of metallographic sections and atomic-emission spectroscopy of the initial material. Oxidation kinetics. X-ray phase analysis (XPA) of the products. Comparison of specimens with the coarse-grained, fine-grained, and submicrocrystal structures	[52]
Electro-explosive powder, particles of sizes 5 and 20 μm	DTA/TG in a layer, heating with a rate of 2, 5, and 10 K min^{-1} at temperatures $T = 323-1473$ K	Air	Effective kinetics, phase composition of specimens in the process of oxidation (XPA)	[53]
99.93% purity Ti	Plates $10 \times 10 \times (2-5)$ mm in size, slow oxidation in a temperature range of 973–1473 K	Air, water vapor	Effective kinetics, XPA of product	[54, 55]
TS0 — titanium sponge manufactured using magnesiothermal technology with vacuum separation, TsMTU 4700-56	Sieve fractions from 53 to 1700 μm in hot gas	Air	Ignition temperature as a function of particle dispersity	[38]
Alloy with 2.5% Ni	Sieve fractions from 53 to 160 μm in hot gas	Air	Ignition temperature as a function of particle dispersity	[38]

Table 2 (continued)

1	2	3	4	5
Calcium-hydride PTS powder. Specific surface of the powder $S_{sp} = 0.09$ m^2 g^{-1} [5]	Sieve fractions from < 45 μm to 250 μm pressed into asbestos-cement cups placed into hot gas	N_2/O_2 mixtures: 0/100, 25/75, 50/50, and 75/25	Ignition temperature and time as a function of particle dispersity and oxygen concentration	[56]
VT1	Spherical particles of the 56–75 and 72–102 μm fractions, tracking facility	Air	Ignition temperature and time as a function of particle dispersity	[57]
	Spherical particles from 880 to 1400 μm in diameter on a holder in a furnace. Specimens of various shapes	Air, pressure up to 40 MPa. N_2/O_2 mixtures	Ignition temperature and time. Effects of the specimen shape (sphere, cylinder, and square plate). High pressure	[57, 58]
Hydride calcium thermal Ti	Explosion of particle suspension in air in a closed volume, narrow fractions and polydisperse powders consisting of 50–100-μm particles	Air	Pressure after explosion. Metal combustion completeness	[59]
Powders	Explosive combustion of particle suspensions in air in a semi-closed vessel $80 \times 80 \times 500$ mm^3. Particles with dimensions 35 μm and 50 nm and concentration of ≈ 0.26 kg m^{-3} [22]; 99.3% purity 44-μm particles manufactured by Nilaco Corp. Japan, concentration of 0.5 and 1 kg m^{-3} [60]; 40 nm particles with concentration of ≈ 1 kg m^{-3} [61]	Air	DTA of initial powders at a heating rate of 10 K min^{-1}. High-speed video shots to record flame velocity and structure. Thermocouple probe measurements. Scanning electron microscopy (SEM) of initial powders and combustion products. X-ray photoelectron spectroscopy (XPES) of combustion products	[22, 60, 61]
Electrolytic TP-6, TU 48-0561-4/0-80, $S_{sp} = 0.11$ m^2 g^{-1}, 57.4% of mass consists of particles smaller than 90 μm	Powder in a gas permeable shell in a muffle furnace	Air	Ignition temperature and combustion rate. Mechanical activation effects	[62]
Ti powder, particle size from 63 to 250 μm	Thermal explosion in a poured density layer under linear heating with a rate of 200 K min^{-1}	Air	Effective activation energy. Chemical analysis of combustion products (results not reported)	[63]
Technical titanium. Deliberate hydrogen addition to attain the maximum concentration of 2.6 mass %	Spherical 5–25-μm particles. Tracking facility, temperature up to 1373 K	Air, oxygen, water vapor, chlorine	Ignition temperature. Effects of injected gases (hydrogen and nitrogen) and oxidizing environment	[64 – 66]
Iodide Ti, 99.98%. VT1-0, VT1-1, OT4, OT4-1, VT6, VT14, VT5-1, PT17, PT3V, and Ti-15Zr	Plate in a high-speed oxygen flow (velocity up to 340 m s^{-1}, pressure up to 30 MPa)	Oxygen and oxygen-containing mixtures	Ignition critical pressure. Blow-off	[67 – 71]
VT1-0	Ignition of a $10 \times 10 \times 1$-mm plate using an 800-W laser; supersonic blow-off	Air	Characteristic temperatures, ignition macrokinetics. Blow-off	[72]
Ti	Wire jump of ∅ 0.5 mm to ∅ 1 mm ignited with a wire	Air enriched with oxygen (up to 100%)	Burning rate as a function of specimen orientation	[73]
Ti	Wire pieces in furnace	Oxygen	Burning product morphology	[73]
VT1	Wire jump of ∅ 0.5 mm to ∅ 4 mm ignited with a wire	Air. Pressure up to 40 MPa	Burning rate as a function of specimen orientation. Pressure required for combustion. High pressure	[58]
99.2% purity Ti	Specimens with dimensions of $\sim 1.6 \times 4 \times 4$ mm ignited from the upper surface using a 100-W laser	Oxygen	Special high-speed video shots. Spectra and glow recorded. Extinguishing with argon and product analysis (XPA and SEM)	[74]
VT1-0	Spherical particles ∅ 4–8 mm. Heated using an inductor in Ar to a specific temperature, after which Ar was substituted with oxygen and ignition event was recorded ('yes-no')	Oxygen	Ignition temperature. Induction heating. Soldered thermocouple probe. Film shooting. Pyrometry using an image converter (EOC) tube	[75]

Table 2 (continued)

1	2	3	4	5
99.99% pure Ti	Specimen 3 mm in diameter and 3 mm in length ignited from butted surface using 100-W laser	N_2/O_2 or Ar/O_2 mixtures containing 0, 10, 20, or 30% of O_2	Direct temperature measurements using soldered thermocouple probe. High-speed video shots. Quenching and analysis of product grinded cuts (SEM and energy-dispersive X-ray spectroscopy (EDX))	[76]
99.95% pure Ti	Specimen 4 mm in diameter and 4 mm in length ignited from the top using focused light of Xe lamp	Oxygen	Temperature measurement using thermocouple probe. High-speed film shots. Recording of emission spectra. Microgravity	[77]
99.894% purity Ti. Admixtures: Fe — 0.03, C — 0.01, N — 0.006, O — 0.06	Rod ∅ 3.2 mm, local ignition	Oxygen	High-speed film shots. Microgravity	[78]
OT-4	Plates with dimensions $10\times35\times0.55$ mm, $10\times35\times1$ mm, $10\times35\times2$ mm. Local ignition from short edge side using a laser	O_2/Ar mixtures (O_2 content from 20% to 100%)	Burning rate. Pressure limits of combustion (up to 3 MPa)	[79]
OT-4, VT1-2, VT5-1, VT6, VT18, Vi8U, VT19, VT20, VT23, VT25, VT25U, VT29, OT4-V, OT4-1V, β_1, β_2	Plates with dimensions $50\times80\times0.3$ mm, $50\times80\times0.5$ mm, $50\times80\times1.5$ mm. Local ignition from short edge side using a laser	Air. Blow-off with a velocity of up to 250 m s^{-1}	Burning rate. Blow-off velocity limits of combustion with variation of plate thickness. Effect of dopants	[80–84]
Powder	Specimens compressed in the form of a $25\times10\times5$-mm parallelepiped	Nitrogen, air, O_2/Ar mixtures	Burning rate; pressure, thermocouple probe, and photo diode signals recorded. Dynamic XPA	[85]
Titanium fine powder (PTM) (calcium hydride, $S_{sp} = 0.12$ m^2 g^{-1}), composition: Ti 98.92%, H 0.38% [86]	Millimeter-sized specimens compressed in the form of a parallelepiped. Density of 1.11–3.33 g cm^{-3}, ignition from specimen's end	O_2/Ar mixtures varying from 10/90 to 100/0	Specimen density and oxygen concentration limits of combustion. Weight method to determine completeness of combustion	[87]
98.9% pure PTM; particle size $\leqslant 90$ μm	Compressed tablets 10 mm in diameter and 7.7 mm in thickness; porosity 33% in a furnace	Oxygen, air	Ignition temperature. Effects of vacuum processing and annealing	[88]
PTM with adsorbed gases: PTM w.1: H2.8, O 2.7; PTM w.2: H 3.0. O 1.9; PTKh 7-1: H 1.4, O 3.3	Poured layers 35×300 mm, 0.5 or 1.5 mm thick. Powders 'as it is' and TFP fractions from <50 μm to >315 μm. Ignition using a wire	Air	Front velocity as a function of particle dispersity and material of the substrate. Inflammability on a heated substrate. Effect of adsorbed gases	[89]
PTM: $S_{sp} = 0.12$ m^2 g^{-1} [5]; powder manufactured by RUSAL: 99.8%. 0.03 mass % of diluted H_2, average diameter (using the Brunauer–Emmett–Teller method to describe adsorption) $D_{32} = 22$ μm, $S_{sp} = 0.06$ m^2 g^{-1} [90]	Poured layer (4-g cone). Ignition using a wire	Air	Production of nitride. Front temperature and velocity, phase composition of combustion products	[90, 91]
Powder manufactured by Grade EP Chemetall	Particle size 4.5 μm. Poured layer $25\times10\times(5-10)$ mm. Ignition using a wire	Oxygen, air, nitrogen	Video shots, 5000 frames per second, temperature measurements using spectra	[92–94]
'Nano-sized' Ti powder obtained by the method of electroexploding wires	Agglomerate-shaped particles with sizes of up to 200 μm. Content of the active metal is 83–85%. Ti as a modifier of combustion composite systems based on HMX (High Melting eXplosive), Al, and a binder	Air	Characterization of initial powders, DTA, and burning rate of composite systems	[32]
Powder obtained by the method of electroexploding wires	Particle sizes of 50–100 nm, $S_{sp} = 15$ m^2 g^{-1}. Content of active metal is 90–99 % [95]. Particle size in Ref. [96] is 14 nm. Ti as a modifier of combustion of composite systems	Air	Characterization of initial powders. Burning rate of composite systems	[95, 96]

Table 2 (continued)

1	2	3	4	5
Powders manufactured by Super Conductor Materials, Inc. (spherical particles)	Spherical particles 82, 250, 500, and 1000 μm in diameter	Air	Video shots, product morphology	[97]
Powders manufactured by Atlantic Equipment Engineers Inc. (spongy particles)	Spongy particles with average size of 30 μm. Electric spark ignition of particles in a monolayer and in a layer ∅18.5 mm and 0.25, 0.5, and 1 mm in height			
Powder	Sieve fractions of 44-, 62-, 105-, 150-, 250-, and 420-μm particles. Ignition in Bunsen gas burner flame	Gas burner flame	Burning time	[98]
PTM-A powder	Irregular-shaped particles with average size of 3.5 –4 μm. Motion in a gas flow heated with plasmatron	Ar/O_2 flow (20/80) at 3000 K	Temperature, as well as granulometric, morphological and phase compositions of particles and products in various flow cross sections	[99]
Powders, type A and type V	Particles with sizes 41–115 μm. Ignition of falling particles in a gas burner	Flame of O_2/Ar or methane/O_2/air mixtures enriched with O_2 to 100%	Video shots. Burning time, particle sizes in dynamics	[100]
Powder manufactured by Atlantic Equipment Engineers, Inc. Purity 99.7%	Spongy 2–25-μm particles. Ignition using laser beam	Air	Burning time determined using time-resolved recording of individual particle glow. Pyrometry	[101]
Powder manufactured by Alfa Aesar. Purity 99%	Particles of 0.9–24 μm in size. Ignition using laser beam	Air	Same plus estimated effect of flow turbulence on burning time	[102]
Powder	Particles of 20 or 25 μm in diameter released in gasification of a mixed specimen in hot gas	Water + ammonium perchlorate (AP) decomposition products, water vapor; AP decomposition products + glycerin	Burning time	[103]
Powder manufactured by CERAC, Inc. Purity 99.5%	Irregular-shaped particles. Narrow sieve fractions in the 15–110-μm range. Electrodynamic levitation. Laser ignition	Air	High-speed video shots. Pyrometry. Burning time	[104]
Raw material: wires manufactured by California Fine Wire Co., ∅102 μm, 99% pure Ti and manufactured by Johnson Matthey, ∅127 μm, 99.99% pure Ti	Particles of 240 and 280 μm in diameter produced and ignited in microarc discharge	Air	Pyrometry. Burning time. Forced quenching, analysis of grinded cuts of residues (SEM, X-ray dispersion spectroscopy at various wavelengths, electron back scattering (EBS) method)	[105]
Raw material: PTM type powder. Purity 98.92%	Free-falling monodisperse particles-agglomerates of 300, 390, and 480 μm in diameter ignited in the combustion products of a metal-free composite system based on AP, HMX, and a binder	Gaseous products of combustion composition, and afterwards air	Combustion and fragmentation times. Granulometric and phase compositions of products and residues. Fragmentation characteristics	[106]
PTM type powder. Purity 98.92%	Coarse (100–330 μm) individual particles ignited in combustion products of a metal-free composite system based on AP and a binder. Specimen placed into a capillary tube	Same	Ejection of burning particles into air with velocity of up to 3 m s^{-1}. Quenching on substrate and precipitation of aerosol that accompanies particle. Transmission electronic microscopy (TEM) of a sediment	[107, 108]
PTM type powder. Purity 98.92%	Sieve fraction of particles less than 20 μm in size as part of a composite system based on AP and a binder	Same	Sampling of combustion products. Granulometric and phase compositions of oxide spherule particles in nano-sized range (TEM)	[109]
Particles 53–66 μm in size	Meker–Fisher gas burner	Burner flame. $CO_2 + 0.77\,O_2$ environment	Ignition time. Burning time	[110]

Table 2 (finished)

1	2	3	4	5
Powders manufactured by Kojundo Chemical Laboratory Co.; average size of particles 10 and 25 μm. Purity 99.9%	Dry mixture with sodium perchlorate in a layer	Gaseous products of mixture combustion in argon	Combustion product particle characteristics: granulometric and phase compositions, photocatalytic activity	[111]
Particles of ≈ 5 μm in size	Ti particle combustion in a coaxial dust burner	Oxygen concentration up to 40%	Spectroscopy. Granulometric composition of combustion product particles	[11, 112–114]
Raw material: PTM type powder, purity 98.92%, $S_{sp} = 0.12$ m^2 g^{-1} [5]	Combustion in chlorine-free mixed compositions on the basis of hydrazine mononitrate and a binder with 15–29% Ti; actually, the burning particles are titanium agglomerates	Gaseous products, of composition combustion and afterwards air	Ti agglomeration in the combustion wave. Granulometric composition of combustion product particles in a micrometer range and spherules in a nanometric range. SEM. Morphology of spherule aggregates	[115]
Raw material: PTM type powder	Combustion in composite systems basis on AP and a binder	Same	Granulometric composition of spherules — combustion product particles in a nanometric range. SEM. Electric charge properties	[109]
Raw material: PTM type powder	Monodispersed agglomerate 320-μm particles and sieve fraction particles (36–40 μm) ignited in the combustion products of a metal-free composite system based on AP, HMX, and a binder. The specimen is placed into a chamber with a nozzle	Same	Ejection of burning agglomerates into air with a velocity of up to 8 m s^{-1}. Granulometric composition of combustion product particles in a nanometric range as a function of the velocity of particle motion in air. Effect of the velocity of motion on the burning time	[116]

reader to rapidly find references to the items and data of interest. Table 3 contains data on the elemental composition of industrial grades of titanium and its alloys. Below, we only quote the grades of materials whose characteristics may be found in Table 3.

We present below qualitative information about the general regularities in the *ignition* of Ti in the form of individual particles, air suspensions, a poured layer, a pressed layer, and compact specimens.

(1) *Effect of the nature of a gaseous environment*. Titanium can ignite and burn in nitrogen, carbon dioxide [2], hydrogen [117], and chlorine [66]. The ignition in oxygen-containing environments depends on the partial pressure of the oxygen. For example, T_{ign} of compact specimens is 1070 K in oxygen, and 1570 K in air [50]. Regularities in ignition were explored in Ref. [51] for Ti powders of industrial grades TU 10-0 and TU 77-7 in a 'layer' located in a muffle furnace filled with oxygen, air, and nitrogen. The specimen had the shape of a cylindrical capsule 6 or 15 mm in diameter and 20 mm in length made of metal gauze and filled with the powder.

Having analyzed data on ignition delay time, the authors of Ref. [51] found that, if ignition occurs in air, the primary role in this process is played by oxygen. If the gas is moving (particles are blown off) with a small flow rate (about 5 cm s^{-1}), the critical temperature diminishes (and at lower temperatures no inflammation occurs), while at higher flow rates (about 23 cm s^{-1}), the temperature increases due to the changed heat exchange conditions for the specimen. The increase in the oxygen content has a two-fold effect on the ignitability. On the one hand, the time of heating to the critical temperature decreases together with the thickness of the oxide film that builds up on the specimen, thus facilitating ignition. On the other hand, heat removal is enhanced when the reaction starts developing, thus hindering the inflammation.

An independent nonisothermal thermogravimetric method was applied in Ref. [51] to determine the kinetics of oxidation in air for TU 10-0-grade powder at a specimen heating rate of 5 and 10 K min^{-1} in a temperature range of 823–973 K. The heat generation rate was described as $dg/dt = k_0 \exp[-E/(RT)] \exp(-bg)$, where g is the amount of heat released in the course of reaction per gram of metal, $k_0 = 7.5 \times 10^{13}$ J (g s)$^{-1}$, $E = 207$ kJ mol^{-1}, and $b = 0.0031$ g J^{-1} is the parameter characterizing the rate of reaction deceleration by the oxide layer being built up. The critical temperature calculated using these kinetic parameters, $T_{ign} = 880$ K, virtually coincides with the value of 900 K determined in experiments with the muffle furnace.

(2) *Dependence of ignition temperature on powder particle sizes*. Figure 1 displays data obtained from original studies [38, 56–58, 118]. It also shows a wide range in which T_{ign} varies, depending on experimental conditions (specimen type, addition of nickel, substitution of air with oxygen). We note that the Ti ignition temperature may be lowered by introducing some alloying additions (data *2* and *3*).

For individual particles, the ignition and combustion times as functions of the gaseous environment temperature are usually reported. We quote here some typical values. If the experiment runs at a temperature of about 1000 K in air and under atmospheric pressure, the equivalent diameter of particles increases from 24 to 254 μm, the ignition time (also referred to as the induction time or ignition delay time) increases from 14 to 40 ms, and the combustion time from 12 to 55 ms [38]. For particles 80 μm in diameter and a temperature of ≈ 1230 K, the induction time is 8 ms, and the combustion time 15 ms. For comparison, in a $CO_2 + 0.77$ O_2 environment and at a temperature of 2800 K, particles with sizes of 53–66 μm are ignited within 0.9 ms [110].

If a powder is oxidized in a layer, the heat generation rate is usually proportional to the specific powder surface S_{sp}, so the dependence of T_{ign} on S_{sp} may be approximated by a

Table 3. Composition* of titanium materials manufactured in Russia.

Material	References	Ti	Cl	Fe	Ni	C	Si	N	H	O	Al	Mn	Zr	Sn	Mo	V	Nb	Cr	Cu
PTM-1	[49]	Base	0.004	Fe+Ni 0.40		0.05	0.10	0.08	0.35										
PTS-1	[45]	Base	0.004	Fe+Ni 0.40		0.05	0.10	0.08	0.35										
TG-100	[46]	min 99.72	0.08	0.06	0.04	0.03	0.01	0.02		0.04									
VT1-0		99.72–99.7		0.25		0.07	0.1	0.04	0.01	0.2	0.7								
VT1-1		99.038–99.7		0.25		0.08	0.1	0.05	0.012	0.15									
VT1-2		97.8–99.7		1.5		0.1	0.15	0.15	0.01	0.3									
OT4		91.83–95.4		0.3		0.1	0.12	0.05	0.012	0.15	3.5–5	0.8–2	0.3						
OT4-1		94.33–97.5		0.3		0.1	0.12	0.05	0.012	0.15	1.5–2.5	0.7–2	0.3						
VT5-1		88.83–93.4		0.3		0.1	0.12	0.05	0.015	0.15	4.3–6		0.3	2–3		1			
VT6		86.45–90.9		0.6	0.05	0.1	0.1		0.015	0.2	5.3–6.8		0.3			3.5–5.3			
VT14		86.85–92.8		0.25		0.1	0.15	0.05	0.015	0.15	3.5–6.3				2.5–3.8	0.9–1.9			
VT18		76.82–82.05		0.15		0.1	0.05–0.18	0.05	0.015	0.14	7.2–8.2		10–12		0.2–1		0.5–1.5		
VT18U		82.11–87.3		0.2		0.1	0.1–0.25	0.04	0.015	0.14	6.2–7.3		3.5–4.5	2–3	0.4–1		0.5–1.5		
VT20		85.15–91.4		0.25		0.1	0.15	0.05	0.015	0.15	5.5–7		1.5–2.5		0.5–2	0.8–2.5			
VT23		84.1–89.3		0.4–0.1		0.1	0.15	0.05	0.015	0.15	4–6.3		0.3		1.5–2.5	4–5		0.8–1.4	
PT3V		91.39–95		0.25		0.1	0.12	0.04	0.006	0.15	3.5–5		0.3			1.2–2.5			
VT19**	[81]										3		1		5	3.5		5.5	
VT25U**							0.2				6		3	1	3.5				
VT29**											1								2
OT4-1V**											3.5					1.5			
β_1**											3			3		15		3	
β_2**													6	4	10				

* Units of measurement: mass %. The maximum value or range is specified for admixtures and dopants. All alloys contain up to 0.3 mass % of impurities in addition to those specified.
** Only additives-ligands are specified.

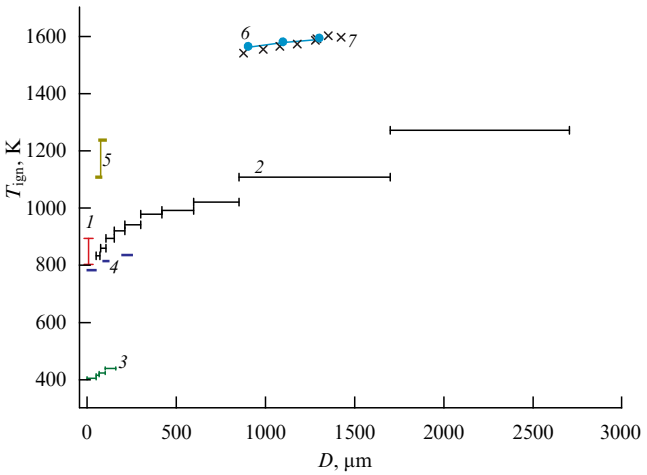

Figure 1. Temperature T_{ign} of Ti particle ignition in air as a function of the particle size (case *4* is for oxygen) under atmospheric pressure. Vertical line *1* shows data [118] for Ti aerosols consisting of 9.6-μm particles if concentration varies from 75 to 200 g m^{-3} (smaller T_{ign} corresponds to larger concentration). The sequence of horizontal segments, 'steps' *2*, displays data [38] for sieve fractions 53–75, 75–105, 105–150, 150–210, 210–300, 300–420, 420–600, 600–850, 850–1700 μm, and larger than 1700 μm of TG-0 grade titanium sponge particles (contains 0.04% Ni). Horizontal steps *3* show a Ti alloy containing 2.5% Ni; sieve fractions < 50, 50–63, 63–100, and 100–160 μm [38]. Three horizontal steps *4* correspond to data [56] for the specimens produced by pressing PTS-grade Ti particles of sieve fractions < 45, 90–120, and 200–250 μm into asbestos-cement cups; experiments were performed in oxygen. The two steps connected by segment *5* show data [57] obtained in a tracking facility for spherical VT1-grade Ti particles whose sizes fall in the ranges of 56–75 and 72–102 μm. The dots connected by *6* and crosses by *7* display the data [57, 58] for spherical VT1-grade Ti particles; the particles were inserted into a furnace with the aid of a holder. Data sets *2* and *5–7* show how T_{ign} varies depending on the Ti grade (TG-0 and VT1). Data sets *2* and *3* illustrate the effect of adding nickel (0.04 and 2.5%) on T_{ign} and indicate how the Ti ignition temperature may be decreased by introducing alloying additions.

linear function [118]. The reaction occurs in the kinetic regime, but it is retarded by the layer of products, the factor that is taken into account in devising kinetic equations.

We conclude that the temperature and nature of the gaseous environment, sizes of particles (or their specific surface), and the chemical composition of the particle material are the key factors that determine the titanium particle ignition time.

(3) *Ignition and combustion of aerosuspensions*. If aerosuspensions ignite and burn in a dusty flame, the particle concentration and fuel-to-oxidizer proportion must be added to the list of key input parameters. The flame propagation rate is an important output parameter. To assess the fire hazard of dust, the concept of minimum explosible concentration (MEC) is engaged [22, 50, 119]. If dust is ignited with an electric spark, the minimum ignition energy (MIE) is used as an ignition characteristic [22, 38, 118]. To assess the destructive impact of an explosion, the maximum explosion pressure P_{max} and maximum rate of pressure rise $(dP/dt)_{max}$ are invoked [22].

For Ti particles whose sizes are less than 40 μm in a 'layer', it was found that MIE = 0.008 mJ, a value equal to 0.5% of Al particles with a comparable size (1.6 mJ) [38]. There is a certain relationship between MEC and T_{ign} [120]. The techniques and the results of explorations of flame propagation across particle suspensions in gases have been reported [22, 29, 60, 61, 100, 120, 121]. A typical list of recorded parameters includes the flame propagation rate, temperature, and geometric structure of the flame. It is noteworthy that the flame propagation rates measured under comparable conditions but in various setups may differ by an order of magnitude. An analysis of these data is beyond the scope of our review. Condensed products of aerosuspension combustion have been studied in Refs [22, 61]. These data are discussed in Section 7. The completeness of metal burning was numerically estimated in Ref. [121] by analyzing the gas composition in a chamber after explosion. In the concentration range under consideration, from 0.08 through 1.275 kg m^{-3}, the fraction of the metal that reacts ranged 57–93%, and, due to incomplete burning, the maximum explosion pressure P_{max} in the chamber was 1/3 to 1/2 the calculated value.

If the specimen type and size are varied, the magnesium T_{ign} in air is known to diminish in the following sequence: bulk specimen → powder → aerosol → aerogel [38]. A similar sequence for Ti cannot be specified due to the scarcity and incompatibility of data. For example, the ignitability of refined iodide Ti particles in a layer and aerosuspension has been compared in Ref. [50]. For T_{ing} on the order of 690–870 K, the ignitability in the aerosuspension was 12–17% higher than in the layer. However, according to monograph [2, p. 241], T_{ign} in the aerosuspension is conversely lower than in the layer (630 and 670 K, respectively). This mismatch seems to be due to the different purity levels of the powders.

We continue the list of the regularities identified in Ti ignition.

(4) *Ignitability characteristics* depend on test conditions and powder properties. In addition to the parameters listed above, such as the gaseous environment composition and pressure, particle composition and size (or, more accurately, the particle size distribution), particle concentration, and metal/oxidizer mass ratio, also of importance are the particle shape (presence or absence of sharp-edge flanges) and state of the surface (oxide film structure, occurrence of defects, adsorbed gases and/or moisture). The heating rate may be a significant factor under thermal explosion conditions. In the case of powder layer surface ignition, the flame propagation velocity depends on the blow-off velocity and direction, layer thickness, substrate material, and other factors. Moreover, the oxidation rate may depend on the process prehistory via the characteristics of the oxide film, which builds up in the preignition period.

To illustrate the surface state effects, we quote results of experiments [62], where Ti powder mechanically processed in a ball mill was ignited. The powder was then input into a muffle furnace in a capsule ∅16 mm made of metal gauze. Data on the granulometric composition in the initial powder and the material processed over 8, 40, and 120 hours are reported in Ref. [62] for TP-6-grade Ti. The powder was somewhat refined as a result of mechanical processing, and the fraction of fine particles diminished (presumably as a result of aggregation); however, the specific surface hardly changed after the 8-hour processing. To prevent powder oxidation, the titanium was processed in a vacuum. The value of T_{ign} in air was found to almost linearly diminish from ≈ 800 to ≈ 600 K, when the duration of the processing increased from 0 to 120 hours.

The authors of Ref. [62] relate a mechanical activation effect with the accelerated burn-out of the powder particle surface layers that experience the strongest deformation in the

course of processing. As a diagnostic method, light-stimulated electron emission was applied, which is the phenomenon observed when a crystal is irradiated with light whose energy of quantum is smaller than the electron work function. The emission is thought to be due to structural defects on the crystal surface, since the layer from which the emission occurs in solid bodies (including Ti crystals) is ≈ 10 nm thick. The emission intensity increased 43-fold after the 120-hour processing. Since the mechanical activation effects persist for a long time (up to six months), this technique may be applied as a method of enhancing the powder inflammability.

The authors of Ref. [63] explored the thermal explosion of Ti specimens in the form of a poured-density powder subjected to linear heating with a rate of 5–200 K min^{-1} in air. In addition to the heating rate, they varied the powder particle size (from 63 to 250 μm) and specimen size (cup diameter ranged from 10 to 26 mm). The temperature was registered using two tungsten-rhenium thermocouple probes located in the center of the cup and near its wall. The effective activation energy was estimated by processing the temperature records. For the variations of particle sizes specified above, it was 142–285 kJ mol^{-1}.

(5) *Effect of gas environment composition on the oxidation rate* (*law*) *and oxide film structure*. The kinetics of Ti particle reaction in a layer is also investigated utilizing conventional thermographic methods. The reaction of powders with particle sizes of 5 and 20 μm with air was studied in Ref. [53] in a temperature range of 323–1473 K applying the thermogravimetry (TG) method with the heating rates of 2, 5, and 10 K min^{-1}. X-ray phase analysis (XPA) was employed to determine the specimen phase composition in the process of oxidation. The experiments performed showed that Ti transforms into rutile, TiO_2, without producing other phases (traces of titanium nitride were observed at a temperature below 700 K). The reaction rate was expressed as $Z\exp[-E/(RT)]$, where R is the molar gas constant. The kinetic parameters Z and E change if the heating rate is varied; their averaged and generalized values for a temperature interval of 700–1400 K are as follows: $Z = 6.1\times 10^{-3}$ cm^2 s^{-1}, and $E = 189$ kJ mol^{-1} [53].

Slow Ti oxidation in air and water vapor (characteristic timeframe is several hours) was studied in Refs [54, 55] in a temperature range of 973–1473 K. Experiments were performed using 99.93% pure specimens with sizes of $10\times 10\times(2-5)$ mm under atmospheric pressure in a weak flow of gas moving with a velocity of 6 cm s^{-1}. At temperatures in the range 1073–1373 K, the 3-hour experiment showed that the oxidation kinetics corresponded to the Evans equation combining the linear and parabolic laws of oxidation rate. This is an indication that diffusion and interphase reactions control the process in a commensurable way. Study [54] reports parameters of the oxidation laws in various temperature ranges. The apparent oxidation activation energy in the linear law case approaches 71 kJ mol^{-1} at $T = 973-1173$ K, and 199 kJ mol^{-1} at $T = 1173-1423$ K. The apparent oxidation activation energy by the parabolic law is 235 kJ mol^{-1} at $T = 973-1123$ K, 510 kJ mol^{-1} at $T = 1123-1223$ K, and 159 kJ mol^{-1} at $T = 1223-1373$ K. The XPA data give evidence that the produced oxide is rutile, TiO_2. The oxide layer in the form of scale is weakly bound with the metal. For $T > 1373$ K, the role of cationic diffusion (outward diffusion of metal and oxide formation at the oxide–gas interface) becomes increasingly important. The Pilling–Bedworth coefficient for rutile equals 1.74, a value that suggests, combined with a low strength of the bond between the oxide layer and the metal, the occurrence of periodic local failures in the oxide layer integrity. This factor facilitates producing rutile with an almost stoichiometric composition. The oxidation rate in water vapor is higher than in air [55].

(6) *Gas admixtures in metals* may affect in an indirect way the particle ignition via the oxide film structure and, in a direct way, the particle oxidation and combustion rates. The effects of adding hydrogen to titanium have been explored in Refs [64, 65]. Experiments were conducted with spherical particles of industrial grade titanium 5 to 25 μm in diameter. If the content of hydrogen increased from 0 to the maximum value of 2.6 mass %, T_{ign} of the Ti particles 5 μm in diameter increased from 933 K to 1163 K, the induction time from 4.8 to 10.2 ms, and the burning time from 1.6 to 6.6 ms (tracking technique data). Effects of the dissolved gases (nitrogen and hydrogen) and oxidizing medium (air, oxygen, water vapor, and chlorine) were also studied [66]. The dependence of the ignition time in various media on the particle diameter has been determined for temperatures ranging 1200–1300 K.

(7) *Effect of metal admixtures*. A relationship has been found for titanium alloys between their ignition temperature and melting temperature (the liquidus line, above which alloys are in a liquid state on the phase diagram of states) [38]. Many patents have been issued for pyrophoric alloy production techniques [38, p. 63]. For example, the addition of 2.5% nickel diminishes the ignition temperature of 50-μm particles to 400 K (see Fig. 1).

(8) *Specific features of Ti alloy ignition with a high-rate flow of an oxygen-containing gas and laser irradiation*. The ignition of Ti specimens of the VT1-0, VT1-1, OT-4, VT6, and VT14 grades under the effect of an oxygen stream outflowing through a nozzle 1.2 to 3 mm in diameter with a velocity of ≈ 340 m s^{-1} was studied in Ref. [67]. The specimen size reached $13\times 30\times(1.5-4.5)$ mm. The full pressure in the immediate vicinity of the specimen surface, which depends on the nozzle diameter and the distance between the nozzle and specimen, may be as high as 30 MPa. The experiments were intended to determine the critical pressure under which the specimen ignited. Ti inflammation was found to be initiated by an electric discharge setting up between the nozzle and specimen. The discharge, being electrostatic in nature, occurs randomly and can be suppressed by coating the specimen with a varnish, enamel, and silicate glass. The discharge is assumed to break down the oxide layer (a juvenile surface emerges) and creates a local overheating that results in inflammation, provided the oxidizing environment pressure is sufficiently high. The alloys explored have been ranked by the critical pressure. It was noted that the specimens ranked in the same sequence as in the case of ignition in oxygen at the formation of a juvenile surface as a result of the mechanical failure (disruption) of the specimens. The results of Ref. [67] suggest ways to affect the inflammability of Ti products or specimens. The inflammability may be diminished by desensitizing the surface by coating, and increased by breaking down the protective oxide layer with an electric discharge.

Studies [68–71] examined conditions and mechanisms of self-ignition of VT1-0, VT5-1, OT4-1, PT17, PT3V, and Ti-15Zr grade titanium alloys in a similar set up of the experiment with oxygen-containing mixtures. Ignition was found to occur only if the metal breaks down as such, although a juvenile surface may emerge at loads that are lower than the breaking load. Inflammation becomes possible

with various methods of destruction or action on a specimen: stretching, bending, impact, friction, rupture, spark discharge, or high-rate blow-off. Depending on the specimen grade, the critical pressure of ignition varies by an order of magnitude, from 0.7 MPa for OT4-2 alloy to 7.5 MPa for 99.98% pure Ti iodide. It was noted that the critical pressure is higher if the destruction surface is smooth (brittle fracture) and lower if the surface is rough (plastic fracture). Preliminary saturation of the surface with hydrogen or nitrogen or making a cut that concentrates stresses facilitated transitions to brittle fracture and in that way increased the critical ignition pressure. The Ti oxidation rate is believed to be limited by diffusion through the TiO_2 layer and almost does not depend on pressure.

A microscopic analysis of the fracture surface showed that ignition begins from local spots where heat removal to the specimen interior is hindered, such as scales partially peeled off the surface and micropeaks. A thermocouple installed on the specimen surface was used to measure the heating temperature (≈ 70 K) immediately prior to fracture in an inert environment. A hypothesis was set forth to explain the ignition mechanism. For the ignition to occur, juvenile surface spots have to be heated to the critical ignition temperature. Each temperature value has its corresponding critical pressure. Estimates show that the temperature corresponding to the critical pressure of 7.5 MPa for Ti iodide amounts to 540 K. The destruction has to develop sufficiently rapidly, so that the heat does not have time for its removal to the specimen bulk. The alloy ignition parameters are not the same due to different both the fracture work and the kinetics of interaction with oxygen. Self-heating occurs owing to the heat of dissociative chemical adsorption of oxygen in metal, so the interaction rate depends on the oxygen pressure ($\sim p^{1/2}$). It was noted [71] that the critical pressure often adopted as the ignition pressure may correspond to only partial melting of some parts of the juvenile surface. The transition to ignition may actually occur at a significantly higher pressure, which may be determined from the thermal explosion conditions. In this approach, heat losses from the locally melted portion of the substance to a semiclosed solid body must be taken into account.

Ti ignition in air using laser irradiation has been studied in Ref. [72]. The published data, which involve a comparatively low laser power (up to 30 W) and a heating duration of 20–1000 s, show that the kinetic parameters are close to the corresponding values in the case of isothermal oxidation. If the power is higher and the specimen is intensely blown off, the ignition character becomes more involved. The author of Ref. [72] experimentally studied how a $10 \times 10 \times 1$-mm plate made of the VT1-0 alloy is ignited from the radiation emitted by a CO_2 laser with power $W = 350-800$ W. The plate was blown off along its surface with a supersonic air stream (Mach number $M = 1.8$); the plate temperature was measured using a chromel–alumel thermocouple pressed into the plate back side. The time during which the temperature across the plate equalized was much less than the duration of the experiment.

The author of Ref. [72] distinguishes two characteristic time instants and two corresponding temperature levels: the instant t_1 when a glow emerges near the specimen surface, which corresponded to the inflection point of the time dependence of recorded temperature $T(t)$, and temperature $T_a = T(t_1)$, which the author interprets as the ignition temperature, and an instant t_2 and temperature $T(t_2)$. The temperature $T_a = T(t_1)$ depends on the radiation power; for example, $T_a = 1250 \pm 25$ K for $W = 360$ W, and $T_a = 1470 \pm 25$ K for $W = 800$ W. The temperature T_a also increased if blow-off was intensified. Sparks emerged at the instant t_2 (which was actually the onset of specimen combustion). The times t_1 and t_2 are on the order of several seconds. The temperature $T(t_2) \approx 1930$ K is close to the titanium melting temperature. If irradiation ceased at the instant t_1, ignition failed to commence. If irradiation was interrupted at the instant t_2, self-sustaining combustion developed, provided there was no blow-off. Study [72] determined the effective kinetic parameters of oxidation; an increase in the radiation absorption coefficient due to the oxide film thickness x growing according to the parabolic law $dx/dt = (k_f/x)\exp[-E/(RT)]$ was taken into account. The following values were determined: $E = 214 \pm 12$ kJ mol^{-1} and $k_f = (8 \pm 4) \times 10^{-2}$ cm^2 s^{-1}. The obtained kinetic parameters are close to those found for isothermal oxidation (for example, $E = 235$ kJ mol^{-1} at 973–1123 K, as reported in Ref. [54]).

We now summarize the experimental information presented above.

Ti ignition proceeds in a diffusion regime because the oxide film building up at the early oxidation stages hinders gaseous oxidizer transfer. Depending on the specimens and experimental conditions, T_{ign} varies in the range of 400–1500 K, temperatures that are lower than the melting points of titanium and its oxide. If ignited in air, the metal reacts with oxygen, and its reaction with nitrogen can be disregarded. The conversion depth during the induction period is not large, and it can be ignored in calculating T_{ign}. Ignition comes into play when heat generation in the diffusion regime exceeds heat removal, the process being controlled by the solubility of the oxide in metal. The estimated effective oxidation-reaction activation energy in the process of ignition is $E \sim 210$ kJ mol^{-1}. The oxide film growth kinetics and heat generation in the chemical reaction should be described using an expression taking into account film diffusion resistance (for example, in the form of the parabolic oxidation law). The experimental data do not indicate that any significant changes occur in the ignition mechanism if the ignition conditions, such as environment parameters (composition, temperature, blow-off rate, etc.), and/or particle properties (size, state of surface, presence of admixtures, etc.) vary. The recorded quantitative changes in the ignition parameters are, on the contrary, qualitatively explained by changes in the experimental conditions. The following ways to facilitate Ti ignition are known: mechanical activation, addition of some alloying metals (Ni, V, Al), and electrostatic breakdown of the oxide shell.

If the specimen disintegrates and a juvenile surface emerges, the temperature at which the thermal balance between heat generation and heat removal collapses changes by the value due to heating as a result of the fracture work. This work energy depends on the alloy properties, which may also affect the specimen morphology in the vicinity of the disruption, local heat removal, and oxidation kinetics.

Overall, titanium ignition corresponds to the classical theory of thermal explosion, according to which an explosion occurs when the heat generation rate exceeds the heat removal rate. A specific feature of metal oxidation is the dependence of the reaction rate on the oxide film thickness and state [122, 123]. Therefore, apart from the temperature value, of importance are the heating rate and the nature and activity of the oxidizing elements.

Table 4. Properties of titanium oxides [124, 125].

Oxide	Syngony	Melting temperature, K	Boiling temperature, K	Thermal stability	Color
Ti_6O				Stable up to $T = 1103$ K	
Ti_3O	Rhombohedral, hexagonal			Stable up to $T = 1673$ K	
Ti_2O	Hexagonal				
TiO (α, β, and γ forms are known)	Cubic, monoclinic	(β) 2100		Stable	Golden, yellow, dark brown, brown-violet
Ti_2O_3	Hexagonal	(β) 2400; 2115 congruently; 2212	(β) 3300	Decomposes when boiling into TiO and TiO_2	Dark violet. Black
Ti_3O_4		—		Unstable	Black
Ti_3O_5	Monoclinic	(β) 2450; 2047	(β) 3600	Only stable at high temperatures	Light and dark blue
Ti_4O_7				Decomposes at 1673–1773 K	
Ti_5O_9	Triclinic				Dark blue
TiO_2	Tetragonal, rutile	2128; 2143 congruently	3200	Decomposes for $T > 2473$ K with a detachment of Ti_3O_5 and then Ti_2O_3	Yellow, red, reddish brown, brownish black
TiO_2*	Tetragonal, anatase				White
TiO_2	Rhombic, brookite				
TiO_3**					

* TiO_2 has five polymorphic modifications.

** The TiO_3 oxide is erroneously included in the reference book [124] (in the first edition, in Table 5 on p. 113) with a reference to [126]. This error was then reproduced in the second edition of that book and other publications. Actually, no data on TiO_3 are available.

4. Combustion of titanium compact specimens. Convection and blow-off effects

Study [73] reports experiments where titanium 0.5 and 1 mm in diameter wires were burned in a cylindrical chamber of $\approx \varnothing 23$ and 38-cm-long that had a window on the side surface. The wire secured in the chamber and directed along its axis was ignited at one end using a spiral heated with an electric current pulse. The experiments were performed under a pressure of 1 atm in air enriched with oxygen up to 100%. Video shots were used to determine the velocity of the combustion zone motion along the wire. The velocity was found to depend on the oxygen content in the atmosphere, wire diameter for various orientations of the wire (horizontally or vertically), and ignition site location (above or below the wire) [73]. A specific feature of the wire combustion is that the material from time to time flows down from the combustion zone, and detachment of the droplet from the wire. The author of Ref. [73] concluded that the combustion rate is controlled by the oxygen diffusion from the ambient air.

Experiments have also been performed in paper [73], where a piece of wire was burned in a small furnace in an oxygen flow. Ti was found to completely burn out, producing a brittle residue of the bluish-black color with a yellow-white layer on the surface. Although vapor-phase combustion was not observed, a similar yellow-white residue was found on the outlet (colder) pipe of the furnace. The described colors are typical of various titanium oxides (Table 4).

The research technique reported in 1959 by Harrison [73] is still in practice. The burning rate is measured for specimens of titanium or its alloys as a function of varying conditions, including composition, velocity, oxidizing gas environment temperature, and specimen geometry and orientation. Additional information about the combustion mechanism is obtained by quenching the specimen combustion and exploring its residues; currently, state-of-the-art electron microscopy facilities are used to that end (energy-dispersive X-ray spectroscopy,[1] wavelength-dispersive spectroscopy,[2] etc.).

Ignition and combustion of millimeter-sized spherical particles and wires made of VT1-grade Ti were studied in Refs [57, 58] under an elevated pressure (up to 40 MPa in air) in a windowed chamber whose volume reached 0.02 m^3. A heater installed inside the chamber warmed up air to 1,800 K. An electromechanical particle feed system was used in the experiments, which enabled igniting 13 particles in sequence without opening the chamber. Ignition temperature dependence was determined for particles whose diameter D ranged $0.8-1.4$ mm with a natural oxide film on their surface under a pressure of 0.1 and 0.5 MPa; this dependence may be described as a linear function $T_{ign}(D)$ (the dependence for 0.1 MPa (curve *6*) is displayed in Fig. 1). The activation energy (184 kJ mol^{-1}) was determined assuming the parabolic oxidation law. The ignition temperature as a function of pressure p, which was determined for a fixed particle diameter (equal to 1.1 mm), may be represented as $T_{ign} \sim 1/p$. If the pressure increased from 0.1 to 10 MPa, T_{ign} decreased from 1600 to 1400 K. The function $T_{ign}(p)$ was fitted under the

[1] EDS (or EDX).
[2] WDS.

assumption that the value of $E = 184$ kJ mol^{-1} is constant in the entire range of explored pressures, 0.1 through 10 MPa, to yield the dependence of the pre-exponential factor k on the pressure: $k = 0.074p^{0.22}$ cm^2 s^{-1}. This formula agrees with the Freundlich sorption isotherm — an empirical equation describing the dependence of the amount of substance adsorbed on an energy nonuniform surface. The following phenomenon has been experimentally observed: after a particle is input into a heater, it incandesces first to a temperature that exceeds the gas temperature, as is evidenced by its bright glow, and then cools down to the gas temperature. If such a brightly glowing particle fell and touched internal elements of the chamber, it always ignited. This phenomenon was interpreted by the authors of papers [57, 58] as a confirmation of the decelerating effect of oxide film under the conditions close to those of inflammation.

The 0.5-to-4 mm in diameter and 150-to-250 mm long wires that were studied in the experiments were ignited from the loose end using a titanium spiral heated by electric current. The wire specimen completely burned out only provided the pressure is high enough; otherwise, the combustion faded out. The required pressure increased with growing wire diameter (for example, it was 7.5 MPa for a diameter of 1 mm, and 10.5 MPa for a diameter of 3 mm). The wires were located horizontally or vertically (in the latter case they were ignited from the top or bottom), and the burning rate was measured using video shots or burning through the reference wires located at a distance of 76–120 mm from each other. Dependences of the linear burning rate on pressure and the wire diameter and orientation were reported by Grachukho et al. [57, 58]. The rate is on the order of 1 cm s^{-1}.

The authors of report [74] explored the combustion of 99.2% pure Ti specimens with sizes of $\sim 1.6 \times 4 \times 4$ mm and weight of 130 mg in oxygen under a pressure of 0.1 MPa. The specimen was located flatwise on a horizontal graphite substrate and ignited from the upper surface with a 100-W CO_2 laser. To record specimen behavior, the experimentalists used high-speed color filming and an innovative high-speed video shooting technique based on Hilbert transformation (HSSHT) (an analog of Toepler's schlieren method) that enables detecting heat generation by observing optical density perturbations, obtaining the records of visible wavelength range spectra with space and time resolutions to identify compounds, and records of integral glow. In addition, the combustion of specimens was quenched using argon, and their residues were explored with the aid of chemical and X-ray structural analyses and scanning electron microscopy. The authors of Ref. [74] suggested the following three-stage physical model of Ti specimen combustion.

Stage 1, lasting ≈ 0.2 s, which includes specimen heating, ignition, and partial melting, actually corresponds to the propagation of combustion process across the specimen. A vapor-phase reaction occurs at a distance of several millimeters above the specimen surface, which is evidenced by heat generation (recorded using HSSHT) and by Ti and TiO lines and bands in the radiation spectra. The reaction zone glow intensity first gradually increases and then decreases. The absolute glow maximum is observed at $t \approx 0.15$ s. The presence of continuous parts in the glow spectrum from reaction zone allows one to assume that the size of the condensed product region in that zone is on the order of 1 μm. Thermal radiation from the reaction zone may significantly contribute to a specimen heating. The reaction rate seems to be limited by the kinetics, although the reaction zone may hinder oxygen diffusion to the surface. A metallographic analysis of the quenched specimens showed the presence of a solid solution of oxygen in titanium (absorption to the solvability limit of 34 at. %) and subsequent production of increasingly heavier oxides.

Stage 2, combustion, begins when the specimen melting front reaches the substrate and continues for 0.2–0.7 s. At the beginning of stage 2, when the specimen still maintains its square shape, signs of the vapor-phase reaction described above are observed. Afterward, the vapor-phase zone narrows to 1–2 mm and 'lands' on the specimen surface, and simultaneously the Ti and TiO bands disappear from the spectrum. The glow intensity gradually increases, reaches its maximum at $t \approx 0.4$ s, and then begins to decrease. A Ti + O mixture was observed inside, and TiO near the surface of a specimen quenched at the beginning of stage 2. The specimens were covered later with a thin layer of heavy oxides.

The authors of Ref. [74] explain the increase and subsequent decrease in the glow intensity in the following way. As oxygen accumulates in the particle (up to the limit of its solubility in the liquid mixture), the Ti vapor concentration in the vapor phase decreases, since the Ti + O mixture whose Ti and O ratio is the same as in Ti_3O_5 and Ti_4O_7 evaporates approximately as TiO_{liq} (in liquid Ti_3O_5) $\rightarrow TiO_{gas}$. In addition, the Ti and TiO concentrations above the specimen surface are reduced due to a significant drop in vapor pressure, as follows from the phase diagram of the system when moving along its composition from Ti to TiO. The Ti and TiO concentrations may be reduced even when the surface temperature increases. The reaction rate is now controlled by the layer of heavy oxides rapidly being built up, which hinders the oxygen diffusion transport inside the specimen, so the specimen temperature and glow gradually decrease until stage 2 ends.

Stage 3 (time interval from 0.7 to 1.0 s) begins with the ejection of one or more particles from the molten specimen. Dispersion of particles enhances and transfers into a continuous ejection of linear showers (the term used by the authors of Ref. [74]). Sometimes, the specimen 'breathes' during this time interval: its size almost doubles and, after the gas bubble bursts, returns to the initial size. The bubble burst is also accompanied by the ejection of fragmentation particles. The fragmented particles ejected at the beginning of the intense fragmentation are not yet fully oxidized and continue burning and fragmenting in flight. HSSHT is employed to observe optical density perturbation regions, the size of which is two to three times larger than the droplet size, evidencing the occurrence of the vapor phase reaction near the surface of the recently produced droplets. At the end of the intense fragmentation, the ejected particles no longer fall apart.

An analysis of collected fragmented particles showed that they are hollow TiO_2 spheres. Prior to the onset of intense fragmentation, the vapor zone disappears, and the specimen surface becomes clearly visible. After the intense fragmentation regime settles, the specimen temperature and glow decrease. As fragmentation evolves, the size of the ejected particles diminishes. If the specimen is frozen in argon in the process of intense fragmentation, the outer layer composition changes from an intermediate oxide (arguably, Ti_2O_3) to TiO_2. There is an internal TiO layer beneath the TiO_2 layer that 'grows into' the Ti + O specimen in the form of dendrite structures. In the opinion of the authors of Ref. [74], 'the

driving force' of the fragmentation is localized at the interface of the TiO_2 and TiO layers, and the observed intense boiling does not supply fresh metal to the surface. The fragmentation phenomenon is due to gases or vapors; however, the gas composition is still not clear.

The specimen begins hardening from the bottom at the end of combustion stage, and, when it is fully hardened, reacting and fragmentation halt.

Clark et al. [74] suggested the bulk specimen ignition being similar to that of Ti particles. Due to conductive heat losses, the bulk specimen temperature may be somewhat lower than that of the particles; this effect results in incomplete metal burning and a more complex picture of oxide production and interaction between them.

Experiments with a similar setup have been performed in Ref. [76], where cylindrical specimens 3.125 mm in diameter and 3.125 mm long made of 99.99% pure Ti were involved. The specimens were heated with a CO_2 laser ($W = 100$ W, wavelength $\lambda = 10.6$ μm) from a flat surface in a nitrogen–oxygen or argon–oxygen atmosphere containing 0, 10, 20, or 30% oxygen under a pressure of 0.1 MPa. Thermocouple Pt/6% Rh and Pt/35% Rh wires 200 μm in diameter were soldered to the specimen side surface. The specimen behavior was recorded using a high-speed video camera; the specimens were also quenched at different stages of the experiment, and specimen metallographic sections were studied using scanning electron microscopy and energy-dispersive spectroscopy.

The authors of Ref. [76] distinguish A and B 'transitions' in the temperature records $T(t)$ that feature a sharp increase in the temperature growth rate. Transition A at a temperature of $\approx 1120-1220$ K is related to the beginning of TiO_2 production. The increased heating rate is due to both an exothermal oxidation reaction and an increase in the surface optical absorption capacity. The temperature jump at 1670 K (transition B) is due to reaction self-acceleration, which does not depend on oxygen concentration. If the specimen is heated for a sufficiently long time, a liquid bead consisting of TiO_2 emerges on its surface, which, after induction period, starts ejecting fragmentation particles. The fragmentation occurs more intensely in an O_2/N_2 atmosphere.

In comparing the results of studies [74, 76], we note that the millimeter-sized Ti specimens were able to maintain self-sustainable combustion in pure oxygen, but failed to do so in environments containing 30% O_2. Due to the build-up of oxide and molten metal on the surface, for the combustion to be maintainable, the titanium must be pre-heated, the oxygen concentration must be high, or the molten metal/oxide layer must be removed from the surface. The last may occur in engineering devices to cause their failure [43].

Experiments have been performed in Ref. [77] with cylindrical 99.95% pure Ti specimens 4 mm in diameter and 4 mm long in motionless oxygen under a pressure of 0.1 MPa. A specimen located on an aluminum-oxide substrate was ignited from the top using a 1000-W xenon lamp with a broad radiation spectrum ($\lambda = 0.3-1.1$ μm). Owing to the usage of an aspheric lens, the density of the radiation flux focused on the specimen surface was as high as 1.75 MW m^{-2}. Light irradiation occurred when a shutter opened, and the shutter was closed immediately after igniting the specimen. The following techniques were applied for measurements: shooting at a rate of 500 frames per second; temperature measurement (a Pt–Pt/13% Rh 125-μm-diameter thermocouple probe was attached to the specimen side surface); emission spectra of gas phase reactions recorded with a frequency of 150 Hz; and measuring gas pressure in the reaction vessel (volume 4.5 l). A distinguishing feature of studies [75] compared to [74, 76] is that the experiments were performed in a microgravity environment (±0.01 g for 20 s) to assess the effect of natural convection on ignition and combustion.

Thermocouple records and video shots [77] have been processed to yield the following results. The specimen is heated first for ≈ 6 s in a virtually linear manner with a rate of over 100 K s^{-1}. A plateau is observed in the $T(t)$ plot at a temperature of about 1100 K, after which the temperature growth rate increases. The authors interpret the plateau as the $\alpha Ti \rightarrow \beta Ti$ phase transition, and the increase in the temperature growth rate as switching from the parabolic oxidation rate law to the linear law. Shortly after this, the specimen surface exhibits visible changes in color and texture due to surface oxidation. The temperature of about 1700 K is considered to be critical: when it is attained, the heat generation rate becomes equal to the heat loss rate, after which the specimen temperature rapidly grows, despite the external source being switched off. The outer surface of the specimen ignites at a temperature that is a few kelvins below the Ti melting point (1933 K). After the ignition, the molten mass consisting of metal and oxide forms a 'cap' in the shape of a spherical segment on the upper surface, which begins propagating downward along the specimen, reaches the substrate, and spreads across it. The reaction becomes more intense and is accompanied by fragmentation — the ejection of fine particles reacting in the gas phase.

The average steady-state propagation velocity was 16.2 mm s^{-1} in the normal gravitation environment and 8.7 mm s^{-1} in the weak gravitation environment. The velocity ratio of 1.86 is in agreement with the predictions of model [127], where the reaction rate was assumed to be limited by oxygen diffusion and convection to the specimen.

Due to the high heating rate (100 K s^{-1}) and significant conduction and radiation heat losses, the ignition temperature (≈ 1900 K) in experiments [77] was several hundred degrees higher than under isothermal conditions. The reduced gravitation does not affect the ignition temperature; however, it almost halves the velocity of molten mass (interaction zone) propagation down the surface of a specimen, thus indicating the significant role the convective lift of the heated gas plays in delivering oxidizer to the reaction zone.

Experiments have been reported in Ref. [78] where 3.2-mm diameter rods made of Ti and other metals were subjected to combustion in oxygen in a falling facility in which microgravity of $10^{-4}-10^{-5}\,g$ was maintained for 2.2 s. Unlike the materials studied in Ref. [77], the materials explored in Ref. [78] (Ti, Al, Fe, and stainless steel) burned under zero gravity more intensely. This was evidenced by the following observations: (1) the velocity of molten mass propagation along the rod was substantially higher than in the normal gravity environment; (2) miniature thin sheets that flickered out in the normal gravitation environment completely burned out in the zero-gravity environment; (3) volatile combustion products emerged that were not observed in the normal gravitation environment. These phenomena were hypothesized to occur because of the higher temperature that develops due to the reacting substance being retained in the form of a molten mass ball and the heated gas being not lifted. The disagreement between the results of Refs [77, 78] seems to be

related to the different geometry of the specimens. Dispersion was observed in Ref. [78] in the course of titanium combustion.

The burning rate and limits for sustainable combustion regarding pressure (up to 3 MPa) have been investigated in Refs [79–84] for 16 titanium materials (listed in Table 2 and their characteristics displayed in Table 3) in the form of plates with dimensions of 10×35 and 50×80 mm and 0.3, 0.55, 1.0, 1.5, and 2.0 mm thick as a function of the combustion environment, blow-off velocity (up to 250 m s^{-1}), and plate orientation and thickness. An O_2/Ar mixture with an oxygen content of 20–100% or air was used as the environment in the blow-off setups. The plates were ignited by means of a fast (1–2 s) local (a 5-to-10-mm region in the middle of the flat front end) heating to the melting point by means of a CO_2 laser. The events developed further following one of two scenarios. If the blow-off velocity was smaller than a critical value, the combustion wave faded out after having passed some distance (usually after molten mass drops were carried away). If the blow-off velocity was higher than the critical value, self-sustainable combustion developed, and the combustion wave reached the back end of the plate. It is assumed that the conductive heat removal setting the critical conditions is responsible for a combustion failure. The dependences of the burning rate on pressure and plate thickness were determined. We quote below the main conclusions.

(1) *Blow-off effect*. The plot of the mass oxidation rate V as a function of temperature has a step-like form (Fig. 2). It should be noted that, according to Ref. [123], the plot of the heat generation rate may be presented in a similar way.

The oxide film is thin in segment *1* and does not hinder the oxidation that occurs in the kinetic regime. When the film becomes sufficiently thick, oxidizer diffusion through the protective oxide film begins limiting oxidation, and its rate diminishes (segment *2*). The curve shape in this segment may differ depending on the kinetics of the reaction slowdown by the oxide layer. The oxide film loses its protective properties at some temperature T^*, and the oxidation rate sharply increases. The growth of the oxidation rate also has a limit that is now related to the diffusive transfer of the oxidizer to the surface of the metal. Segment *3* comes to a stage where oxidation occurs again with a reduced rate, since it is limited by the oxidizer diffusion in the gas phase. The blow-off boosts the oxidation rate in segment *3*, thus facilitating supply of the oxidizer to the surface. The blow-off may also affect the oxidation rate in segment *2* due to the removal (stripping off) of reaction products that hinder oxidation.

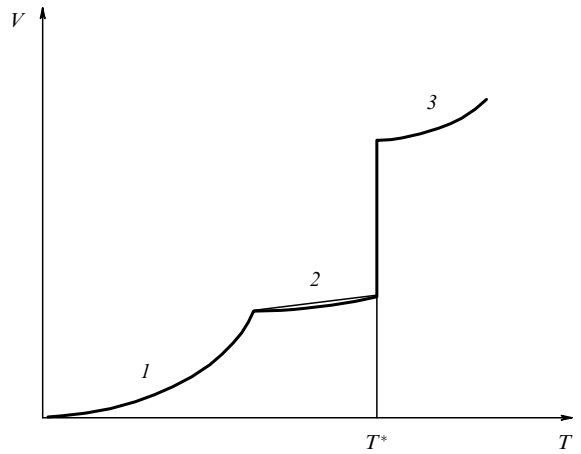

Figure 2. Schematic dependence of the titanium oxidation rate V on temperature (see details in the text).

(2) *Physical picture of combustion of the plate*. There is a region in the metal close to the blown off edge where it is heated from the initial temperature to the melting point; the width of that region depends on the heat diffusivity of the metal and the burning rate. There is a melt layer on its surface that moves under the effect of the gas flow from the front surface to the side surface and hardens on it, creating a ledge from which drops can break. If the blow-off is strong enough, the melt of metal and oxide may drop from time to time, as a result of which the oxidation regime changes.

(3) *Effect of air nitrogen*. Results of experiments performed with air and a mixture of 21% O_2 and 79% Ar were virtually the same, enabling the conclusion that nitrogen behaves in the case being considered as an inert diluent.

(4) *Effect of material properties*. Alloys may be subjected to combustion burn in the diffusion or kinetic regime, depending on their elemental composition. Dopants show their effectiveness via modification of the molten layer properties (its thickness, viscosity, and capacity to settle on the specimen). For example, combustion fading occurred for some alloys as a result of large drops being stripped off. There is a wealth of observable effects, and it is difficult to make any unambiguous conclusions regarding improving or worsening of ignition and combustion characteristics. Ti alloys with a β structure can dissolve up to 2% hydrogen, and the specimens were locally melted (at the site of heating) and fragmented as a result of the igniting effect, but they remained unfired. As a result of annealing in a vacuum at a temperature of 1073 K for 1 h to remove the hydrogen, dispersing was no longer observed, and the specimen became ignitable. This observation agrees with the results reported in Refs [64, 65, 88] that show that the adsorbed hydrogen reduces the reaction capacity of powders. The dispersion character depends on the heating rate. If the specimen was heated to the melting point during a time interval of $\geqslant 5$ s, dispersing did not occur; if, however, the specimen was heated for $\leqslant 1$ s, it developed following the explosive character.

Specific features of the combustion of specimens made of grade St.20 steel and titanium alloys in an $N_2 + O_2$ flow were compared in Ref. [81]. Unlike the combustion of steel, the combustion of titanium alloys becomes more intense (the burning rate more than doubles) if the velocity of the blow-off flow exceeds 30 m s^{-1}. The main reason for the effect is that the shape of the molten mass spread and geometric sizes of the combustion zone change. For the same reason, the burning rate also depends on the angle of attack of the incident gas flow [82].

We now summarize the results presented in this section. An important role in the combustion of bulk Ti specimens is played by the following processes and factors:

(1) conductive propagation of heat across the specimen;

(2) convective heat exchange with the ambient gas. Suppression of convection in the zero-gravity environment may facilitate or hinder combustion, depending on the specimen geometry;

(3) build-up and removal of substances (initial and/or products) from the region close to the reacting zone. Product removal combined with diffusion facilitates the supply of oxidizer; it is controlled by the gravity force magnitude and direction, blow-off flow, and the effects of spread and stripping of drops that depend, in particular, on the alloy

composition and specimen geometry (wire, plate, or cylinder).

Ti ignition proceeds substantially nonstationary and consists of stages. A transition between regimes (stages) and acceleration of the reacting usually occur at $T \approx 1155$ K (related to the $\alpha\text{Ti} \rightarrow \beta\text{Ti}$ transition and the beginning of oxide production) and $T \approx 1670$ K (supposedly due to autocatalysis). Some studies [73, 74] found indications of vapor-phase reacting at the initial stages of the process (even prior to metal melting). Fragmentation (ejection of fine particles) occurs closer to the end of combustion, seemingly as a result of phase transitions, which leads to the release of gases. The conductive heat transfer to a less heated part of the specimen causes critical phenomena and sets limits on combustion (regarding oxygen content, pressure, and blow-off velocity). Convective heat losses may have unexpected impacts. For example, a thick wire may burn more slowly than a thin one and feature more restricting combustion limits. Single or repeated events of droplet detachment affect the critical conditions and combustion parameters.

The phenomena listed above may also affect titanium *particle* combustion. Corresponding factors and effects may be divided into attributive and 'boundary' ones. The attributive set (i.e., inherent in titanium of any form or geometry) comprises the following: oxidation reactions that primarily occur in a molten metal–oxide mixture; the presence of various oxides; phase transitions; and dispersing. The boundary set includes droplet detachment and the influence of geometry on that phenomenon.

It should be noted as well that the oxidation reaction rate is limited in most studies by the transfer of oxygen, as a result of which it insignificantly changes under pressure variations [58].

5. Specific reacting of pressed and poured specimens, aerogels, and aerosuspensions

Specimens that consist of contacting Ti particles require exploration as a subject of importance for practice. For example, pressed specimens, which are intermediate between the bulk and poured specimens, are utilized in technological combustion. Specimens were explored in Ref. [85] and had the form of a $25 \times 10 \times 5$-mm parallelepiped. The horizontally located specimen was burned in a vessel that contained a gaseous atmosphere consisting of nitrogen, air, or an argon–oxygen mixture under a pressure of 0.1 MPa. The specimen burned on the surface without changing its sizes. Signals from a pressure probe, thermocouple probes, and photo diodes were recorded.

A unique feature of experiments [85] is that diffraction patterns of X-ray scattering were recorded with a time resolution. The vessel had a beryllium window transparent to X-rays; the beam from an X-ray source (Cu anode), having passed through a monochromator, was projected onto the side surface of the specimen as a 14×2.5-mm spot. It was captured after being reflected by a detector (1024 elements, angle $2\theta = 33^\circ$, where θ is the diffraction angle), with a frequency of one scan per second. This enabled experimentalists to gather information about the phase composition in real time, since the typical specimen combustion time was 8–40 s. The authors of Ref. [85] have determined, as a result, the time dependence of the recorded phase intensity. In the case of combustion in $O_2 + Ar$, the production of TiO_2 begins prior to or concurrently with the $\alpha\text{Ti} \rightarrow \beta\text{Ti}$ transition. TiO_2 is also the final product, and none of its other intermediate phases has been found. If the combustion occurs in air, the production of TiN_x nitrides and $Ti_3O_{3-x}N_x$ and $TiO_{2-x}N_x$ oxynitrides is observed.

In study [56], PTS grade Ti powder of various sieve fractions was compressed flush with the top into an asbestos-cement cup 10-mm high under a pressure of 9600 kg cm^{-2}. The cup was rapidly input into a furnace heated to a specific temperature (up to a maximum of 1070 K). When ignition occurred, a bright glow emerged near the specimen surface. It was found that if the particle sizes increased (sieve fractions of < 45, 90–120, and 200–250 μm were used), both specimen gas penetrability and T_{ign} increased as well (783, 817, and 873 K, respectively [see Fig. 1, data set *4*]). Gas penetrability is undoubtedly of importance for oxidizer supply into the specimen; however, the increase in particle sizes and decrease in S_{sp} proved in this case to be more important factors that increased the ignition temperature.

The following comments should be made regarding the effect of the gas nature. In experiments where specimens were pre-heated in inert argon to be moved afterwards to an oxidizing environment, a significant decrease in the ignition time has been observed. At the same time, T_{ign} only decreased by ≈ 20 K. If oxygen was diluted with nitrogen, T_{ign} increased up to 793, 808, 833, and 845 K for the N_2/O_2 ratio equal to 0/100, 25/75, 50/50, and 75/25, respectively. Simultaneously, the oxidation occurred in air (or in a 75/25 mixture of N_2/O_2) faster than in pure oxygen. This is explained by a mismatch of crystal lattices and the densities of the oxide and nitride, as a result of which the oxynitride film produced in air is prone to cracking, thus facilitating gas access to the surface.

Critical conditions have been studied in paper [87] for compressed particles made of PTM-grade Ti specimens in the form of a millimeter-sized (up to 7 mm) parallelepiped under a pressure of 0.1 MPa as a function of the O_2/Ar gas mixture composition (10/90, 15/85, 20/80, 50/50, 75/25, and 100/0) and specimen density (1.11–3.33 g cm^{-3}). A weight method has been proposed to determine the completeness of combustion and the oxide film thickness and density. The method is based on the assumption that Ti partially transforms into TiO_2. The completeness of combustion was found to decrease monotonically as the specimen density decreased, and a limiting density value has been determined which, if exceeded, results in combustion disruption. There is also a minimum density: if the density is lower than this value, the character of combustion changes; namely, specimens partially melt, lose their shape, and start dispersing (molten material spray-back is observed). The limiting density values depend on the O_2/Ar ratio; the completeness of combustion increases as the oxygen content grows. The observed regularities are primarily due to changes in heat conductivity with variations in the density of specimens.

The effect of vacuum thermal processing on specimen ignition was explored in Ref. [88] for specimens made of pressed PTM grade Ti (particle sizes of < 90 μm, 98.9% purity, cylinders $\varnothing$10 mm and 7.5 mm long, 33% porosity). It should be noted that industrial grade titanium powders often contain an admixture of hydrogen. For example, it was reported in Ref. [86] that PTM grade 98.92% pure Ti powder with an average particle size of 40 μm contains 0.38 mass % of hydrogen. In experiments [88], the specimens were first subjected to oxidation in air at a temperature of 473 K for

2 hours and, next, to vacuum processing. It was found that even 5-minute long vacuum processing noticeably changes the ignition temperature, and, unlike the temperature, the duration of the processing is not of importance. If the processing temperature ranges 620–870 K, T_{ign} diminishes from ≈ 740 K to ≈ 670 K, and, if it is over 870 K (870–1170 K), T_{ign} increases from ≈ 670 K to ≈ 740 K. The authors of Ref. [88] explain this behavior by changes in surface reactivity, in the area of a reacting surface, and in the pellet porosity due to the sintering of particles. If heated to a moderate extent, the metal reacts with the gas with the production of solid interstitial solutions that enhance the reactivity of the material. The oxide film does not build up but, on the contrary, partially dissolves in the metal. As a result of vacuum annealing at a higher temperature, the effect wears off due to the sintering of particles and the ensuing reduction in the specific surface area and porosity of the specimen. The data reported in Ref. [88] suggest a technique to improve Ti powder ignitability by applying combined processing (weak oxidation followed by vacuum annealing).

Study [89] explored the combustion of PTM and PTKh powders poured as a $0.5\times35\times300$-mm or $1.5\times35\times300$-mm layer in a depression made in a substrate. The combustion wave front velocity was recorded by eight directional photodiodes installed along the depression. Both the material of the substrate (metal and asbestos-cement) and powder fractional composition were varied. A number of features specific to the process have been found: oscillatory and spotty combustion, the ejection of burning particles, and a multistage structure of the combustion wave.

Combustion of metallic aerogels intended for the production of nitrides was explored in Refs [16, 18, 90, 91]. If PTM grade powders burn in air, the temperature growth rate in the combustion front is as high as 400 K s^{-1}; this is related to combustion of the hydrogen dissolved in metal particles [86, 128]. The powders pressed in a layer burn in air in a two-stage regime, nitride being produced at the first stage [91].

Thus, in the case of filtration combustion of porous metallic systems and aerogels, the gases adsorbed (dissolved) in metal play an important role. The nitrogen contained in the oxidizing environment may affect the combustion process more efficiently than in the case of a monolith specimen and, in particular, cause multistage combustion. Chemical bonding of air nitrogen determines the combustion product composition; the parameters that control nitride production in the most significant way are the maximum combustion temperature and the final product cooling rate. If quenched properly, the products may contain up to 88 mass % of TiN [91].

Adsorbed hydrogen reduces in some cases the powder reactivity. However, it can be removed by thermal processing in a vacuum. Moreover, a combined processing that includes weak oxidation and subsequent vacuum annealing may improve Ti powder ignitability.

An intermediate case was explored in experiments [92–94] that combines specific features of combustion of aerogel, an aerosuspension system, and individual particles. EP grade Ti powder (average size of particles 4.5 ± 1.5 μm) manufactured by Chemetall Co. was burned in experiment [92] in a layer with the sizes of $(5-10) \times 25 \times 10$ mm in pure oxygen under a pressure of 0.1 MPa in a windowed vessel. The powder weight was about 1 g. The layer was ignited from one end with an electric spiral using a small amount (< 0.1 g) of a paste-like pyrotechnic igniter. The process was filmed using a Motion Pro X3 video camera (5,000 frames per second, frame duration 10–50 μs). To record spectra in the visible and ultraviolet (UV) ranges ($\lambda = 190-1000$ nm), an MCS 601 Carl Zeiss spectrometer was applied, and emission spectra were recorded with high resolution using an Andor Technologies DV420-OE silicon diode matrix (1024×256 elements) and an Oriel Instrument MS 257 monochromator. The time resolution of the system was 10 ms. Spectra in the near-infrared (IR) region ($\lambda = 1.0-2.2$ μm) were measured using a PGS-NIR 2.2 Carl Zeiss spectrometer via a small hole and light guide. The vessel was continuously ventilated during the experiment with a flow rate of 2.8 g s^{-1} to maintain constant pressure and a sufficient amount of oxygen.

Upon activation of the igniter, the combustion wave front passed across the specimen in ≈ 30 ms. During that 30 ms and subsequent approximately 50 ms, a significant part of burning Ti particles was ejected to a height of 50–100 mm due to expansion of heated oxygen. As ≈ 200 ms elapsed after the combustion initiation, a brightly glowing blown-off two-phase region emerged on the layer (resembling a bedcover by its almost flat relief); this region ≈ 3 mm thick had an incandescent orange–red crown ≈ 1 mm thick. Gaseous or liquid matter was ejected from time to time. White tracks perpendicular to the surface are indicative of the ejection of fine particles or hot gases from the molten mass. Glowing fine particles were also observed above the surface. At a distance from 5 to 20 mm above the surface, somewhat larger particles were observed that glowed increasingly more strongly as they moved away from the surface. Some of those particles exploded in the manner specific to titanium. After 3 to 5 s, the crown vanished, the blown-off 'surface' of the molten mass became brighter, and, concurrently, the number of comparatively large ejected and exploding particles significantly increased. It should be recalled that a similar phenomenon (shower) was observed in Ref. [74], where monolith Ti specimens were burned in oxygen. After approximately 2 s, the number of ejected particles diminished, indicating the end of the reaction and molten mass cooling and hardening.

An analysis of the video shots enabled separating two types of particle 'production'. Type 1 refers to particles with sizes of $\approx 100-300$ μm (actually, titanium agglomerates) that are ejected from the molten layer and move away from it with a constant velocity and glow intensity increasing with time. Type 2 includes particles whose sizes are significantly less than 100 μm. They are not seen leaving the layer; these particles seemingly emerge on the crown edge owing to their increased brightness and visible sizes. Type 2 particles are observed about 100 times more frequently during the time that the crown exists and dispersing occurs.

After the particles leave the crown, their brightness first increases and then decreases until they become invisible. Ultra-close-up video shots of a particle surface showed some motion, indicating that these particles are molten. Sometimes, an increase and decrease in brightness were observed several times in sequence. Some particles swelled and fragmented without complete destruction, i.e., having the mother particle preserved. The explosion-like fragmentation, where fragments are dispersed in a star burst manner, has only been observed for a small number of particles.

An analysis of emission spectra revealed the following: (1) the peaks at wavelengths 560, 670, and 710 nm are characteristic of TiO and are responsible for the red–orange glow of the crown; (2) the radiation in the $\lambda = 1.0-2.2$-μm range has a continuous spectrum that is well described by Planck's law. This observation enabled estimating the

maximum temperatures of the melt (2750 K) and dispersed particles (3000 K). Both temperatures are significantly lower than the adiabatic value (4000 K for the ratio $Ti/O_2 \approx 65/35$). It is generally supposed that if a burning particle moves in the environment containing an excess of gaseous oxidizer, the optimal proportion may be attained between the fuel and oxidizer; however, Ti oxidation does not relate to a direct transformation of Ti into TiO_2, being instead an exothermal process of continuous oxygen dissolution in solid or liquid titanium, in which various oxides are formed (TiO, Ti_2O_3, Ti_3O_5, ..., TiO_2), and concurrently higher oxides may decompose producing lower oxides.

The authors of Ref. [92] hypothesized the following picture. As the poured layer is burning, increasingly large amounts of oxygen are dissolved in Ti particles. Since the layer is not uniform, hot spots emerge, from which particles may be ejected as a result of spontaneous local gasification. TiO vapors may condense on the crown boundary, producing small but already observable particles. When those particles move, TiO vapors may condense on the their surfaces, eventually oxidizing them to TiO_2. Owing to this, a liquid particle may grow, heat up, and become prone to oxide evaporation and decomposition. Near the point of saturation with oxygen concentration, the particle may spontaneously decompose and explode. Ti combustion in the system under consideration is driven not only by fuel evaporation and oxidizer diffusion towards the particle. The significant features of the process are determined by the exothermal dissolution of oxygen atoms in Ti melt and evaporation and decomposition of various oxides. The authors of Ref. [92] expand in this way the list of possible sub-processes constituting the Ti particle combustion mechanism.

Similar experiments have been conducted in air and nitrogen under a pressure of 0.1 MPa [93, 94]. Unlike the red–orange crown that emerges in the process of burning in pure oxygen [92], which was described above, if combustion occurs in air, a bright white glowing surface appears that seems to be dense but, nevertheless, is blown through and bubbles. It bursts in some places and, in the zones where vapor-like Ti escapes, red–orange local flames emerge (similar to the crown observed in combustion in oxygen, thus indicating the presence of TiO). Particle ejections are observed in the case of combustion in air, primarily at the beginning of the process, while they are virtually absent at its end, in contrast to combustion in oxygen, where they are observed during the entire process. In the case of combustion in oxygen, the gas phase temperature is ≈ 3000 K, and the surface temperature, which remains approximately constant, is about 2200–2400 K. In the case of combustion in air, the surface temperature also varies in the range of 2200–2400 K, but for a shorter time (≈ 5 s instead of 9 s) and afterward begins to decrease. The gas phase temperature equals ≈ 2400 K. Overall, burning in oxygen and air occurs in a similar way and differs from burning in nitrogen. In the case of combustion in air and oxygen, the temperature is over the melting points of metal and oxide. It is, therefore, probable that the metal reacts as a boiling melt, and, in addition, gases dissolve in the metal. The combustion temperatures are significantly lower in all cases (oxygen, air, and nitrogen) than the calculated thermodynamically equilibrium values. The reason for this difference is that the powder layer reacts with the gas flow in the diffusion regime and, likely, under the nonstoichiometric relation between the components.

We can now draw some conclusions. High-speed video recording, spectroscopic, and pyrometric methods have been used to obtain data about the complex character of the reacting of fine (≈ 5 μm) Ti particles in a layer. The spatial nonuniformity and occurrence in stages of the combustion, ejections and fragmentation of agglomerates with sizes of 100–500 μm, and evaporation and decomposition of various oxides — these are the characteristic features observed if combustion occurs in oxygen and air. The combustion mechanism on a single-particle level includes exothermal dissolution of oxygen and the formation of a mixture of various oxides. Higher oxides may decompose, producing lower oxides. The combustion temperature in the layer remains lower than the adiabatic values but is over the melting point of the metal and oxide and may exceed the TiO_2 decomposition temperature and, if combustion occurs in oxygen, the boiling temperature of TiO_2, as a result of which the metal reacts as a boiling melt.

The list of the most explored types of gas dispersion systems containing titanium includes gas suspensions and dust two-phase flames. The ignition of Ti suspensions in gas has been studied in Refs [50, 64], and the combustion of aerosuspensions in Refs [22, 60, 61, 64, 129]. Typical experimental setups are displayed in Table 2. Aerosuspension particles with sizes from 5 to 40 μm and concentrations ranging from the minimum explosible concentration (MEC) (≈ 0.05 kg m^{-3}) to 1 kg m^{-3} have been explored. A comparison of Ti particles with sizes of 35 μm and 50 nm has been reported in Ref. [22]. The DTA/TGA method (differential thermal analysis/thermogravimetric analysis) at a heating rate of 10 K min^{-1} was applied to establish that the 35-micrometer particles commence intensely reacting at $T \approx 873$ K, while the 50-nanometer particles do so at a temperature as low as $T \approx 673$ K. The velocity with which flame propagates across the aerosuspension with a concentration of 0.26 kg m^{-3} was 0.2 and 0.4 m s^{-1} for the 35-micrometer and 50-nanometer particles, respectively. Differences have been observed in the flame structure; in particular, in the case of nanometer particles, more intense microexplosions occurred, accompanied by a characteristic sound. SEM images of the initial particles and combustion products are presented in Ref. [22]. The initial 35-micrometer particles have an irregular faceted shape, while the nanometer-sized particles are aggregates of virtually spherical particles ≈ 50 nm diameter. X-ray photoelectron spectroscopy was employed to determine that the products of combustion of the 35-micrometer particles consist of 85% TiO_2 and 15% Ti_2O_3. The products of the combustion of 50-nanometer particles contain 61% TiO_2, 18% Ti_2O_3, 8% TiO, and 13% TiN. The authors of paper [22] assumed that the particles were liquid in the process of burning, which is evidenced by their predominantly spherical shape, and consist of an oversaturated Ti–O–N solution. Larger particles may contain a titanium core that is liquid in the outer layers and solid in the particle interior. Particle microexplosions occur as a result of the release of the nitrogen phase.

The second type of aero dispersion system currently under intense study comprises specially arranged two-phase flames intended for the so-called gas dispersion synthesis of oxides [11, 13, 113, 114]. The essence of the method is that micrometer-sized metal particles are burned in stationary laminar dust flames. This method features a high purity of the target product (oxide), a low production cost, high efficiency, environmental safety, and the capacity to control

the product properties by varying the flame parameters. It is possible, in particular, to ensure a significant yield of spherical 20–100-nm particles. The oxide nanoparticle characteristics are reviewed in Section 7. It is worth emphasizing here an unusual feature. In contrast to the turbulent regime that is usually arranged to enhance combustion intensity in heat generation facilities, a laminar flame is preferable for technological purposes. The reaction zone is, in this case, narrow, has virtually the same thickness across the flame surface, featuring large temperature gradients in pre- and post-flame zones and no signs of recirculation of the combustion products. Due to this, the metal burns and combustion products condense along the entire flame height under virtually the same conditions, thus facilitating the production of the narrow fractions of combustion products. Attempts to boost facility performance by making the flame turbulent result in the condensed combustion products being polydisperse.

It is noteworthy that burning Ti particles in a dust flame in the range of concentrations that may be implemented in practice is similar to burning individual particles.

6. Burning of individual titanium particles

We begin this section by providing useful information about titanium powders and particles considered to be an object of research. One can distinguish sponge-shaped particles, spherical particles, nanoparticles, and spherical particles and titanium agglomerates produced in the course of experiment. Industrial grade Ti powders (for example, the PTM grade) usually consist of particles with an irregular 'spongy' shape with a broad size dispersion [49, 106, 130] (Fig. 3). Some studies explore specifically such particles or their sieve fractions.

The burning of suspensions of nanoparticles in air has been studied by Yu ey al. [22]. Mixed compositions with the addition of Ti nanopowders playing the role of combustion characteristic modifiers have been explored in Refs [32, 95, 131]. Powders obtained by the method of electrically exploding wires [95] had sizes of 50–100 nm, $S_{sp} = 15$ m^2 g^{-1}, and contained 90% to 99% of the active metal. Study [96] reported on preparing the Ti powders where the average size of particles was 14 nm with a root-mean-square deviation of 8 nm. The particle shape is complex, and the particles are often faceted, so when viewed as plain photo images they may look like triangles, rectangles, or hexagons.

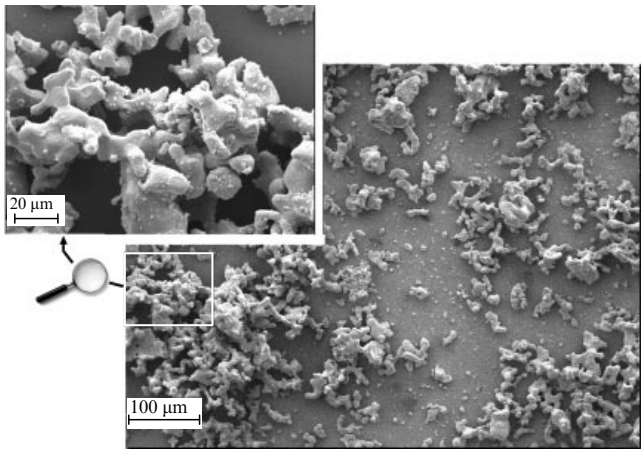

Figure 3. Scanning electron microscope image of Ti particles.

For research purposes, it is desirable to have objects that may be clearly described, preferably spherical particles. However, the author of this review is aware of only one work [97] where electric spark ignition of commercially grade spherical Ti particles in a layer was studied (the average diameter of the particles manufactured by Super Conduction Material, Inc. was 82, 250, 500, and 1000 μm). Some studies explored *millimeter*-sized particles having the shape of a cylinder, parallelepiped, or sphere [57, 58, 74–77]. There are also papers where spherical titanium microparticles were produced with the sizes, for example, of 10–50 μm [132] and 5–32 μm [133]; currently, some manufacturers also offer spherical Ti microparticles [134, 135].

Following paper [99], one can distinguish two groups of experimental methods intended for studying the mechanisms and kinetics of high-temperature interactions between metals and gases. The first group comprises track type techniques, where microparticles move in a gas flow, and the second group includes studies of millimeter-sized models: individual particles fixed on a suspension or substrate, wires, foils, etc. More detailed information about the process may usually be obtained in the latter case; however, the applicability of these data to microparticles is a matter for discussion. It should be added that the methods are available that enable producing burning spherical Ti particles having a specific size directly in the course of experiment [106, 136].

A list of studies published in 1960–2005, in which Ti particle combustion was explored, is reported in paper [104]. The methods that were involved to obtain information are in most cases identical: video recording, photodetectors/pyrometry, particle quenching/sampling, and analysis of residues. The following methods were used for igniting particles: heating in the carrier gas in a tracking facility, plasmatron, gas burner flame, laser beam, and inductor (see Table 2). The main parameters being measured comprised ignition and combustion times.

We consider next basic studies in which the combustion of individual particles was explored.

According to classification [98], Ti belongs to *nonvolatile substances* with a *soluble oxide*. Such substances feature easy ignitability of even comparatively large particles but a low burning rate. Clear-cut tracks and large combustion times are evidence of surface combustion. Ti particles were noted to burn more slowly than Mg, owing to which they are used in pyrotechnics to produce eye-catching long and bright sparks. Fragmentation is a specific feature of Ti particle combustion. The burning of Ti particles usually ends with an explosion in which fragments fly away in a characteristic star burst manner. Another specific feature of Ti is its ability to dissolve gases [64, 65, 103, 125, 137, 138]. Titanium may contain up to 30 at. % (16.67 mass %) of oxygen, and up to 20 at. % of nitrogen [52, 125, 138]. This feature should be taken into account in analyzing data obtained with the aid of gas burners, which serve as a typical tool for studying metal particle ignition and combustion (see Table 2).

It was noted in Ref. [64] that experiments in which the ignition and combustion times are determined in an environment consisting of combustion products of a mixed composition on the basis of glycerin and ammonium perchlorate (AP) [103] and experiments in an oxygen–hydrogen burner yield virtually identical results for Al particles, while their results are substantially different for Ti particles. The hydrogen available in the burner flame proved to be absorbed by Ti particles via dissolution. As a result, particle properties

change, as was shown in experiments [137], where hydrogen was dissolved in Ti. An X-ray structure analysis showed that the dissolved hydrogen converts titanium from αTi phase to γTi. The dissolved hydrogen was shown to diminish chemical activity of Ti as a result of γTi being produced on the well-developed powder surface [64, 65]. The diminished activity manifests itself in an increase in ignition time and temperature and combustion time. If, for example, 2.6 mass % of hydrogen is added to the specimen, the induction time of a 5-micrometer particle at a temperature of 1300 K increases from 4.8 to 10.2 ms, while the combustion time from 1.6 to 6.6 ms [64]. The quoted data were obtained in a track facility in air. Gas dissolution is an exothermal process. Gas forms a solid solution residing at interstitial lattice sites and occupying the vacancies intended for the oxidizer, as a result of which pre-flame reactions are retarded. There is no clear-cut boundary during oxidation between oxide and metal. Dissolved gases reduce the metal combustion rate as a result of endothermic counter-diffusion and increase the combustion time.

Study [99] provides detailed information about the combustion of PTM-A grade powder in an Ar/O_2 environment (80/20). The powder consists of irregular-shaped particles with a count mean size of 3.5–4.0 μm. Argon heated in a plasmatron arc was supplied with a flow rate of 1.5 g s^{-1} into a mixing chamber, where oxygen was added with a flow rate of 2.35 g s^{-1}, and Ti powder was input with a flow rate of 0.005 g s^{-1}. The powder was added using a weak argon flow through a 2-millimeter-sized pipe oriented along the chamber axis. The gas carrying the particles was then transported to a 4-cm-diameter and 50-cm-long measurement channel . The gas temperature and velocity at the channel inlet were 3000 K and 11 m s^{-1}, and at the outlet 1800 K and 6 m s^{-1}. The particle velocity corresponded to the gas flow rate. The concentration of particles was small, owing to which they can be considered individual particles. The measurement channel had windows for taking photos and pyrometry measurements, and inlets for probes and thermocouples. A two-beam stroboscopic photographic pyrometer was involved in determining particle velocities and temperatures (photos were taken from perpendicular directions to identify particles). Particles from different flow cross sections were sampled with the aid of $6 \times 6 \times 2$-mm plates that were inserted for a short time into the flow. To prevent further oxidation of deposits, the plates were blown off with argon. To sample fine oxide particles, plates made of polished quartz were utilized, and for sampling large metal droplets they were made of compressed asbestos. The sampled particles were explored using optical and electron microscopes, and a DRON-3 X-ray diffractometer.

The authors of Ref. [99] noted explosions of particles (both star-like and incomplete in the form of bright 'nodes' on tracks). The most intense particle fragmentation was observed as the gas outflowed from the channel into cold air. The pyrometric temperature of the particles ranged 2400–2600 K, attaining the maximum value at a distance of 5–30 cm (6–43 ms if recalculated in terms of time). Lines of TiO and atomic Ti were observed in the radiation spectrum near the channel entrance. As a result of thermophoresis, the particle motion along the channel involves sedimentation on the wall of both large particles and highly dispersed products — white particles whose sizes are less than 100 nm. Beginning from a distance of ≈ 25 cm, this fraction starts dominating and, at the end of the channel, its proportion amounts to 95%. According to XPA, large particles with sizes of several or dozens of micrometers consist of TiO_2 in the form of rutile, sometimes with an admixture of Ti, while small particles (< 100 nm) consist of TiO_2 in the form of anatase.

The authors of work [99] do not rule out the possibility that metal particles may be additionally oxidized already on the channel wall, producing rutile as a result. Plots are presented in Ref. [99] demonstrating how the particle size distribution functions in the 0–30 μm range are transformed at five distances along the channel. The distribution functions are plotted as histograms separately for metal and oxide particles. The last particles appeared as light transparent balls; the metal particles had a dark, almost black, surface with interference colors that are indicative of the presence of a thin oxide film. The phase composition of the oxide particles selected on the plates was the same as the composition of the particles on the wall (large particles consisted of rutile, and fine particles of anatase). The phase composition of incompletely burned particles corresponded to Ti–O solid solutions, lower oxides, and nonstoichiometric Ti_nO_{2n-1} oxides. The authors of Ref. [99] assert in their conclusion that in their experiment a combined combustion regime occurred. If particles get into a flow with a temperature of 2500–3000 K, vapor-phase combustion is possible, as evidenced by the presence of fine oxide particles (< 100 nm) in combustion products. As metal burns out and the temperature diminishes, the process seems to switch to the heterogeneous regime. The combustion becomes more complex due to fragmentation, which involves the rapid burning of fragments (probably in the vapor-phase regime), this factor apparently affecting the transformation of the particle size distribution functions.

In summarizing, study [99] describes the morphology of particle combustion products and points to the production of particles with sizes of less than 100 nm and the possibility of a combined vapor-phase-heterogeneous particle combustion.

Study [100] explored the combustion of particles with sizes of 41–115 μm for various oxygen concentrations (up to 100%). Falling particles were ignited in a gas burner in a flat flame of a methane/oxygen/argon or methane/oxygen/air mixture. The video recording technique utilized made it possible to record changes in particle sizes. The ratio squared of the current diameter D and initial diameter D_0 was found to linearly depend on the time $(D/D_0)^2 \sim t$. The particle exploded if its size diminished to $0.7D_0$, regardless of oxygen concentration and initial particle size. The authors of Ref. [100] related the decrease in particle size to partial evaporation of oxide products, and explosions of the particles, with an instantaneous release of volatile components. The combustion time of 58-μm diameter particles decreases monotonically from ≈ 120 ms to ≈ 4 ms, as the molar fraction of oxygen in the mixture increased from ≈ 0 to $\approx 85\%$. The combustion rate constant is 0.5 mm^2 s^{-1}, if the molar fraction of oxygen increases to 85%. The combustion time is ≈ 10 ms in both mixtures, with the atmospheric content of oxygen being 20.7%. It is this point, summarizing the published data on titanium particle combustion times, that is displayed in Fig. 4 (the data reported in Ref. [100] are shown as a pentagonal star in the inset).

In experiment [98], Ti particles with sizes of about 44, 62, 105, 150, 250, and 420 μm (sieve fractions) were ignited in a Bunsen gas burner, and the combustion time t_b was determined as a function of the diameter D: $t_b = 4.55(D/1000)^{1.59}$ (where t_b is measured in seconds, and D in

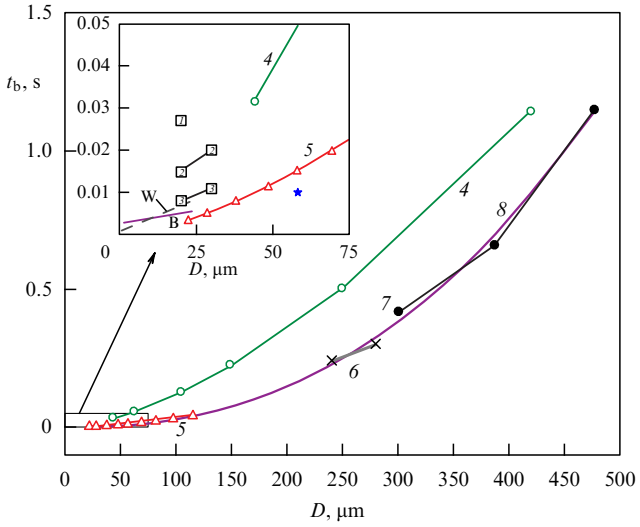

Figure 4. Ti particle burning time t_b as a function of size D. The inset shows on an enlarged scale the fine particle region delimited with a rectangle. The star in the inset presents the data reported in Ref. [100] for particles with $D = 58$ μm. Environment: gas burner flame with methane for an atmospheric oxygen concentration of 20.7%. Segment B corresponds to the data of Ref. [101] for 2–25-μm particles ignited in air when passing a laser beam. Approximation suggested in Ref. [102]: $t_b = (2.62/1000)\,D^{0.24}$. Dotted segment W corresponds to data from Ref. [102] for 0.9–24-μm particles ignited in air when passing a laser beam. Approximation suggested in Ref. [102]: $t_b = (1.09/1000)\,D^{0.63}$. Squares numbered *1*, *2*, and *3* are data from Ref. [103] for a specimen consisting of powdery AP with 1% Ti and water or glycerin used as a binder. The Ti particles that are released during specimen gasification burn in various media: (square *1*: water + AP decomposition products; squares *2*: water vapor; squares *3*: AP decomposition products + glycerin), $D = 20$ and 25 μm. Unfilled dots and curve *4* show data from Ref. [98]. Environment: gas burner flame enriched with oxygen. Approximation: $t_b = 4.55(D/1000)^{1.59}$, $D = 44-420$ μm. Triangles and curve *5* show data from Ref. [104]. Environment: air, laser ignition. Approximation: $t_b = 1.29(D/1000)^{1.56}$, $D = 15$–110 μm. The oblique crosses signs connected by segment *6* show data from Ref. [105]. Particles with $D = 240$ and 280 μm were produced in air in a microarc discharge. Approximation in Ref. [102]: $t_b = 0.09(D/1000)^{1.45}$. Filled dots connected by segments of straight lines *7* show data from Ref. [139] for particles of 'agglomeration origin', $D = 300$, 390, and 480 μm, burning in air. Curve *8* presents results of joint processing of data [104, 105, 139]. Environment: air. Approximation: $t_b = 5.81 \times 10^{-7} D^{2.35}$, range of D is 15–480 μm. In all approximation formulas, t_b is expressed in seconds, and D is micrometers.

micrometers) (see unfilled dots and curve *4* in Fig. 4). Data presented in Ref. [98] should be considered estimates, due to an uncertainty in particle sizes caused by their nonspherical shape and in environment composition and temperature, which, moreover, varied along the burner height. An effect from hydrogen may also be significant [64, 65].

A microarc method is described in Ref. [136] that enables producing individual burning particles of various metals, including Ti. The method is based on forming a liquid metal droplet as a result of fast melting in a pulse discharge of the electric arc between a thick cold cathode and a consumable wire anode. This technique yields freely falling droplets with well reproducible dimensions and initial temperatures and velocities. The size of produced droplet may be set in the range of 50–500 μm with an accuracy of ±5%. The initial droplet temperature may be varied for most metals from the melting temperature to a temperature close to the boiling point, so the droplets produced in an oxidizing medium immediately ignite. The process was video recorded, the

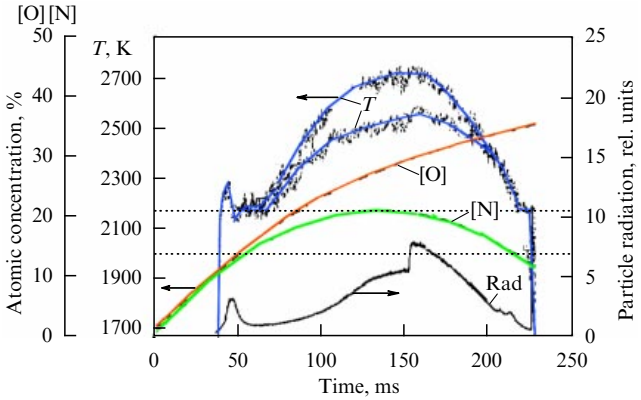

Figure 5. Data [105] obtained in combustion of 240-micrometer Ti particles in air: temperature (T) and radiation (Rad) in the process of burning and the atomic concentrations of oxygen [O] and nitrogen [N] in the interior of a particle quenched at various instants of time. Unprocessed temperature records (with 'noise') of two experiments are displayed. These records provide insight into the reproducibility of the results for different particles. Approximation dependences are presented for [O] and [N] concentrations. Horizontal dotted lines show temperature ranges in which the following phases exist: lower region (up to ≈ 1973 K), solid Ti; intermediate region (1973 < T < 2173 K), liquid αTi + TiO mixture; and upper region (T > 2173 K), liquid Ti + O solution.

brightness temperature was captured, and quenched particles were analyzed.

This method was applied in work [105] to produce spherical particles 240 and 280 μm in diameter using a 99% and 99.99% pure wire as the anode. No qualitative differences have been found in the burning of those particles. The burning particle temperature history was recorded by measuring the brightness temperature at three wavelengths (488, 510, and 640 nm) using a pyrometer. The particles were quenched at various instants of time, and their internal structure and composition were studied. The authors of Ref. [105] preferred 'fast' quenching under the assumption that it would enable them to freeze and preserve the phases that existed in burning. The particle was quenched by impingement onto a 12-μm-thick aluminum foil over a time interval of ≈ 0.3 ms. The particle embedded into the foil and got stuck in it. The results obtained in air under atmospheric pressure are presented below.

The combustion time of 240- and 280-micrometer particles was 240 and 300 ms, respectively (oblique crosses in Fig. 4 connected by segment *6*). Particle combustion always ended with an explosion. The collected fragmented products were fine particles, the color of which was similar to that of Ti_2O_3 (Ti_2O_3 crystals are usually dark violet or black [see Table 4]); however, the authors did not explore them. A radiance brightness jump was observed at $t \approx 150$ ms (Fig. 5) that was not accompanied by noticeable temperature perturbations. The $T(t)$ dependence is ∩-shaped with the maximum at ≈ 2773 K, a temperature that is substantially lower than the metal and oxide boiling points. Particle explosion was preceded by a reduction in temperature to 2050 ± 50 K. The phase diagram demonstrates that various phase transformations occur at this temperature, including the formation of eutectic Ti_2O_3. When the particle exploded, a radiance brightness jump was also observed.

Metallographic sections of 240-micrometer particles quenched at various moments in time were used in Ref. [105] to explore in detail their internal structure utilizing diffraction

of back scattered electrons [3] and scattering spectroscopy at various wavelengths. The measurements failed to find noticeable changes in the diameter occurring in the process of burning. The particle composition evolution is represented as triangular Ti/O/N diagrams (in at. %). The overall picture does not depend on the 'depth': the distance between the point of analysis and the particle surface. Random variations of the local concentrations of O and N atoms occur in 'antiphase', so their sum barely changes.

At the initial stage of burning, which corresponds to a freezing time in the range 55–140 ms, the particle is rich in nitrogen, the amount of which becomes substantially smaller at time 170–230 ms, i.e., after the brightness jump. The overall time dependence of nitrogen atom content is $\cap$-shaped: it begins at zero, then attains the maximum value of ≈ 20 at. % at $t \approx 140$ ms and diminishes to 12 at. % by the end of burning at $t \approx 240$ ms (see Fig. 5).

The content of oxygen atoms increases monotonically in the process of burning from 0 to ≈ 38 at. % (see Fig. 5). The number of Ti atoms per unit volume does not change during the entire combustion process; this circumstance, combined with temperature measurements (the combustion temperature being lower than the metal and oxide boiling points) and invariable particle diameter, enables one to suggest that reactions in the gas phase are insignificant, although the particle is surrounded by a glowing zone. The Ti, O, and N atoms present in the particle interior not as an oxide film or nitride inclusions but in the form of a triple system-solution.

The authors of Ref. [105] explain the jump in glow brightness at a temperature of ≈ 2573 K that occurs at approximately half of the combustion time by the release of a αTi phase rather than TiN production accompanied by the release of gaseous nitrogen. They also link the brightness jump at a temperature of ≈ 2073 K at the end of burning with the production of γTiO and βTi_2O_3 phases from the Ti–O solution. According to the phase diagram, these substances are produced at a temperature of 2023 K and oxygen concentration ranging 32–56%. The latter values correspond to those found in the experiment ($T \approx 2073$ K and [O] ≈ 38 at. %). The reduction in temperature initiates production of compounds close to stoichiometric γTiO and βTi_2O_3 and is accompanied by the solidification of these compounds, as a result of which nitrogen is released in the form of internal bubbles. The latter process may result in emergence of cracks and a fresh αTi surface. The reacting of this surface with oxygen causes a temperature jump, gas expansion inside bubbles, and particle explosion.

Thus, the authors of Ref. [105] explain the temperature and radiance brightness jumps and particle explosions by the emergence of phase transitions and note that a more accurate interpretation of experimental data requires a phase-state diagram of the triple Ti–O–N system at higher temperatures. The Ti particle combustion mechanism must include phase transitions along with the dissolution of gases and vapor-phase and heterogeneous reactions.

An innovative experimental technique was applied in Refs [107, 108]. Titanium (purity 98.92%) 100–330-μm particles were added in a countable number to a metal-free AP + binder composition, which was used to fill a quartz capillary tube whose inner diameter measured 2.5 mm. The particles were ignited one by one in the process of composite burning and ejected from the capillary tube with a velocity of 1–3 m s^{-1}. The motion of the burning particles was recorded using high-speed video shots. A glass substrate was installed on the particle motion trajectory at an angle of $5^\circ - 17^\circ$ with respect to the particle velocity vector. The oxide aerosol from the tail accompanying the burning particle was deposited by means of thermophoresis on transmission electron microscopy grids fixed on the substrate. The advantage of the method is that the obtained aerosol sediment provides information about the oxide particle characteristics near the surface of the burning mother particle, i.e. at the early stages of their growth (age < 0.1 ms). The typical combustion time of the mother particles of the size under consideration is about 300 ms. The particle stays in the capillary tube for no longer than 50 ms, and the time of particle combustion in air prior to its collision with the substrate, which was varied by changing the distance from the capillary tube to the substrate, and was equal to 50–100 ms.

The authors of Refs [107, 108] explored in this way particles that burned for approximately 50 ms in metal-free composition products and afterwards burned for no less than 50 ms in air. The results obtained for the oxide particles correspond, therefore, to burning of the mother particle in air and its quenching at $\approx 1/3$ of the total combustion time. These findings are discussed in Section 7 devoted to nanoparticles.

Sequential explosions of particles (further disintegration of fragments) are described and illustrated with high-speed video shots [109]. To explain the fragmentation phenomenon, the results of paper [105] displayed in Fig. 5 have been involved, and the following physical picture of Ti particle combustion has been suggested. The liquid titanium droplet temperature rapidly increases after ignition, as a result of an exothermal reacting. Due to oxygen and nitrogen diffusion, the droplet is a liquid Ti–O–N solution. The data reported in Ref. [105] show that during the first 150 ms of burning, the droplet temperature reaches ≈ 2670 K and then diminishes to ≈ 2050 K. The temperature drop after 150 ms of combustion is related to the reduced heat generation rate.

Ti–O and Ti–N phase diagrams show that a reduction in temperature initiates the formation of γTiO and βTi_2O_3 nonstoichiometric compounds, which is accompanied by their solidification, since the phase transition temperature for the Ti–O system at an oxygen concentration of ≈ 40 at. % is ≈ 2100 K. At the same time, the current concentration and temperature levels prevent the TiN solid phase from being formed. As a result, when a solid shell emerges, gaseous nitrogen is liberated in the form of bubbles in the interior of the particle beneath the shell. The inner pressure increases, and, when the ultimate strength is exceeded, the shell breaks. The process becomes even more vulnerable, since the shell break may result in the emergence of a fresh αTi surface, its active reacting with oxygen in the air that involves heat release, and, eventually, gas expansion inside the bubbles and an 'enhanced' particle explosion. The lower limiting concentration of nitrogen was estimated in Ref. [109] to be 8 at. %. This value approximately corresponds to data reported in Ref. [105], according to which the nitrogen concentration prior to the explosion of the 240-micrometer particle ranges 10–17 at. %.

Some comments on this description seem to be in order. First, the reason for the reduced heat generation rate after burning for 150 ms has not been finally clarified. This may be related to the exhaustion of gas saturation capacity without the emergence of a new phase or to increased diffusion

[3] BSE.

resistance of the near-surface particle regions. Second, no clearly pronounced shell has been observed in exploring quenched particles; therefore, the suggested fragmentation mechanism needs to be justified. Third, the fragmentation occurs in the process of burning in a nitrogen-free environment (for example, in an Ar/O_2 mixture (80/20) [99] and pure oxygen [92]). Consequently, the release of gaseous nitrogen is not the single 'driving force' of fragmentation. Experiments should be performed in various environments to obtain additional information regarding phase transformations and combustion mechanisms.

Combustion of 15–110-micrometer Ti particles was studied in Ref. [104] using electrodynamic levitation and laser ignition. Irregular-shaped particles were separated into narrow fractions (20–25, 25–32, 32–44, 44–53, 53–63, 63–75, 75–90, 90–106, and 106–125 μm), individually suspended in a levitator, and ignited with the light of a 60-W CO_2 laser with a wavelength of 10.6 μm. The particles melted after ignition and acquired a spherical shape. The combustion process was recorded with a high-speed video camera (Vision Research Phantom v5.1) through an Infinity K2 long-focus optical microscope. The shooting parameters were as follows: interval between frames, 500 μs; frame duration, 10 μs; and image size, 768 × 768 pixels. The size of each particle being studied prior to its ignition was determined from an appropriate particle's image. Burning particle glow was recorded using a light guide and Hamamatsu H6780-20 photomultiplier (PMT). The laser was disabled when the specified radiance intensity was attained. The main results of the study [104] are as follows.

In qualitative terms, particles in the size range under consideration burn in a similar way; however, the quantitative parameters depend on the particle sizes. The particle is surrounded at the initial combustion stage by a bright halo, whose size is three to five particle diameters. The halo exists during approximately 1/4 of the particle burning time (this time is about 5 ms for a 60-micrometer particle). The halo manifests itself in the glow intensity record as a peak followed by an extended plateau-like region, the amplitude of which is $\approx 1/5$ of the peak amplitude. The particle diameter did not really change in the process of burning, and the combustion always ended with an explosion. The second radiance peak, which corresponds to that explosion, is very narrow, and its amplitude is approximately 2/3 that of the first peak. The particle combustion time t_b as a function of the size D may be approximated with a power-law function $t_b = 1.29(D/1000)^{1.56}$, where t_b is measured in seconds, $D = 15-110$ μm, and the determination coefficient $R^2 = 0.95$ (triangles and curve *5* in Fig. 4). The calculated thermodynamic adiabatic temperature of the Ti reacting with air is ≈ 3400 K, while, according to measurements [105], the actual combustion temperature of 240-micrometer particles is 2700 K (see Fig. 5). In any event, the particle temperature is below the boiling temperature 3560 K of titanium, in agreement with the picture of predominantly surface (i.e., nonvapor-phase) Ti combustion; at least during the last 3/4 of the combustion timeframe, when halo is no longer observed.

'Surface' combustion involves adsorption of oxygen and nitrogen on the particle surface and dissolution of those gases in molten titanium accompanied by the formation of a liquid Ti–O–N phase-solution uniformly distributed across the molten titanium. The dissolution is assumed to occur sufficiently fast, so the process is controlled either by adsorption kinetics or by gaseous reagent transport to the particle surface. Therefore, the particle glow intensity does not change during almost the entire burning time. An insignificant change in the particle diameter in the process of burning is due to different densities of the oxides and Ti. An estimate shows that the maximum increase in the particle diameter corresponds to the complete transformation of Ti into TiO_2. The final particle diameter equals in this case 1.17 times the initial value. If Ti transforms into Ti_3O_5, Ti_2O_3, or TiN, the ratio of these diameters fall in the range of 1.15–1.00. The authors of Ref. [104] note that the power index in the dependence they found, $t_b \sim D^{1.56}$ (for $D = 15-110$ μm), agrees perfectly well with that in the dependence $t_b \sim D^{1.59}$ (for $D = 44-420$ μm) reported in Ref. [98], but the values of t_b in Ref. [98] are approximately three times larger (see Fig. 3). The increased burning time in Ref. [98] seems to be due to the experiments having been performed with the burner in a gaseous environment with a nonspecified composition. It could be a manifestation of the effect of gases dissolved in metal; the dissolution may occur directly in the burner flame. Dissolved hydrogen is known to diminish the chemical reactivity of Ti [64, 65].

Ignition and combustion of particles passing through a CO_2 laser beam focused onto a ≈ 330-μm diameter spot were studied in Refs [101, 102]. Particles supplied via a capillary tube moved with a carrier gas velocity of ≈ 0.9 m s^{-1} (Reynolds number Re ≈ 0). The time of particle combustion in air was registered optically wih the aid of a photomultiplier tube and optical filters transmitting light with wavelengths of 589, 532, and 568 nm (589 and 532 nm are needed for blackbody radiation pyrometry, and 568 nm for recording the luminous track). The particle size was determined using light scattering techniques. The following approximation dependences have been found for particles from different manufacturers (see Table 2) with the sizes of 2–25 μm used in Ref. [101], and 0.9–24.0 μm in Ref. [102]: $t_b = (2.62/1000)\,D^{0.24}$ and $t_b = (1.09/1000)\,D^{0.63}$ (straight lines B and W in the inset to Fig. 4). The maximum (2900 K) and average (2800 K) temperatures were recorded [101]. Particle burning finished with an explosion. A distinguishing feature of experiments [102] is air turbulization near the feeding capillary tube cut. A comparison with experiments without air turbulization showed that the average combustion temperature increases due to turbulization by 100–200 K, and the combustion time decreases by 20–30%.

Particle combustion in AP decomposition products was studied in Ref. [122]. The experimental setup was as follows. The specimen was made of a powdery AP with an addition of 1% titanium (particle size $D < 50$ μm) in the form of a ball; water or glycerin was utilized as a binder. The ball was inserted into a high-temperature gas flow. When the specimen-ball was gasified, individual metal particles and AP decomposition products (water vapor, hydrogen chloride, and nitrogen oxide) or products of combustion of the AP + glycerin stoichiometric mixture were supplied to the flow. The flow, whose temperature was as high as 1300 K, was maintained using a SC (globar) furnace; an oxygen–hydrogen burner was utilized to attain higher temperatures. The particle behavior was recorded using photographic methods, as in the tracking approach. The burning time as a function of particle sizes (20–30 μm) in water vapor, AP + water decomposition products, and products of AP and glycerin combustion is displayed in the inset to Fig. 4 (squares labeled *1*, *2*, and *3*). Typical combustion times of 20-μm Ti particles in the

above-mentioned media are ≈ 15, 27, and 9 ms, respectively. The combustion always ended with a star-like explosion.

An innovative technique for producing monodisperse burning particles of an agglomeration origin was developed and implemented by the author of this review in Refs [106, 116, 139]. The specimens consisted of a metal-free matrix structure into which a certain number of identical small-sized inclusions were added; those inclusions were made of a metallized composition containing 69% PTM grade Ti. If the specimen burned, each inclusion became a burning agglomerate-particle, the size and mass of which were predetermined by the inclusion composition and dimensions. Matrix combustion products created a flow of high-temperature oxidizing gases that ignited the inclusions and ejected them into the ambient air. It is worth emphasizing the advantages of this method for producing particles. First, it does not need any special equipment such as a spark gap switch [136] or levitator and laser [104]. Second, the size (several hundred micrometers) and origin (coalescence of many fine particles) of the particles obtained are similar to those of the titanium agglomerates that are produced in the combustion of composite propellants with powdery titanium.

Particles of 300, 390, and 480 μm in size and burning in air in free fall have been studied in Ref. [139]. The combustion process is described as follows (Fig. 6).

The especially bright glow emerging after particles leave the specimen continues for about 0.3 s and attains the maximum at $t \approx 0.15$ s. After the ≈ 0.3 s timeframe elapses, the particle acquires a spherical shape (indicating that the titanium boiling point, at 1933 K has been attained); the radiance intensity diminishes and remains afterward invariable almost until the end of combustion. It may be supposed that the bright glow and self-heating of the particle at the beginning of the combustion process are due to heat generation in the heterogeneous oxidation reaction that occurs in the kinetic regime. It should be noted that the authors of Ref. [105] also observed an intensity jump at $t \approx 0.15$ s and the radiation maximum in the combustion of initially monolithic particles 240 μm in diameter. They linked the observed phenomena to phase transitions occurring in the particle at a temperature of ≈ 2623 K. However, the data reported in Ref. [139] show that the particle is not fully molten at $t \approx 0.15$ s.

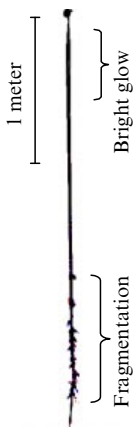

Figure 6. Negative photo image of the track of a 480-micrometer titanium agglomerate-particle burning in free fall in air. The '1 meter' segment shows the spatial scale of the image. The flame of the specimen ejecting the particle is seen at the beginning of the track (in the upper part of the picture). The flame size is negligible in comparison to the distance the particle passes in air. The bright glow of the particle after it leaves the flame is seen as track thickening. If particles are larger than 300 μm, the 'fir-tree branch' fragmentation regime usually develops: it looks like a time-expanded 'jettison' of many fine fragment particles from the mother particle kept intact.

The further sequence of events in the particle combustion process is as follows: fragmentation begins, fragmentation ends, and combustion terminates. Characteristic times in the occurrence of these events are reported in Ref. [139]. The fragmentation of the comparatively large particles under study is distinguished by a large number of fine fragmentation particles being 'jettisoned' from the mother particle, while the latter is preserved (the ejected fragment tracks in the photo resemble a fir-tree branch (see Fig. 6)). The particle mass, diameter, and fall velocity diminish in the process of fragmentation. After the fragmentation ends, the particle radiation strength gradually decreases, and shortly after that the particle is no longer visible. The time after which the particle can no longer be observed by its own radiance is supposed to be the combustion end time. The burning times for particles of 300, 390, and 480 μm in diameter reported by Ref. [109] are shown in Fig. 4 (data *7* — solid dots connected by straight lines). The same figure displays curve *8*, a joint approximation of data from Refs [104, 105, 139] in the form $t_b = 5.81 \times 10^{-7} D^{2.35}$, range of 15–480 μm, and coefficient of determination $R^2 = 0.997$. It should be emphasized that the burning time calculated using this formula for $D = 1200$ μm is $t_b = 10$ s. It is specifically the time that was determined in Ref. [57] for VT-1 grade 1200-μm diameter titanium particles. Based on this agreement, one may assume that the equation quoted above is also valid for particles whose size is over 480 μm. The power index equal to 2.35 indicates the diffusion-limited reacting; this refers not only to oxidizer transport to the particle surface but also to the process developing in the particle interior. The dissolved gases and emerging oxide phases decelerate the particle reacting. A comparison of various approximation formulas ($t_b \sim D^{1.56}$ for $D = 15-110$ μm, $t_b \sim D^{1.85}$ for $D = 15-280$ μm, and $t_b \sim D^{2.35}$ for $D = 15-480$ μm) enables one to conclude that, as the particle size increases, the role of the reacting deceleration factors is also enhanced.

Upon the end of combustion, the mother-particle residue is a golden-yellow sphere whose diameter is 0.5–0.8 times the initial diameter; it consists of a substance with the ratio of O/Ti atoms varying from 1 to 5, on average, $TiO_{2.76}$ (data of energy-dispersive X-ray spectroscopy), without a clearly expressed structural division into a core and shell. The fragment particles, which are described by a logarithmic normal distribution, look as though they consist of metal or oxide. A particle size analysis of fragments larger than 10–25 μm has shown that, if the parent source particle diameter diminishes from 480 μm to 300 μm, the fragment dimensions diminish 'on average' until the fragment mode size decreases to ≈ 30 μm. This effect is presumably related to sequential splitting of the fragments into smaller ones. The larger the particle, the larger the number of fragmentation events that occur. A particle size distribution analysis of fragments larger than 0.5 μm has shown that a single 300-micrometer mother particle produces over 6000 fragments with the mode size of ≈ 2 μm, and the total volume of the measured fragments whose sizes are in the 0.5–110 μm range is $\approx 1/3$ of the initial mother-particle volume [139].

The effect of the blow-off velocity on the combustion time of agglomerate 320-μm diameter particles has been estimated

in Ref. [116]. The blow-off was shown to intensify the combustion process, as a result of which the burning time diminishes from 0.45 s to 0.26 s, if the blow-off velocity increases from 0.9 to 7.9 m s^{-1}. This result is in qualitative agreement with the data from Ref. [102] on the combustion of 0.9–24-μm particles in turbulent air.

We now generalize data on the combustion of individual titanium particles in air under atmospheric pressure (and, in some examples, in oxygen and argon-oxygen mixtures).

Combustion regime. Bright glow is observed in many cases at the early combustion stage with the intensity maximum occurring at $t \approx 0.15$ s. Examples include: 240- and 280-μm diameter particles produced by the electric-spark method in air [105]; agglomerate 300-, 390-, and 480-μm diameter particles [139] in air; $1.6 \times 4 \times 4$-mm specimens in oxygen [74]; and 4.5-μm particles in a poured $25 \times 10 \times 5$-mm layer in oxygen and air [92–94]. For smaller particles (for example, 20–125 μm in air [104]) that burn for less than 0.15 s, a radiant halo is observed at the early combustion stage that exists for approximately 1/4 of the particle combustion time.

Analyses of the metallographic sections of particles quenched at this combustion stage show a solid solution of oxygen in titanium (adsorption up to a 34 at. %) [74, 105]. Peaks are observed in radiation spectra at the wavelengths of 560, 670, and 710 nm, characteristic of TiO, which is the reason for the red-orange glow [92]. Lines and bands of not only TiO but also Ti have been observed in Refs [74, 104, 105]. Optical methods were used in the case of bulk specimens [74] to detect heat generation at a distance of several millimeters above the specimen surface.

The quoted observations indicate the titanium reacting at the initial stage in the vapor phase. This reacting, which probably occurs in the kinetic regime, is an exothermal process of continuous oxygen dissolution. It develops first in solid and later in liquid titanium and is accompanied by the formation of various oxides: TiO, Ti_2O_3, Ti_3O_5, ..., TiO_2. The higher oxides may decompose in this process with production of lower oxides [92] and also evaporate, likely, with subsequent full oxidation of the vapors in the gas phase.

Under the experimental conditions that facilitate intense reacting (external heating, high oxygen concentration), metal also seems to evaporate. Some studies have observed that the phase composition in the particle interior changes with time. Given that the radiation intensity maximum followed by a reduction in the intensity was observed in various experiments at about the same moment in time (≈ 150 ms), one may assume that the combustion process is driven by a reaction that occurs in the *condensed phase* in a fixed-thickness layer, while the vapor-phase reaction *above the surface* maintains the formation of disperse combustion products and radiance.

The reduction in the reacting rate and radiance intensity after the radiance attains its maximum at some moment in time is related to changes in the particle phase composition in a layer of corresponding thickness. From that moment on, the combustion process gradually switches to the diffusion regime: the reacting rate is limited by oxidizer transport from the surface of a particle to its interior. It is of importance that the titanium particle does not have a clearly pronounced metal–oxide interface in either of the monolithic particles quenched at various moments in time [105] and titanium agglomerates where combustion was completed [139]. The reacting rate reduction results in a decrease in temperature and vanishing of the reaction zone in the gas phase in the vicinity of the particle; the reactions now occur in the particle interior in a kind of heterogeneous regime. As was noted above, the diffusion deceleration becomes stronger as the particle size grows, a pattern that can be observed as a growth of the power index in the dependence $t_b \sim D^n$. In other words, a decrease occurs in the rate of the external oxidizer transfer through the surface layers, which primarily consist of the substance that has already reacted, to the particle interior, where the substance still retained the capacity to reacting.

Fragmentation. Particle explosion or ejection of fragments is most probably caused by the release of gas in the particle interior as a result of changes in its phase composition. If the combustion occurs in air, the gas released is, arguably, nitrogen; however, no direct evidence in favor of this suggestion is available. The role of nitrogen in particle combustion and fragmentation is still unclear. It may be assumed that the phase composition of rather large (200–500 μm) burning titanium particles varies with time, and there is a radial gradient of component concentrations. The temperature and concentration conditions occur at some moment in time and in some spatial area above the mother particle surface that result in the release of the gaseous phase. The gas release results in the ejection of fragment particles, the dimensions of which correlate with the thickness of the layer external with respect to the gas release zone. The process is repeated until the substance capable of reacting is exhausted in the particle. The estimated thickness of the fragmented layer for 300–480-μm particles is ≈ 30 μm, since the minimum particle size after which they are no longer fragmented is about 30 μm [139]. This value is a rather rough upper estimate; it can be refined provided detailed information on the fragment particles is available.

According to paper [139], if the diameter of the burning agglomerate particles diminishes from 480 to 300 μm, the fragmentation start time and fragmentation duration decrease as well. For example, the fragmentation duration for 480-, 390-, and 300-μm particles equals 0.22, 0.13, and 0.09 s, respectively. Extrapolating this dependence to smaller particles one can estimate the particle diameter for which the fragmentation duration is close to zero. This value for particles of agglomerate origin is about 100 μm, so it may be expected that a particle whose size is less than 100 μm undergoes fragmentation in a 'star-like' manner — a one-off explosion where fragments are ejected as star prongs. These arguments explain why star-like fragmentation is substituted with the fir-tree branch fragmentation if the particle diameter increases, and the multiple fragmentation of large particles was observed in Refs [92, 107, 108, 139].

Particles as research objects. In analyzing the experimental methods utilized for selecting, preparing, and characterizing the particles to be studied, the following should be noted. The standard technique based on utilizing narrow sieve fractions of irregular-shaped particles inevitably adds some uncertainty, giving rise to the particle size being defined as an effective value. Various methods are applied to heat such particles: gas burners, plasmatrons, lasers, and mixed-composition combustion products. Conditions change in all of the techniques listed above as the particle moves, adding in this way uncertainty to experimental results. However, the last method (heating in mixed composition combustion products) physically simulates the conditions that occur if the Ti particle burns as part of a composite system. If the burning particles are ejected into the air, specific but quite definite conditions are available to researchers. Therefore,

this method of heating and ignition seems to be the most promising if combined with the use of monodisperse particles. A method widely applied for producing large burning particles is based on inserting metallized inclusions, agglomerate 'nuclei', into a metal-free matrix [106]. However, the issue of how the combustion parameters of monolithic and agglomerate particles correspond to each other remains open.

7. Characteristics of oxide particles produced in titanium combustion

We consider below the characteristics of the dispersed oxide produced in the titanium combustion and focus our attention on nanoparticles. We refine first the terminology adopted. The term 'TiO_2 nanoparticles synthesized in the process of combustion' is usually used in publications in referring to the nano-sized particles obtained by decomposing a precursor containing titanium and the subsequent oxidation of Ti clusters in a gas burner flame [140]. Sometimes, the detonation of a gas [141] or solid substance [142] is used instead of the burner. It should be noted that, unlike the gas dispersion synthesis of oxides in laminar dust flames [11, 13, 113, 114], the turbulent flames available in gas burners may be superior to laminar flames (a higher precursor concentration is permissible [143]). The following substances may be utilized, for example, as the precursors: $TiCl_4$, $Ti(OC_3H_7)_4$, $TiO(NO_3)_2$, and $TiOSO_4(2H_2O)$. Titanium compounds are employed in standard gas- and liquid-phase methods to produce TiO_2 [144]. Ultrasound [145] or plasma [146, 147] techniques may be applied to intensify the process. There is a wealth of such studies that usually contain: (1) a description of the original synthesis method (reagents and process setup); (2) the determined characteristics and properties of the TiO_2 particles produced (specific surface and morphology of the particles; sizes of crystallites and coherent scattering region; phase composition; and, less frequently, photocatalytic activity), and (3) a comparison with popular commercial Degussa P25 and Hombikat photocatalytic agents.

In this review, when speaking about the TiO_2 particles obtained in combustion, we mean *metal titanium combustion products*.

Of special interest are photocatalytically active nanometer-sized TiO_2 particles and their capacity to decompose organic substances and purify water and air [148–150]. For this reason, we first provide basic information about such particles obtained applying standard methods and next proceed to titanium metal combustion products.

TiO_2 nanoparticles, which have a spherical (or, less frequently, polyhedral or cubic [151]) shape, are referred to as spherules. The spherule diameter is usually not over 100 nm. This value is not an intrinsic feature of these particles but is due to researchers' efforts to obtain particles of the smallest sizes possible, i.e., a material with the largest specific surface S_{sp}. It has been demonstrated that various organic substances, live cells, bacteria, and viruses located on the surface of TiO_2 particles may be fully oxidized to CO_2, H_2O, and an inorganic residue (or subjected to conversion) under the exposure to light. Light irradiation of the specimens at a level of 1–2 mW cm^{-2} was attained in most studies using mercury lamps. The quantum yield of the decomposition reaction was determined in some studies as a function of irradiation intensity and wavelength. A list of the reactions catalyzed by TiO_2 is presented in handbook [124].

The sizes and crystallographic structure of the TiO_2 nanoparticles produced may be controlled by varying the precursor concentration and burner flame and dissolution gas parameters (actually by changing the temperature and residence time). Particles with sizes of 5.8–15.5 nm and an anatase content of 68.3–100% were obtained, for example, in work [152]. The degree of hydration and number of oxygen vacancies were shown to affect in a dominant way the crystallographic structure and absorption band. These parameters may be modified in the process of synthesis in solution by using special reagents [153].

The role of surface defects (oxygen vacancies), adsorbed molecular oxygen, and surface hydroxyl groups in the photooxidation of chloromethane CH_3Cl to H_2CO, CO, and H_2O was studied in Ref. [154]. The presence of hydroxyl groups and water on the oxide surface was shown not to be a prerequisite for the photooxidation process.

The most important issue analyzed in most studies is the effect of the phase composition and dimensions (or the specific surface) of photocatalytic particles on their efficiency. The activity of TiO_2 specimens (in the form of powders of various origins and structures) with respect to benzene and phenol in aqueous solutions was studied in Ref. [155]. The photocatalytic activity of anatase having $S_{sp} = 11.5$ m^2 g^{-1} was shown to be more than twice the activity of rutile having $S_{sp} = 6.7$ m^2 g^{-1}. However, the nanoparticles are known to aggregate if placed into water [156]. It is therefore difficult to make final conclusion regarding the effect of particle sizes in this case.

TiO_2 nanoparticles were obtained in Ref. [157] from $TiCl_4$. The spherule size changed (from 15 to 30 nm) and their phase composition varied (anatase proportion of 45–80%), depending on the $TiCl_4$ precursor concentration in a gas flame and oxidizer supply rate. The authors of Ref. [157] found that the anatase mass proportion affects TiO_2 photocatalytic activity more substantially than the particle size in decomposing an organic dye (methylene blue), bacteria, and gaseous ammonia. Anatase is usually more active; however, this is not always true. For example, rutile, whose crystallite size ranges 65–100 nm, is more active in the solid-phase reaction with strontium nitrate than is anatase, whose crystallite size falls in the range 10–12 nm [158]. The irregular-shaped particles with $S_{sp} = 3.05$ m^2 g^{-1} rich in rutile were shown in Ref. [111] to exhibit a higher activity than spherical particles with $S_{sp} = 1.45$ m^2 g^{-1} rich in anatase. The activity was determined with respect to methanol and acetic acid by placing the particles into the corresponding aqueous solutions and irradiating them with a 400-W mercury lamp at a wavelength $\lambda > 290$ nm.

The quoted examples show that the functional properties of the photocatalytic materials essentially depend on the conditions under which TiO_2 particles are synthesized, so information about relations between the activity of the material and particle size distribution, porosity, crystallographic structure, and the presence of active centers on the particle surface is required in each specific case. The adsorption properties of the TiO_2 surface, which depend on the relative content of amorphous and crystalline particles in the specimen, may also affect in a substantial way the functional properties of photocatalytic agents [159]. It is still unclear why the photocatalytic activity of TiO_2 specimens with very similar properties may be so different [148].

Photocatalytic activity also depends on the light wavelength. The intensity of solar light incident on Earth's surface

is not large ($\approx 10^{13}$ quanta per cm^2 per s on a sunny day) in TiO_2's own absorption band ($\lambda \approx 300-400$ nm). If TiO_2 is used in an aerosol state to decompose toxicants in the atmosphere under the solar irradiation effect, to enhance the decomposition reaction quantum yield, it is recommended to shift the absorption band edge to the visible region using dopants. The issues related to doping TiO_2 are considered in many publications (see, for example, reviews [160, 161]). Table 5 displays data on the effect of some dopants that were reported in studies not included in those reviews and data on the effect of Cl from Ref. [161], since they are of especial interest.

We assumed earlier [115] that the presence of chlorine is undesirable and excluded AP from the formulations of pyrotechnic systems containing titanium. However, doping TiO_2 with chlorine may yield not only a negative [156, 162, 182] but also a positive [161] effect. As was shown in Ref. [161], the TiO_2 surface properties may be improved by doping it with halogens as a result of enhanced acidity, hydroxyl radical production, and the formation of oxygen vacancies or Ti^{3+}. Chlorine in the TiO_2 crystal substitutes O^{2-}. The optical properties (absorption band position and width) depend on the nature of dopants, but chlorine usually changes the optical properties only insignificantly.

The quoted data on doping with specific elements, including chlorine, are controversial and cannot be generalized. In practice, experimental data must be obtained for each case, depending on nanoparticle properties, the substance to be decomposed, and external conditions. For composite systems whose components contain chlorine, specified data are also needed. The 'ban' on using AP can probably be lifted in some cases; should this be the case, the options to develop formulations of the pyrotechnic compositions containing TiO_2 will be substantially extended.

We consider now the characteristics of disperse condensed products of titanium metal combustion. The list of these products includes the following types: mother particle residues, fragment particles, oxide particles produced in the combustion of fragments in the predominantly heterogeneous regime, and finely dispersed oxide particles (products of combustion in the vapor-phase regime or condensation products, in particular, spherules). Data were presented above about the component and phase compositions of the quenched and final residues of Ti particle combustion. Below, the available scant data on the characteristics of submicron particles are also displayed.

The photocatalytic activity of products of the combustion of mixtures of Ti metal particles with $NaClO_4$ has been measured in Ref. [111]. The 10- and 25-μm Ti particles manufactured by Kojundo Chemical (99.9% pure) were mixed with an oxidizer in a ball mill. The mixture was then placed into a graphite boat in the form of a poured-density layer and ignited with a graphite foil strip in an argon environment. The typical size of product particles was 100–1000 nm. In the case of 10-μm Ti particles, the product particles had an irregular shape, $S_{sp} = 3.05\ m^{-2}\ g^{-1}$, and were rich in rutile. In the case of 25-μm Ti particles, the product particles were spherical, had $S_{sp} = 1.45\ m^2\ g^{-1}$, and were rich in anatase. The conventional size of the particles calculated using the value of S_{sp} was 500 and 1000 nm, respectively. If the commercial Degussa P-25 photocatalytic agent was utilized (its activity is adopted as the unit), the activity of the rutile particles (with larger S_{sp}) and anatase particles was 0.46 and 0.01 in methanol conversion and 0.37 and 0.05 in acetic acid conversion. The activity was assessed on the basis of hydrogen or carbon dioxide yield. The authors of Ref. [111] came to the conclusion that, in the synthesis under consideration, which includes gasification, nucleation, and crystal growth and occurs under conditions

Table 5. Dopants and additives affecting photocatalytic properties of TiO_2.

References	Increased catalyst activity	Decreased catalyst activity	Shift of absorption band edge
[162]	Oxide SiO_2/TiO_2 doped with 0.2% of Ce	NO^{3-}, SO_4^{2-}, Cl^-	
[163]*	Ethanol, H_2O_2	NO^{3-}, SO_4^{2-}, Cl^-, CO_3^{2-}	
[164]	Al and Fe combined		
	SO_4^{2-}	HCO^{3-}	
	Cl^-, no effect		
[165]	Zn in $ZnTiO_3$, $ZnSO_4$, ZnO, and $Zn_2Ti_3O_8$ crystallites		
[161]	F, Cl, Br, I		Diminishes the band gap
[166]	Li, Zn, Pt^0	Co^{3+}, Cr, Ce, Mn, Al, Fe^{3+}	Co^{3+}, Cr, Mn, Fe^{3+}
[167]	Fe^{3+}, Mg, Co^{2+}, Cr		Co^{2+}, Cr, Mg, Fe^{3+}
[168]	La^{3+}, N		N
[169]	Li		Li
[170]	F		
[171]	C		C, N, S
[172]	Cr, Mo		Cr, Mo
[173]	Fe^{3+}		
[174]	Fe^{3+}, Mn^{3+}, Mo^{5+}, Ru^{3+}, Os^{3+}, Re^{5+}, V^{4+}, Rh^{3+}	Co^{3+}, Al^{3+}	Ru^{3+}
[175]	N		N
[176]	Pt	Mn, Cu	
[177]	N		N
[178]	Nd^{3+}		
[179]	Mn		Mn
[180]		Fe^{3+}, Cr^{3+}, V^{5+}, Mn^{2+}, N	Fe^{3+}, Cr^{3+}, V^{5+}, Mn^{2+}, N
[181]**	SnO_2		SnO_2
[182]***	Zr, PO_4^{3-}, SO_4^{2-}	NO^{3-}, Cl^-	
[183]****	Fe^{3+}, Ag		Fe^{3+}, Ag

* Polyoxometalate nanocatalytic agent based on Y-doped TiO_2.

** Two precursors were added to the burner flame to produce a mixed SnO_2/TiO_2 oxide.

*** The Zr ions dope not only the surface layer but also the TiO_2 lattice.

**** Doping with Fe^{3+} ions and depositing of Ag particles on the catalyst surface.

where the adiabatic temperature of the flame is lower than the oxide boiling point, the target product phase composition and particle size distribution are controlled by the initial titanium particle sizes.

Study [99] explored the evolution of PTM-A grade powder particles with an average size of ≈ 4 μm moving in a heated gas for several dozen milliseconds, described the morphology of mother particle residues separated into metal and oxide, and discovered oxide particles (anatase) whose size was less than 100 nm. The last observation allowed the authors of Ref. [99] to hypothesize a combined vapor-phase-heterogeneous regime of Ti particle combustion.

A method for gas-dispersed synthesis of oxides by burning micrometer-sized metal particles in stationary laminar dust flames was described in Refs [11, 13, 113, 114]. The facility included a coaxial dust burner and systems that produced dust, sample condensed combustion products, and performed spectral diagnostics of the flame. As reported in Ref. [11], if Ti particles ≈ 5 μm in size are burned in a gas-disperse flame (particle concentration of 10^{12} m^{-3}, oxygen concentration of 40%, and temperature in the flame 3000–3100 K), the spherules produced have a count average size of $D_{10} = 40$ nm and a root-mean-square deviation of 16 nm. The particle size distribution is described by a logarithmic-normal function with the following parameters: median of 38 nm, mode of 35 nm, and width of 0.38. The authors noted a weak dependence of the oxide parameters on external conditions (Ti particle concentration and initial size), provided a sustainable dust flame is maintained.

To affect the granulometric composition of the synthesized oxide, the authors of Ref. [114] suggest controling the nucleation and condensations processes by adding admixtures that feature either a high electron affinity and easily bind electrons to produce electronegative ions (substances containing C, F, Cl atoms) or a low electron work function of a metal (Ba). It is assumed that an important role is played in the high-temperature oxide condensation zone by the electric charges of the particles emerging due to particle ionization as a result of electron capture or detachment. The ions perform as condensation centers, and, if their number increases, the combustion product fineness increases as well. Pilot experiments with Al grade powder showed that the spherule diameter D_{10} may be changed from 103 to 34 nm by adding admixtures in the amount of 5% of the metal mass; however, experiments with Ti particles have not been performed. In assessing the options to control the spherule dimensions using admixtures, it should be taken into account that the presence of some elements reduces the TiO_2 photocatalytic activity (see Table 5).

The authors of Ref. [111] assert that, if the oxygen concentration is over 40% (while the Ti particle concentration is maintained constant at a level of 10^{12} m^{-3}), the yield of TiO_2 nanoparticles is significantly enhanced, reaching several dozen mass percent, and this phenomenon is due to the transition from the heterogeneous combustion regime to the gas-phase regime with heterogeneous production of suboxides and their subsequent full oxidation in the volume around the particle. The increased combustion intensity facilitates, in this case, the production of nanoparticles. Generically, the more intense combustion results in attaining higher temperatures in the reaction zone, while the size and properties of the particles being produced substantially depend on subsequent cooling [16, 18, 91]. If combustion occurs in air, a nitride may be produced alongside the oxide under certain conditions [22, 90].

For chlorine-free mixed compositions that contain 15–29% metallic titanium, ammonium nitrate, and an energetic binding matrix, the granulometric compositions were determined in Ref. [115] for condensed combustion products, namely, particle mass distributions in the entire range of sizes and detailed particle size distributions in a nanometer range. The combustion of composition samples occurred in air, owing to which the particles, the titanium agglomerates ejecting from the combustion surface of the centimeter-sized specimen, burned most of the time in air.

The following techniques were applied in Ref. [115] and other studies of ours to sample and diagnose aerosols and dispersed phases of burning condensed systems: highly efficient Petryanov filters, a vacuum sampler, a diffusion aerosol spectrometer (DSA), an Andersen type five-cascade aerosol impactor, a thermophoretic precipitator, a chamber with a nozzle to 'accelerate' burning particles, and video microscopy in a Millikan type optical cell. Most of the listed techniques are innovative; their capacities and limitations were analyzed in reviews [184, 185], which also contain data on the dispersity, morphology, structure, phase (crystal) composition, and electric charges of oxide TiO_2 nanoparticles, — the products of Ti combustion products.

We briefly present now those results. The aerosol particles of the TiO_2 oxide 'smoke' are fractal chain-branched aggregates with outer dimensions varying from a fraction of micrometer to several micrometers that consist of spherules, the diameter of which ranges from several manometers to several hundred manometers (Fig. 7). For the compositions [115] that contain 15–29% titanium, the yield of oxide smoke particles smaller than 5 μm was $\approx 5\%$ of the Ti mass, so the aim to enhance the yield of finely dispersed oxide is still of importance. An X-ray phase analysis showed that the smoke particles are TiO_2 in the crystalline forms of rutile, anatase, and brookite.

Most of the aggregates bear both positive and negative electric charges. The particle charge distribution function has the form of a Gaussian curve symmetric with respect to zero. The characteristic aggregate charge amounts to several units of the elementary charge. The TiO_2 particle charge distribution is 1.4 to 3 times broader than the equilibrium Boltzmann distribution at room temperature. Some large aggregates bear distributed charges, and, if the polarity of an external electric field reverses, they are turned through 180°.

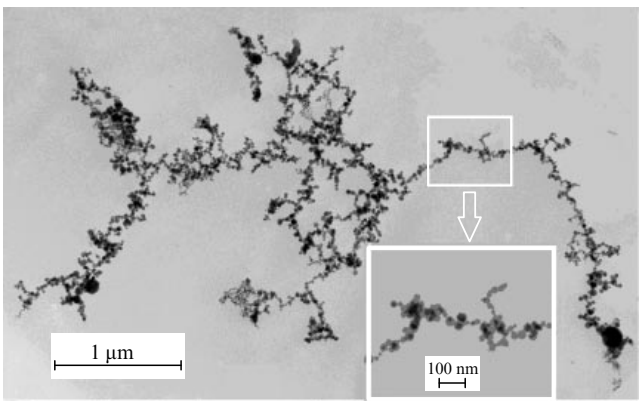

Figure 7. Typical morphology of the aerosol TiO_2 particle — an aggregate consisting of nano-sized spherules.

The aggregate morphology is described by the fractal dimension D_f determined from the power-law function $M \sim D^{D_f}$ that sets the relation between the aggregate mass M and its characteristic size D. The D_f value characterizes aggregate 'compactness'. If $D_f \approx 3$, the aggregate shape is close to spherical, while if $D_f \approx 1$, the aggregate looks like an almost linear chain of spherules. The D_f value depends on the aggregate production mechanism. In particular, $D_f \approx 1.80$ if aggregates are united as a result of diffusion-limited cluster–cluster aggregation (DLCCA). For TiO_2 aggregates, D_f is always less than 1.8; usually $D_f = 1.5-1.7$, indicating the effect of long-range electrostatic interactions. As a result of the presence of the charges, linear spherule chains emerge in the aggregate structure, this phenomenon being manifested in a reduction in D_f. The reduction in D_f with respect to $D_f = 1.80$, which follows from the DLCCA model, characterizes the role of the Coulomb interaction between the coagulating aggregates. Video microscopy was applied to directly record the aggregate coagulation events. The aggregates move prior to unification with acceleration and connect with each other primarily by means of protruding spherule chains.

Chain-like TiO_2 aggregates have been found in the smoke tail of burning individual Ti particles whose sizes varied between several dozen and several hundred micrometers. A tail deposited on a substrate using the thermophoretic technique is an aerogel should this term be interpreted in a standard way as a 'solidified' smoke. The aerogel is produced due to a high concentration of spherules and the charges they bear.

The parameters of dispersity and structure of aerosol TiO_2 particles that are produced in burning various compositions on the basis of ammonium nitrate, hydrazine mononitrate, and AP, which contain a PTM grade titanium powder, were found to be very similar. In particular, the corresponding values of the aggregate fractal dimension ($D_f \approx 1.55$) and spherule size ($D_{10} \approx 23$ nm) are virtually the same. The size distributions of spherules produced in the combustion of individual 300- and 20-micrometer particles as part of a mixed composition are also close to each other. The spherule size distribution function is actually independent of the mixture composition and initial size of burning Ti particles, a feature that essentially distinguishes Ti from Al [186]. The invariability of TiO_2 smoke characteristics enables one to look for ways to control the parameters of the oxide nanoparticles produced. A feasible solution is to make the burning particles move with a high velocity with respect to the gas. A small chamber with a nozzle was designed to this end in Ref. [116]. The experiments were performed with d 320-μm particles of agglomeration origin that were prepared applying the technique developed in Ref. [106]. An increase in the blow-off velocity from 0.9 to 7.9 m s^{-1} was shown to reduce the spherule size from 28–30 nm to 19 nm. The burning time also diminished from 0.45 to 0.26 s. Thus, the motion (blow-off) of particles may be considered a technique effecting the combustion parameters and properties of the nanoparticles being produced. It should be emphasized that this purely physical method does not require adding dopants, as was suggested in Refs [11, 114].

The TiO_2 aerosol evolution may be schematically represented in the following way [187]. First, spherules emerge and grow at some distance from the burning particle due to nucleation and condensation. The oxide particles grow near the condensation zone by way of coalescing. As the particles move away from the burning particle, their temperature decreases, and when it falls below the oxide melting point, the particles start crystallizing. Instead of coalescing, the spherules now unite into aggregates. Later, on when already far away from the burning particle, the aggregates can unite and change their structure (for example, become more compact via 'curling up'). An important role in spherule aggregation, as well as aggregate coagulation and restructuring is played by the electrostatic forces that emerge due to the presence of electric charges.

There are, thus, accomplishments in exploring the dimensions and morphology of TiO_2 oxide aerosol particles produced as a result of Ti metal combustion. However, the chemical properties and, especially, the photocatalytic activity have not been studied to a satisfactory extent. The photocatalytic properties of Ti combustion products have been specifically evaluated in only some studies [111, 188, 189]. The TiO_2 powder obtained by the method of electrically exploding titanium wire in an argon-oxygen atmosphere (15 vol.% O_2) has been studied in Refs [190, 191]. The powder, which did not contain unburned Ti, consisted of spherules whose size ranged from 6 to 400 nm, had a mode in the 20–30 nm region, and had an average diameter $D_{10} = 60$ nm. Its photocatalytic properties were studied in decomposing $H_2C_2O_4$ in a solution. The activity of the electro-explosive powder is superior to that of the commercial Degussa P25 powder with regard to the oxalic acid decomposition rate but is inferior to it regarding the final conversion. In the opinion of the author of Ref. [191], this is due to the S_{sp} values: 17 and 55 m^2 g^{-1} for the electro-explosive TiO_2 and Degussa P25, respectively. The powder phase compositions were also different: the anatase/rutile ratio was equal to 77/23 for the electro-explosive TiO_2, and 84/16 for Degussa P25.

Overall, the available limited data on the photocatalytic activity of the TiO_2 produced in Ti metal combustion do not suggest that the conceptual option of employing a TiO_2 aerosol cloud to fight local emissions of pollutants should be rejected.

8. Titanium combustion mechanism

We present here an up-to-date view on the titanium oxidation, ignition, and combustion mechanisms.

Reaction mechanisms of millimeter-sized compact specimens heated at a moderate rate (not over several degrees per second) are the most studied. Figure 8 schematically depicts 'stages' 0–6 in the oxidation of such specimens.

Stage 0. Initial state, room temperature (298 K). Titanium is covered with a natural X-ray-amorphous protective film about 3.5 nm thick [192] (from 1 to 10 nm, depending on the study) of almost stoichiometric TiO_2 oxide. The film spontaneously builds up during approximately 50 days, and after that period its growth ceases. Owing to that film, the titanium is resistant to corrosion at temperatures of up to 773–823 K.

Stage 1. At temperatures of 473–623 K, oxidation occurs by way of building up the oxide film according to a logarithmic law; oxygen only dissolves in the metal in insignificant amounts. If the film thickness is not large, the transferred oxygen maintains Ti oxidation to TiO_2.

Stage 2. At temperatures of 673–873 K, the logarithmic oxidation law changes to the parabolic law due to dissolution of oxygen. Substantial oxygen dissolution is known to begin

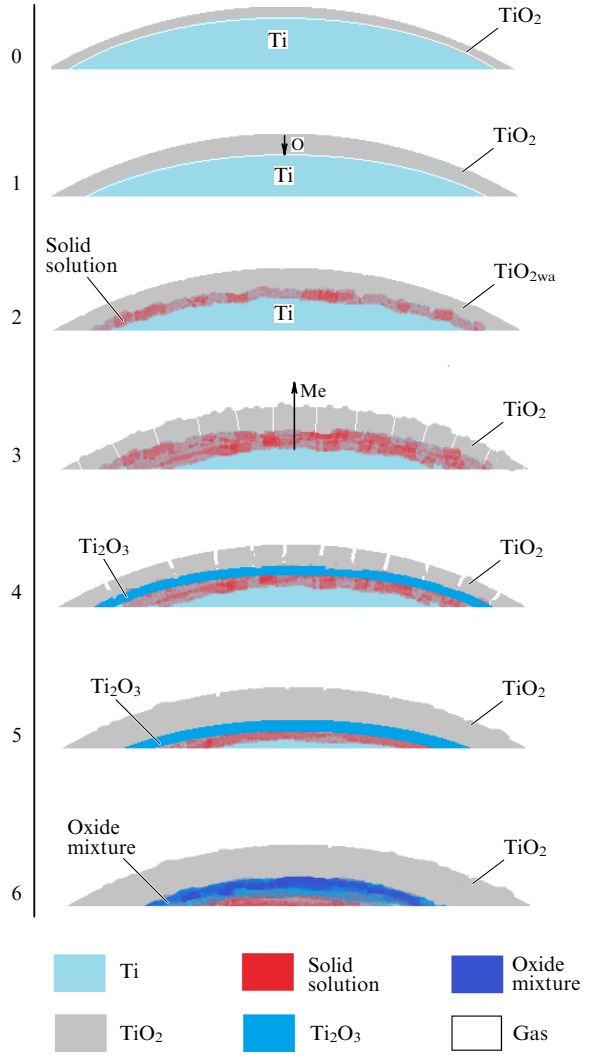

Figure 8. (Color online.) Compact Ti specimen oxidation in the case of a moderate heating rate (see a description of stages 0–6 in the text).

at temperatures of 673–683 K; however, the dissolution kinetics have not been sufficiently studied [137, p. 52]. The initial oxidation stage consists of oxygen dissociation and penetration of its atoms into crystal lattice interstitial sites. The titanium metallic properties are preserved in this process, and the system is a solid solution. The oxygen maximum solubility in αTi is 14.5 mass % at a temperature of 293–1873 K, and 2 mass % in βTi at $T = 2013$ K. The maximum nitrogen solubility is 7 mass % in αTi at $T = 1323$ K, and 2 mass % in βTi at $T = 2293$ K [128, 137]. The low-temperature allotropic αTi modification with a hexagonal crystal lattice transforms at a temperature of 1155 K into the βTi modification with a volume-centered cubic lattice. The latent heat of the allotropic transition is 700 (or 570–850) cal mol^{-1} (mol = g atom). The frequently observed increase in the oxidation rate in the temperature range of 1123–1273 K is related to the changes in the crystal structure; however, the speed-up mechanism has not been determined yet. Experiments have shown that the oxide film growth is related to oxygen diffusion via vacant anion nodes. At temperatures of 1140–1160 K (near the αTi → βTi transition), the Ti atomic thermal capacity diminishes by approximately 10%. It should be noted that the αTi → βTi transition temperature depends on the presence of admixtures. For example, iron that is always present in magnesiothermal titanium reduces the transition temperature from 1155 K to 1103 K. In stage 2, there is usually an oxide layer on the surface, and a solid solution of oxygen in titanium beneath it.

Stage 3. At a temperature of about 1273 K, the oxide film starts losing its protective properties, and oxidation speeds up. This phenomenon is supposedly related to the amount of dissolved oxygen, its concentration gradient, and film thickness. The crystal lattice parameters of the solid solution and oxide are mismatched, as a result of which the oxide film deforms and cracks. At temperatures on the order of 1173–1373 K and higher, the role of cationic diffusion becomes noticeable. Titanium dioxide is an n-type semiconductor that features an excess of metal in the form of ions located in interstitial lattice sites. The metal ions diffuse through the oxide layer to be oxidized afterward on the outer surface. Actually, the interdiffusion of titanium and oxygen occurs. The oxide is produced not only at the metal–oxide interface, but also at the oxide–gas interface. Deviations from the parabolic oxidation law may occur at this stage. The oxide layer structure is analyzed in Ref. [52]. It is noted that at a temperature of over 1073 K pores and voids emerge.

Stage 4. At some temperature in the range of 293–1933 K (the specific value depends on the ratio of the oxygen dissolved in metal and consumed for oxide production, the presence of admixtures, the heating rate, and the prehistory), a new phase emerges in the system. This phenomenon is due to saturation of the system with oxygen over the solubility limit. The new phase is initially a solid solution based on TiO with a face-centered cubic lattice. Oxygen is an interstitial element, since its atoms are smaller than titanium atoms. If the oxygen content further increases, the Ti_2O_3 phase emerges, for example, in the $\alpha Ti + \alpha TiO \rightarrow \beta Ti_2O_3$ reaction, at a temperature of 1193 K, to be followed by the emergence of a TiO_2 phase [125]. The content ratio of the oxygen dissolved in the metal to the oxygen incorporated into the oxide depends on temperature, time, and availability of admixtures. We quote for guidance several values: at 1173 K, 80% of the oxygen is dissolved in the metal; at 1223 K, 45%, and at 1273 K, 30%. Consequently, the remaining oxygen is consumed to produce the oxide.

Stage 5. An oxide film forms and oxygen dissolves in the metal concurrently. TiO_2 builds up on the outer surface, and Ti_2O_3 on the 'inner' one. TiO may be present at the metal–oxide interface [52]. It is generally accepted that TiO_2 is the main compound in the oxide layer, while other layers are thin and insignificant. Simulation is usually based on the assumption that oxygen diffuses through the TiO_2 layer. The Ti–O system phase diagram [124, 125] shows that, if oxygen concentration is high (at $T = 673$ K, oxygen concentration is as high as 56 at. %), various oxides may be present, beginning with the lower suboxides Ti_6O, Ti_3O, and Ti_2O to Ti_3O_5, Ti_2O_3, and Ti_nO_{2n-1} (Magnéli phases, $n = 4, \ldots, 10$), and to the higher TiO_2. Some information about known titanium oxides is displayed in Table 4. The suboxides Ti_6O and Ti_3O may coexist with metal Ti, if the oxygen concentration is less than 35 at. % (Ti_6O at temperatures of up to 1073 K, and Ti_3O and Ti_2O at temperatures of up to 2173 K). At temperatures close to the melting point of βTi, 1933 K, Ti and Ti_2O may coexist, if the oxygen concentration is < 50 at. %; TiO and Ti_2O, if the concentration is 50–55 at. %; TiO and Ti_2O_3, if the concentration is 55–60 at. %; Ti_2O_3 and Ti_3O_5, if the concentration is 60–62 at. %, and the

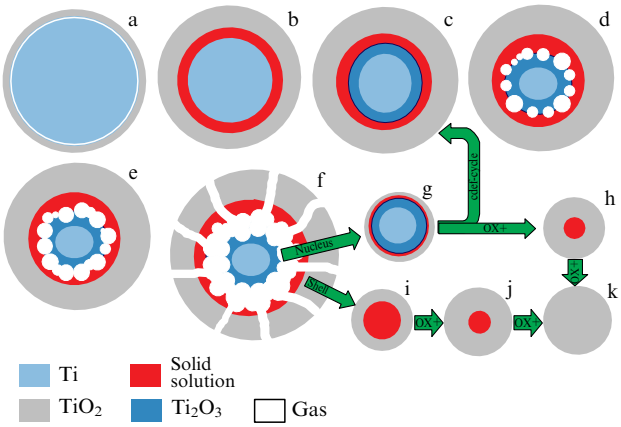

Figure 9. (Color online.) Diagram of titanium particle reacting. (a) Oxide film builds up without oxygen dissolution. (b) Solid solution of oxygen in metal emerges. (c) Phase Ti_2O_3 emerges. (d) Gaseous phase emerges. (e) Bubbles inflate. (f) Fragmentation. The 'core' case: production of a particle (g) similar to that shown in figure c; cdef-cycle occurs followed by full (OX+) particle oxidation (h) to the final particle (k). The 'shell' case: gradual oxidation (OX+) to the final particle: (i) → (j) → (k).

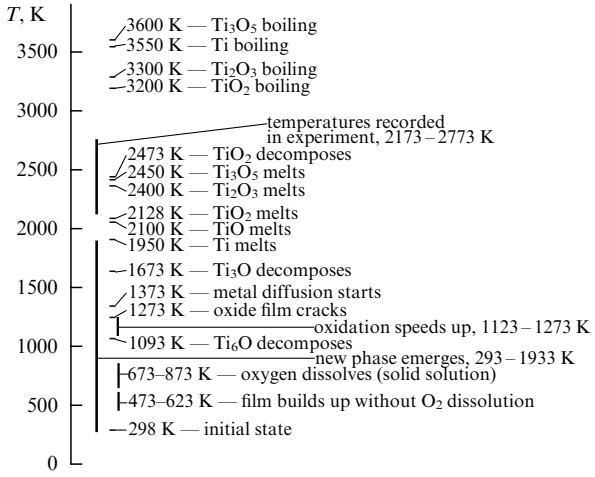

Figure 10. Characteristic temperatures in titanium particle combustion; Refs [125, 193] and experimental data for air. If a 4.5-μm particle burns in a layer, the temperatures are 2200–2400 K [93]. In the combustion of individual 240-μm particles, temperatures of 2173–2723 K were recorded in Ref.. [105].

Magnéli phases, if the oxygen concentration is 63–67 at. %. The lower boundary of the TiO_2 phase corresponds to an oxygen concentration of 65.5 at. %, and the oxygen content in a stoichiometric oxide is 66.7 at. % [192]. Overall, the system evolves towards an increasing amount of the higher TiO_2 oxide [52, 125, 192]. As emphasized in Ref. [52], the published data on the mechanisms and kinetics of compact Ti oxidation in air are controversial, and data about the presence of nitride phases in oxidation products are not available.

Stage 6. Numerous phases coexist, and lower oxides gradually transform into higher ones.

Reacting of submillimeter-sized particles (< 500 μm), including titanium agglomerates, and titanium specimens at high heating rates ($\geqslant 100$ K s^{-1}) exhibit some specific features (Fig. 9). The process develops first in a similar way: stages a, b, and c for a particle are similar to stages 1, 2, and 4 for a bulk specimen, described above. Differences emerge beginning at stage d. The particle temperature starts decreasing in the process of burning, and, according to the current particle state viewed as its coordinates in a composition–temperature phase diagram, a situation may occur when a new phase is supposed to emerge in the gaseous state in the particle interior. Gas 'bubbles' emerge as a result of this process. The most probable reason for the particle temperature diminishing is that the heat exchange conditions change as a result of the heat generation rate being reduced due to an increase in diffusion resistance of the oxide film shell being built up and the heat loss level remaining unchanged. The composition of the released gaseous phase may vary (diluted gases, lower oxides). At stage e, the amount of gas in the particle increases, and the pressure in the bubbles grows. As a result of these processes, the oxide shell locally or fully breaks (stage f), which is observed as particle fragmentation. The surface tension gathers the produced fragments into spherical particles. The fragment particles have various compositions and, hence, exhibit various behavior patterns. Two limiting cases may be distinguished: a fragment primarily consisting of the mother particle's inner central part material (core), and a fragment primarily consisting of the mother particle's outer part material (shell).

In the former case (core), the particle (Fig. 9g) contains large amounts of substances that can be further oxidized (lower oxides and, probably, metallic titanium). A particle at the 'g' stage (Fig. 9g) is similar to the mother particle at the 'c' stage (Fig. 9c) but on a reduced scale. It is natural to expect that such a particle will intensely react, since the gaseous oxidizer gains access after the fragmentation to the material that is able to react. Oxidation and fragmentation are repeated many times [the c–d–e–f cycle (see Fig. 9)], and the particle size diminishes at each step. The cycle iterates until the particle has 'resources' for active reacting. If the material capable of reacting is essentially exhausted, the fragmentation terminates, and the particle is gradually fully oxidized (noted as OX+ in Fig. 9) to finally transform into an oxide particle (stages 'h' and 'k').

In the latter case (shell), the fragment particle (Fig. 9i) does not have the resources for subsequent fragmentation and reacts in the gradual oxidation regime (Fig. 9i, j, k).

Figure 10 shows the levels and ranges of temperatures of particular processes and events specific to titanium combustion and the temperatures being measured in experiments. Temperatures of 2173–2723 K were recorded in Ref. [105] for 240-μm particles. It is this range that is shown in Fig. 10. The temperature range in other studies is usually narrower: it is, for example, 2500–3000 K in plasmatron [99] or 2200–2400 K, if a particle layer burns in air [93]. One can assert that the characteristic experimental temperatures are significantly higher than the melting points of Ti and TiO_2 and, sometimes, the TiO_2 decomposition temperature (see Table 4). The accelerated oxidation at $T \sim 1100$ K is usually ascribed to the $\alpha Ti \rightarrow \beta Ti$ phase transition.

9. Conclusion

Beginning approximately in 2005, studies of the Ti particle combustion mechanism resumed in some countries applying state-of-the-art experimental techniques. High-speed video shots and time-resolved spectroscopy or pyrometry are now used for recording the combustion process, and the enhanced capacities of electron microscopy (energy-dispersive X-ray

spectroscopy, scattering spectroscopy at various wavelengths, back-scattered spectroscopy, etc.) are implemented to analyze combustion residues. The revived interest in Ti particle combustion is partly a result of the prospect of using nano-sized TiO_2 to deactivate local pollutions of atmospheric air. A possible way to implement this idea is to develop a pyrotechnic device that will efficiently transform metallic Ti into photocatalytic TiO_2 particles and scatter them in the air.

To implement this idea, it is necessary to resolve many issues similar to those that were encountered in designing and developing rocket engines powered by aluminized composite propellant, beginning from the design of the composite propellant structure and ending with the oxide product propagation in the atmosphere. One of the most important tasks is to arrange effective burning of Ti particles in the air; to solve this problem, it is necessary to study combustion mechanisms. Based on an analysis of the published data, we make some conclusions and outline areas for future explorations.

To activate the ignition and combustion of Ti *particles*, including those contained in composite systems, it is necessary to study options for preliminary degassing of Ti particles by vacuum annealing and doping Ti with admixtures of metals that facilitate ignition but do not suppress TiO_2 photocatalytic activity. Vanadium, magnesium, and chrome may be selected as candidates for such dopants. Mechanical activation should be tested as a mechanism for producing alloys or adding dopants to the mixture. The important issue of the 'lifetime' of the mechanical activation effects still remains open. It is of interest as well to assess the capacities of the electric arc or spark 'activating' effect on the flame of a burning titanium-containing mixture.

The mechanism of Ti particle combustion in air under atmospheric pressure may be briefly described as follows. The combustion occurs at the initial stage in the kinetic regime in the condensed and vapor phases. It is accompanied by the production of a nano-sized oxide above the particle surface and emergence of bright radiance. This stage may be referred to as 'pyrophoric'. The oxide film is still thin and can peel off the metal; its diffusion resistance is insignificant, and, due to the comparatively low thermal conductivity of titanium, metal can locally heat to temperatures that are over the melting point. This regime is maintained by the external diffusion of gaseous oxide from the ambient environment to the particle surface and from there to the particle interior, where oxygen is continuously dissolved in solid or liquid titanium in an exothermal process.

When the oxygen concentration comes close to the maximum oxygen solubility in titanium, the production of various oxides begins: TiO, Ti_2O_3, Ti_3O_5, ..., TiO_2. As oxygen atoms keep accumulating, the amount of higher oxides increases, and those of lower oxides decreases. The higher oxides may at the same time decompose and produce lower oxides, evaporate, and fully oxidize in the gaseous phase. As a result of the oxide product build-up in the particle volume, oxidizer diffusion transport to the particle interior is hindered due to the emergence of additional *internal* diffusion resistance. The reaction rate diminishes, the temperature decreases, the amount of the released heat proves to be insufficient for vaporizing semiproducts, and the process switches to a kind of heterogeneous regime. A radial concentration gradient of component-semiproducts exists in particles several hundred micrometers in diameter. As the near-surface temperature decreases, temperature and concentration conditions may occur in the near-surface layer approximately 30 μm thick, below which the gas phase is released, causing fragmentation of the burning particle. Larger particles (several hundred micrometers in size) continuously eject surface layer fragments in some time interval, but the mother particle is preserved. If the particle is sufficiently small (from several micrometers to several hundred micrometers), even a single explosion may destroy the mother particle, transforming it into a set of fragments.

Overall, titanium particle combustion develops according to the combined vapor-phase-heterogeneous mechanism, the description of which should be elaborated in more detail. The following parameters must be determined or refined: oxygen penetration and dissolution rates; the kinetics of oxide phase production, interaction, and evaporation; the nature of the gas disrupting the particle; the role of nitrogen; and components and paths of chemical condensation reactions that proceed in the gas phase. It is very desirable to have the phase diagrams of the Ti–O-N system. Experiments where particles 50–500 μm in size are burned in environments of various compositions, characteristic times are recorded, and the phase composition of the mother particle residues and fragment granulometric compositions are determined would seem to be very informative.

TiO_2 *nanoparticles are primarily produced* at the initial, 'pyrophoric' stage of particle combustion, when the visible gas-phase reaction occurs (bright radiance), and fragments undergo combustion. The mass yield of the nanoparticles increases if combustion is intensified by: (1) increasing oxygen concentration in the environment; (2) increasing temperature owing to an external heat source, increased fineness of the particles, or the collective effect of combustion in a layer; and (3) using blow-off (or the motion of a particle with high velocity in a motionless environment). The blow-off technique facilitates delivery of oxygen to the particle and, possibly, to its interior due to the partial removal of combustion products. The blow-off technique seems, therefore, to be a promising method to affect burning Ti particles. To implement its capacities and attain the required parameters of the oxide particles (size and mass yield), experiments must be performed where the spherule characteristics will be determined for various sizes and velocities of the mother particles. Next, a multiparametric optimization will be needed, with consideration of motion and burning characteristics such as fragmentation and combustion times, particle acceleration, and relative velocity of particle motion averaged over the time interval of interest.

The *photocatalytic activity* of the TiO_2 particles produced in Ti combustion must be explored further. The data that are currently available look rather promising. Issues of utmost importance as regards the combustion of Ti particles incorporated into a pyrotechnic composition are as follows: Is the presence of chlorine allowed and may AP be used? The second issue is related to the search for active dopants. Mg seems to be a candidate if viewed from the perspective of combustion process arrangement.

It should be noted that if attempts to develop an aerosol with the required photocatalytic process in the combustion regime fail, there is a 'fallback': an undoubtedly effective ready-to-use TiO_2 powder may be dispersed using an explosion or a pyrotechnic gas generator [194]. There is, however, a problem that is intrinsic to this option: the photocatalytic agent properties must be preserved for a long time. No such problem exists if TiO_2 is produced '*in situ*'.

Acknowledgments

The author is profoundly grateful to R S Zakharov, O V Netskina, and S A Khromova for their assistance in selecting publications; to A M Baklanov, V E Zarko, V V Karasev, A A Onishchuk, V N Panfilov, V N Simonenko, and G S Surodin as co-authors of the original papers that were used in preparing this review, and to A A Paletskii for his valuable critical comments on the text of the article.

This work was supported by the Russian Foundation for Basic Research in frames of the 19-03-00294 project.

References

1. Ivanov B A *Bezopasnost' Primeneniya Materialov v Kontakte s Kislorodom* (Safety in Using Materials in Contact with Oxygen) (Moscow: Khimiya, 1984)
2. Bulanov V Ya et al. *Diagnostika Metallicheskikh Poroshkov* (Metal Powder Diagnostics) (Moscow: Nauka, 1983) p. 225
3. Pokhil P F et al. *Gorenie Poroshkoobraznykh Metallov v Aktivnykh Sredakh* (Combustion of Powdered Metals in Active Environments) (Moscow: Nauka, 1972)
4. Paushkin Ya M, Chulkov A Z (Eds) *Raketnye Topliva* (Propellants) (Moscow: Mir, 1975)
5. Zhukov B P (Ed.) *Energeticheskie Kondensirovannye Sistemy: Kratkii Entsiklopedicheskii Slovar'* (Energetic Condensed Systems. Concise Encyclopedic Dictionary) (Moscow: Yanus-K, 2000)
6. Yagodnikov D A *Vosplamenenie i Gorenie Poroshkoobraznykh Metallov* (Ignition and Combustion of Powdered Metals) (Moscow: Izd. MGTU, 2009)
7. Sarner S F *Propellant Chemistry* (New York: Reinhold, 1966); Translated into Russian: *Khimiya Raketnykh Topliv* (Moscow: Mir, 1969)
8. Shidlovskii A A *Osnovy Pirotekhniki* (Basics of Pyrotechnics) (Moscow: Mashinostroenie, 1973)
9. Papers Published in the Proceedings of the International Pyrotechnics Seminars 01 (1968)-39 (2013) http://www.intpyrosoc.org/wpcontent/uploads/2015/08/IPSTOC19682013.pdf
10. Vadhe P P et al. *Combustion Explosion Shock Waves* **44** 461 (2008); *Fiz. Goreniya Vzryva* **44** (4) 98 (2008)
11. Poletaev N I, Zolotko A N, Doroshenko Yu A *Combustion Explosion Shock Waves* **47** 153 (2011); *Fiz. Goreniya Vzryva* **47** (2) 30 (2011)
12. Morokhov I D, Velikhov E P, Volkov Yu M *Sov. Atom. Energy* **44** 235 (1978); *Atom. Energ.* **44** 3 213 (1978)
13. Kryukov A Yu *Adaptatsiya Vnutrikamernykh Protsessov i Elementov Konstruktsii Energoustanovok na Poroshkovom Goryuchem k Tekhnologiyam Polucheniya Ultra- i Nanodispersnykh Materialov* (Adjusting Internal Chamber Processes and Structural Elements of Energy Generation Facilities Powered by Powder Fuels for Manufacturing Ultra- and Nanodisperse Materials) (Perm': Izd. Permsk. Nats. Issled. Politekh. Univ., 2012)
14. Huang H T et al. *Combustion Explosion Shock Waves* **49** 541 (2013); *Fiz. Goreniya Vzryva* **49** (5) 39 (2013)
15. Merzhanov A G, Sychev A E "O samorasprostranyayushchemsya vysokotemperaturnom sinteze" ("On self-propagating high-temperature synthesis"), http://www.ism.ac.ru/handbook/ shsfr.htm
16. Gromov A A et al. *Gorenie Nanoporoshkov Metallov* (Metal Nanopowder Combustion) (Tomsk: Deltaplan, 2008)
17. Ivanov V G et al. *Combustion Explosion Shock Waves* **30** 569 (1994) *Fiz. Goreniya Vzryva* **30** (4) 167 (1994)
18. Il'in A P, Gromov A A *Gorenie Alyuminiya i Bora v Sverkhtonkom Sostoyanii* (Aluminum and Boron Combustion in Hyperfine State) (Tomsk: Izd. Tomskogo Univ., 2002)
19. Wolfhard H G, Glassman I, Green L (Eds) *Heterogeneous Combustion: A Selection of Technical Papers Based Mainly on the American Institute of Aeronautics and Astronautics Heterogeneous Combustion Conf., Palm Beach, Florida, December 11–13, 1963* (New York: Academic Press, 1964); Translated into Russian: *Geterogennoe Gorenie* (Moscow: Mir, 1967)
20. Beckstead M W *Combustion Explosion Shock Waves* **41** 533 (2005); *Fiz. Goreniya Vzryva* **41** (5) 55 (2005)
21. Grigoriev I S, Meilikhov E Z (Eds) *Handbook of Physical Quantities* (Boca Raton, NY: CRC Press, 1996); Translated from Russian: *Fizicheskie Velichiny* (Moscow: Energoatomizdat, 1991)
22. Yu J et al. *Fuel* **181** 785 (2016)
23. Zubkov L B *Kosmicheskii Metall: Vse o Titane* (Space Metal: Everything about Titanium) (Moscow: Nauka, 1987)
24. Veiga C, Davim J P, Loureiro A J R *Rev. Adv. Mater. Sci.* **32** 133 (2012)
25. Rogachev A S, Mukasyan A S *Gorenie dlya Sinteza Materialov: Vvedenie v Strukturnuyu Makrokinetiku* (Combustion for Synthesis of Materials: An Introduction to Macrokinetics) (Moscow: Fizmatlit, 2012)
26. Athawale B K, Asthana S N, Singh H *J. Ener. Mater.* **22** (2) 55 (2004)
27. Shekhar H, Singh H, in *8-ISICP Eighth Intern. Symp. on Special Topics in Chemical Propulsion: Advancements in Energetic Materials and Chemical Propulsion, Cape Town, South Africa, 2009. Program and Book of Abstracts*, p. 77
28. Pang W et al. *Propellants Explosives Pyrotech.* **38** 852 (2013)
29. Komarov V F et al. *Energetic Materials: Characterization, Modelling and Validation, 40th Intern. Annual Conf. of ICT, Karlsruhe, Germany, 2009*, p. 108
30. Matias T et al. *Energetic Materials for High Performance, Insensitive Munitions and Zero Pollution, 41st Intern. Annual Conf. of ICT, Germany, Karlsruhe, 2010*, p. 95
31. Makhov M N *Gorenie Vzryv* **8** (2) 256 (2015)
32. Komarova M V et al. *Polzunovskii Vestn.* (4–1)112 (2010)
33. Shafirovich E Ya *Fizika Aerodispersnykh Sistem* (Physics of Air Dispersion Systems) Vol. 31 (Kiev–Odessa: Vishcha Shkola, 1987) p. 63
34. Weiser V et al., in *Energetic Materials: Performance and Safety. 36th Int. Annual Conf. of ICT and 32nd Int. Pyrotech. Seminar, Karlsruhe, Germany, 2005,* p. 102
35. Kofstad P *High-Temperature Oxidation of Metals* (New York: Wiley, 1966); Translated into Russian: *Vysokotemperaturnoe Okislenie Metallov* (Moscow: Mir, 1969)
36. Bai A S et al. *Okislenie Titana i Ego Splavov* (Oxidation of Titanium and Its Alloys) (Moscow: Metallurgiya, 1970)
37. Nedin V V et al. *Vzryvoopasnost' Metallicheskikh Poroshkov* (Explosive Hazard of Metal Powders) (Ed. O S Nichiporenko) (Kiev: Naukova Dumka, 1971)
38. Zlobinskii B M, Ioffe V G, Zlobinskii V B *Vosplamenimost' i Toksichnost' Metallov i Splavov* (Inflammability and Toxicity of Metals and Alloys) (Moscow: Metallurgiya, 1972)
39. Voitovich R F, Golovko E I *Vysokotemperaturnoe Okislenie Titana i Ego Splavov* (High-Temperature Oxidation of Titanium and Its Alloys) (Kiev: Naukova Dumka, 1984)
40. Markshtein G Kh *Raketnaya Tekh. Kosmonavtika* (3) 3 (1963)
41. Markshtein G Kh *Vopr. Raketnoi Tekh.* (4) 30 (1968)
42. Frolov Yu V *Fizika Aerodispersnykh Sistem* (Physics of Air Dispersion Systems) Vol. 17 (Kiev–Odessa: Vishcha Shkola, 1987) p. 82
43. Rhein R, Baldwin J "Literature Review on Titanium Combustion and Extinction", Naval Weapons Center Report No. NWC TP 6167 (China Lake: Naval Weapons Center, CA, 1980)
44. Zarko V E, in *Modeling and Performance Prediction in Rockets and Guns* Ch. 10 (Eds S R Chakravarthy, S Krishnan) (New Delhi: Allied Publishers Limited, 1998) p. 300
45. PromMetall. Titan, Splav Titana (Titanium and Titanium Alloy), http://prom-metal.ru/marochnik/titansplav-titana
46. Marochnik Stalei i Splavov. Poisk (Grade Guide of Steels and Alloys. Search), http://www.splav-kharkov.com/quest-form.php (Enter the values corresponding to Ti content, in percent, for example, from 80 to 100, into corresponding fields and click 'Search')
47. Shipsha V G "17. Titany i titanovye splavy" (Titanium grades and alloys), in *Metally i Splavy* (Metals and Alloys) (Ed.Yu P Solntsev) (St. Petersburg: NPO Professional. NPO Mir i Sem'ya, 2003); http://www.naukaspb.ru/spravochniki/Demo%20Metall/3j17.htm
48. Metotekhnika. OST1 90013-81. Splavy Titanovye: Marki (Titanium Alloys. Grades), http://www.metotech.ru/ost_90013_81.htm; see also: Metotekhnika. Metal titan. Opisanie (Titanium Metal. Description) http://www.metotech.ru/titan-opisanie.htm; Metotekhnika. Standarty na Titan. GOSTy, TU (Standards for Titanium,

State Standards, Specifications), http:// www.metotech.ru/titan-gost.htm
49. AO POLEMA. Titan i Ti Splavy. Titanovy Poroshki (Titanium and Ti Alloys. Titanium Powders), http://www.polema.net/titan-i-ti-splavy.html
50. Popov E I *Fizika Aerodispersnykh Sistem* (Physics of Air Dispersion Systems) Vol. 17 (Kiev–Odessa: Vishcha Shkola, 1978) p. 65
51. Chernenko E V, Griva V A, Rozenband V I *Combustion Explosion Shock Waves* **18** 513 (1982); *Fiz. Goreniya Vzryva* **18** 5 20 (1982)
52. Korshunov A V et al. *Izv. Tomskogo Polytekh. Univ.* **319** (3) 10 (2011)
53. Schulz O et al. *Thermochim. Acta* **517** 98 (2011)
54. D'yachkov V I *Russ. J. Appl. Chem.* **77** 1397 (2004); *Zh. Priklad. Khim.* **77** 1409 (2004)
55. D'yachkov V I *Russ. J. Appl. Chem.* **79** 896 (2006); *Zh. Priklad. Khim.* **79** 908 (2006)
56. Rozenband V I, Chichev V A, Afanas'eva L F *Combustion Explosion Shock Waves* **12** 26 (1976); *Fiz. Goreniya Vzryva* **12** (1) 31 (1976)
57. Grachukho V P, Gurevich M A, Savel'ev M I *Combustion Explosion Shock Waves* **14** 26 (1978); *Fiz. Goreniya Vzryva* **14** (1) 35 (1978)
58. Grachukho V P, Gurevich M A, Osetrov S B, in *Gorenie Kondensirovannykh Sistem* (Combustion of Condensed Systems) (Chemical Physics of Combustion and Explosion Processes, Exec. Ed. A G Merzhanov) (Chernogolovka: OIKhF, 1977) p. 81
59. Alekseev A G, Sudakova I V, Tsidelko T I, in *Fizika Aerodispersnykh Sistem* (Physics of Air Dispersion Systems) (Exec. Ed. D I Polishchuk) (1986) p. 20
60. Gao W et al. *Sci. Tech. Energ. Mater.* **75** (1) 14 (2014)
61. Gao W et al. *Powder Technol.* **321** 154 (2017)
62. Voyuev S I et al. *Combustion Explosion Shock Waves* **19** 267 (1983); *Fiz. Goreniya Vzryva* **19** (3) 18 (1983)
63. Lukyanov V V, Peregudov A N, Barzykin V V, in *Khimicheskaya Fizika Protsessov Goreniya i Vzryva. XII Simpozium po Goreniyu i Vzryvu, Chernogolovka, 11–15 Sentyabrya, 2000* (Chemical Physics of Combustion and Explosion Processes. 12th Symp. on Combustion and Explosion. Chernogolovka, 11–15 September, 2000) (Chernogolovka, 2000) p. 33
64. Fedoseev V A, in *Fizika Aerodispersnykh Sistem* (Physics of Air Dispersion Systems) Vol. 17 (Kiev–Odessa: Vishcha Shkola, 1978) p. 50
65. Sadlii T P, Grigorenko I N, in *Fizika Aerodispersnykh Sistem* (Physics of Air Dispersion Systems) Vol. 17 (Kiev–Odessa: Vishcha Shkola, 1978) p. 67
66. Sadlii T P et al., in *Fizika Aerodispersnykh Sistem* (Physics of Air Dispersion Systems) Vol. 29 (Kiev–Odessa: Vishcha Shkola, 1986) p. 29
67. Bolobov V I *Combustion Explosion Shock Waves* **29** 138 (1993); *Fiz. Goreniya Vzryva* **29** (2) 12 (1993)
68. Bolobov V I *Combustion Explosion Shock Waves* **38** 639 (2002); *Fiz. Goreniya Vzryva* **38** (6) 37 (2002)
69. Bolobov V I *Combustion Explosion Shock Waves* **39** 677 (2003); *Fiz. Goreniya Vzryva* **39** (6) 77 (2003)
70. Bolobov V I, Podlevskikh N A *Combustion Explosion Shock Waves* **43** 405 (2007); *Fiz. Goreniya Vzryva* **43** (4) 39 (2007)
71. Bolobov V I *Combustion Explosion Shock Waves* **53** 165 (2017); *Fiz. Goreniya Vzryva* **53** (2) 47 (2017)
72. Strakovskii L G *Combustion Explosion Shock Waves* **18** 579 (1982); *Fiz. Goreniya Vzryva* **18** (5) 96 (1982)
73. Harrison P L, in *Seventh Intern. Symp. on Combustion* (London: Butterworths Sci. Publ., 1959) p. 913; Translated into Russian: *Voprosy Goreniya. Materialy VI i VII Mezhdunarodnykh Simpoziumov po Goreniyu* (Ed. S A Goldenberg) (Moscow: Metallurgizdat, 1963) p. 222
74. Clark A, Moulder J, Runyan C, in *Fifteenth Intern.Symp. on Combustion* (Pittsburgh, PA: The Combustion Institute, 1975) p. 489
75. Derevyaga M E, Stesik L N, Fedorin E A *Combustion Explosion Shock Waves* **12** 493 (1976); *Fiz. Goreniya Vzryva* **12** (4) 544 (1976)
76. Andrzejak T A, Shafirovich E, Varma A *Propellants Explos. Pyrotech.* **34** 53 (2009)
77. Abbud-Madrid A, Branch M C, Daily J W, in *26th Intern. Symp. on Combustion* Vol. 2 (Pittsburgh, PA: The Combustion Institute, 1996) p. 1929
78. Steinberg T A, Wilson D B, Benz F *Combust. Flame* **88** 309 (1992)
79. Bakhman N N, Kuznetsov G P, Puchkov N N *Combustion Explosion Shock Waves* **36** 470 (2000); *Fiz. Goreniya Vzryva* **36** (4) 60 (2000)
80. Efimov B G et al. *Combustion Explosion Shock Waves* **25** 158 (1989); *Fiz. Goreniya Vzryva* **25** (2) 29 (1989)
81. Borisova E A et al. *Combustion Explosion Shock Waves* **27** 294 (1991); *Fiz. Goreniya Vzryva* **27** (3) 35 (1991)
82. Efimov B G, Kuzyaev P N *Combustion Explosion Shock Waves* **30** 788 (1994); *Fiz. Goreniya Vzryva* **30** (6) 68 (1994)
83. Efimov B G, Kuzyaev P N *Combustion Explosion Shock Waves* **31** 652 (1995); *Fiz. Goreniya Vzryva* **31** (6) 37 (1995)
84. Efimov B G, Zaklyaz'minskii L A *Combustion Explosion Shock Waves* **30** 178 (1994); *Fiz. Goreniya Vzryva* **30** (4) 46 (1994)
85. Khomenko I O et al. *Combust. Flame* **92** 201 (1993)
86. Khidirov I *Russ. J. Inorg Chem.* **60** 1263 (2015); *Zh. Neorg. Khim.* **60** 1381 (2015)
87. Bakhman N N, Kuznetsov G P, Puchkov V M *Combustion Explosion Shock Waves* **34** 292 (1998); *Fiz. Goreniya Vzryva* **34** (3) 50 (1998)
88. Vadchenko S G, Grigor'ev Yu M *Combustion Explosion Shock Waves* **15** 54 (1979); *Fiz. Goreniya Vzryva* **15** (1) 64 (1979)
89. Chernenko E V, Pivtsov A L *Combustion Explosion Shock Waves* **26** 684 (1990); *Fiz. Goreniya Vzryva* **26** (6) 68 (1990)
90. Gromov A A et al. *Powder Technology* **214** 229 (2011)
91. Gromov A A "Zakonomernosti protsessov polucheniya nitridov i oksinitridov elementov III–IV grupp szhiganiem poroshkov metallov v vozdukhe" ("Patterns in production of nitrides and oxynitrides of the elements of groups III–IV by burning of metal powders in air", Thesis for the Degree of Dr. Sci. (Engineering) (Tomsk: Tomsk. Polytech. Univ., 2007)
92. KeIzenberg S et al., in *ECM 2009, European Combustion Meeting, Vienna, Austria, 14 – 17 April 2009*, p. 1
93. Weiser V et al., in *7th Workshop on Pyrotechnic Combustion Mechanisms, Rotterdam, The Netherlands, 22 August 2009*, p. 15
94. Roth E et al., in *Energetic Materials for High Performance, Insensitive Munitions and Zero Pollution, 41st Intern. Annual Conf. of ICT, Karlsruhe, Germany, 2010*, p. 129
95. Sakovich G et al., in *Energetic Materials*: *Insensitivity, Ageing, Monitoring, 37th Int. Annual Conf. of ICT, Karlsruhe, Germany, 2006*, p. 166
96. Sedoi V S, Ivanov Yu F, OsmonoIiev M N, in *Energetic Materials*: *Reactions of Propellants, Explosives and Pyrotechnics, 34th Int. Annual Conference of ICT, Karlsruhe, Germany, 2003*, p. 145
97. BeIoni E, Dreizin E L *Combus. Sci. Technol.* **183** 823 (2011)
98. Gordon D, in *Solid Propellant Rocket Research* Vol. 1 (Ed. M Summerfeld) (New York: Academic Press, 1960); Translated into Russian: *Issledovanie Raketnykh Dvigatelei na Tverdom Toplive* (Ed. M Summerfeld) (Moscow: IL, 1963) p. 181
99. Dolganov A P et al. *Izv. Akad. Nauk Latv. SSR Ser. Fiz. Tekhn. Nauk* (2) 106 (1990)
100. Makino A et al. *Nensho no Kagaku to Gijutsu* **4** 11 (1996)
101. Badiola C, Dreizin E L *Proc. Combustion Inst.* **34** 2237 (2013)
102. Wang S, Mohan S, Dreizin E L *Combust. Flame* **168** 10 (2016)
103. Sadlii T P, Grigorenko I N, in *Gorenie Kondensirovannykh Sistem* (Combustion of Condensed Systems) (Chemical Physics of Combustion and Explosion Processes, Exec. Ed. A G Merzhanov) (Chernogolovka: OIKHF, 1977) p. 93
104. Shafirovich E, Teoh S K, Varma A *Combust. Flame* **152** 262 (2008)
105. MoIodetsky I E et al. *Combust. Flame* **112** 522 (1998)
106. Glotov O G *Combustion Explosion Shock Waves* **49** 299 (2013); *Fiz. Goreniya Vzryva* **49** (3) 50 (2013)
107. Khromova S A et al., in *Nonequilibrium Processes* Vol. 2 *Plasma, Aerosols, and Atmospheric Phenomena* (Eds G Roy, S Frolov, A Starik) (Moscow: TORUS PRESS, 2005) p. 225
108. Karasev V V et al., in *Energetic Materials*: *Insensitivity, Ageing, Monitoring, 37th Int. Annual Conf. of ICT, Karlsruhe, Germany, 2006,* p. 124
109. Karasev V V et al. *Combustion Explosion Shock Waves* **42** 649 (2006); *Fiz. Goreniya Vzryva* **42** (6) 33 (2006)
110. Davis A *Combust. Flame* **7** (4) 359 (1963)
111. Kitamura Y et al. *Powder Technol.* **176** 93 (2007)
112. Ageev N D et al. *Combustion Explosion Shock Waves* **26** 669 (1990); *Fiz. Goreniya Vzryva* **26** (6) 54 (1990)

113. Zolotko A N et al. *Combustion Explosion Shock Waves* **32** 262 (1996); *Fiz. Goreniya Vzryva* **32** (3) 24 (1996)
114. Zolotko A N et al., in *Gas Phase Nanoparticle Synthesis* (Eds C G Granqvist, L B Kish, W H Marlow) (Dordrecht: Kluwer Academic Publ., 2004) p. 123
115. Zakharov R S, Glotov O G *Vesn. Novosib. Gos. Univ. Ser. Fiz.* **2** (3) 32 (2007)
116. Glotov O G, Surodin G S, Baklanov A M *Combustion Explosion Shock Waves* **55** (1) (2019) in press; *Fiz. Goreniya Vzryva* **55** (1) 49 (2019)
117. Dolukhanyan S K, Nersisyan M D, Borovinskaya I P, in *Gorenie Kondensirovannykh Sistem* (Combustion of Condensed Systems) (Chemical Physics of Combustion and Explosion Processes, Ed. A G Merzhanov) (Chernogolovka: OIKhF, 1977) p. 96
118. Fedotova V S, in *Problemy Inzhenernoi Okhrany Truda* (Problems of Industrial Safety) Issue 13 (Exec. Ed. P I Polukhin) (Moscow: Metallurgiya, 1970) p. 49
119. Drozdenko V I et al., in *Fizika Aerodispersnykh Sistem* (Physics of Air Dispersion Systems) Vol. 31 (Kiev–Odessa: Vishcha Shkola, 1987) p. 34
120. Alekseev A G, Sudakova I V *Combustion Explosion Shock Waves* **19** 564 (1983); *Fiz. Goreniya Vzryva* **19** (5) 34 (1983)
121. Alekseev A G, Sudakova I V, Tsidelko T I, in *Fizika Aerodispersnykh Sistem* (Physics of Air Dispersion Systems) Vol. 30 (Kiev–Odessa: Vishcha Shkola, 1986) p. 20
122. Merzhanov A G *Raketnaya Tekh. Kosmonavtika* **13** (2) 106 (1975)
123. Breiter A L, Mal'tsev V M, Popov E I *Combustion Explosion Shock Waves* **13** 475 (1977); *Fiz. Goreniya Vzryva* **13** (4) 558 (1977)
124. Samsonov G V (Ed.) *The Oxide Handbook* (New York: IFI/Plenum, 1982); Translated from Russian: *Fiziko-Khimicheskie Svoistva Okislov* (Moscow: Metallurgiya, 1978)
125. Lyakishev N P (Exec. Ed.) *Diagrammy Sostoyaniya Dvoinykh Metallicheskikh Sistem. Spravochnik* (State Diagrams of Binary Metal Systems. Reference Book) Vol. 3 Book 1 (Moscow: Mashinostroenie, 2001)
126. Brewer L *Chem. Rev.* **52** 1 (1953)
127. Sato J, Sato H, Hirano T *Combust. Flame* **51** 279 (1983)
128. Moroz L S et al. *Titan i Ego Splavy* (Titanium and Its Alloys) Vol. 1 (Ed. L S Moroz) (Leningrad: Sudpromgiz, 1960)
129. Cashdollar K L, Zlochower I A *J. Loss Prevent. Process Industr.* **20** 337 (2007)
130. Pohlman N A, Roberts J A, Gonser M J *Powder Technol.* **228** 141 (2012)
131. Jaggi C et al., in *Energetic Materials for High Performance, Insensitive Munitions and Zero Pollution. 41st Int. Annual Conf. of ICT, Germany, Karlsruhe, 2010*, p. 35
132. Nersisyan H H et al. *Mater. Chem. Phys.* **141** 283 (2013)
133. Choi S H et al. *Arch. Metall. Mater.* **62** 1057 (2017)
134. Sigma-Aldrich is now Merck, cat. 578347 Aldrich. Titanium, https://www.sigmaaldrich.com/catalog/product/aldrich/578347?lang=en&region=RU
135. OOO NORMIN. Sfericheskie poroshki titana i titanovykh splavov (Spherical powders of titanium and titanium alloy), http://normin.ru/products/165/
136. Dreizin E A *Combustion Explosion Shock Waves* **39** 681 (2003); *Fiz. Goreniya Vzryva* **39** (6) 82 (2003)
137. Pul'tsin N M *Vzaimodeistvie Titana s Gazami* (Interaction Between Titanium and Gases) (Moscow: Metallurgiya, 1969)
138. Fromm E, Gebhardt E *Gase und Kohlenstoff in Metallen* (Berlin: Springer-Verlag, 1976); Translated into Russian: *Gazy i Uglerod v Metallakh* (Gases and Carbon in Metals) (Moscow: Metallurgiya, 1980)
139. Glotov O G *Combustion Explosion Shock Waves* **49** 307 (2013); *Fiz. Goreniya Vzryva* **49** (3) 58 (2013)
140. Memon N K et al. *Combust. Flame* **160** 1848 (2013)
141. Ouyang X et al. *Combustion Explosion Shock Waves* **44** 597 (2008); Li X et al. *Fiz. Goreniya Vzryva* **44** (5) 112 (2008)
142. Qu Y et al. *Propell. Explos. Pyrotech.* **36** 75 (2011)
143. Wang J et al. *Proc. Combust. Inst.* **33** 1925 (2011)
144. Myronyuk I F, Chelyadyn V L *Phys. Chem. Solid State* **11** 815 (2010)
145. Wang X-K et al. *Chem. Eng. J.* **189–190** 288 (2012)
146. Vemury S, Pratsinis S E *Appl. Phys. Lett.* **66** 3275 (1995)
147. Liu Z et al. *Phys. Proc.* **18** 168 (2011)
148. Savinov E N *Soros. Obrazovat. Zh.* **6** (11) 52 (2000)
149. Besov A S et al. *J. Hazardous Mater.* **173** 40 (2010)
150. Haque M M, Bahnemann D, Muneer M, in *Organic Pollutants Ten Years After the Stockholm Convention — Environmental and Analytical Update* (InTech, 2012) p. 293
151. Jõks S et al. *Appl. Catalysis B* **111–112** 1 (2012)
152. Zhao Y et al. *Mater. Chem. Phys.* **107** 344 (2008)
153. Yu F et al. *Chin. J. Catalysis* **34** 1216 (2013)
154. Lu G, Linsebigler A, Yates J T (Jr.) *J. Phys. Chem.* **99** 7626 (1995)
155. Korsunovskii G A *Zh. Fiz. Khim.* **52** 2276 (1978)
156. Shih Y, Lin C *Environ. Sci. Pollut. Res.* **19** 1652 (2012)
157. Jang H D, Kim S-K, Kim S-J *J. Nanopart. Res.* **3** 141 (2001)
158. Torkhov D S et al. *Dokl. Ross. Akad. Nauk* **394** 775 (2004)
159. Sotnikova L V et al. *Yuzhno-Sib. Nauch. Vestn.* **1** (3) 47 (2013)
160. Nah Y-C, Paramasivam I, Schmuki P *Chem. Phys. Chem.* **11** 2698 (2010)
161. Sun H et al. *Chem. Eng. J.* **162** 437 (2010)
162. Yu L et al. *J. Environ. Sci.* **24** 1777 (2012)
163. Wang Y, Lu K, Feng C *J. Rare Earths* **31** 4 360 (2013)
164. Yuan R et al. *J. Hazardous Mater.* **262** 527 (2013)
165. Wang Y, Xue X, Yang H *Vacuum* **101** 193 (2014)
166. Brezová V et al. *J. Photochem. Photobiol. A* **2** 177 (1997)
167. Ranjit K T, Viswanathan B *J. Photochem. Photobiol. A* **107** 215 (1997)
168. Wei H et al. *J. Mater. Sci.* **39** 1305 (2004)
169. Picquart M et al. *J. Mater. Sci.* **37** 3241 (2002)
170. Hattori A, Tada H *J. Sol-Gel Sci. Technol.* **22** 47 (2001)
171. Choi Y, Umebayashi T, Yoshikawa M *J. Mater. Sci.* **39** 1837 (2004)
172. Wilke K, Breuer H D *J. Photochem. Photobiol. A* **121** 49 (1999)
173. Wang C et al. *J. Mater. Chem.* **13** 2322 (2003)
174. Choi W, Termin A, Hoffman M R *J. Phys. Chem.* **98** 13669 (1994)
175. Gole J L et al. *J. Phys. Chem. B* **108** 1230 (2004)
176. Sivalingam G et al. *Appl. Catalysis B* **45** 23 (2003)
177. Irie H, Watanabe Y, Hashimoto K *J. Phys. Chem. B* **107** 5483 (2003)
178. Xie Y, Yuan C *J. Chem. Technol. Biotechnol.* **80** 954 (2005)
179. Obolenskaya N L et al. *Fundament. Issled. Khim Nauki* **1** 796 (2013)
180. Kolesnik I V "Mezoporistye materialy na osnov dioksida titana" ("Mesoporous materials on the basis of titanium dioxide"), Thesis for Degree of Cand. Sci. (Chemistry) (Moscow: Lomonosov Moscow State Univ. Faculty of Chemistry, 2010)
181. Ifeacho P, Wiggers H, Roth P *Proc. Combust. Inst.* **30** 2577 (2005)
182. Gao B et al. *Appl. Catalysis A* **375** 107 (2010)
183. Sun T et al. *Chem. Eng. J.* **228** 896 (2013)
184. Glotov O G et al., in *Gorenie Tverdogo Topliva. Sb. Dokl. VII Vseross. Konf. s Mezhd. Uchastiem* (Solid Fuel Combustion. Reports Delivered at the 7th All-Russia Conf.) Pt. 3 (Novosibirsk: Izd. Inst. Teplofiziki SO RAN, 2009) p. 184
185. Glotov O G, Zarko V E, in *Energetic Nanomaterials: Synthesis, Characterization, and Application* (Eds V E Zarko, A A Gromov) (Waltham, MA: Elsevier, 2016) p. 285
186. Glotov O G et al. *Dokl. Phys. Chem.* **413** 59 (2007); *Dokl. Ross. Akad. Nauk* **413** 2206 (2007)
187. Glotov O G *Russ. J. Phys. Chem. A* **82** 2213 (2008)
188. Zakharenko V S, Khromova S A *Ekolog. Khim.* **15** (4) 226 (2006)
189. Zakharenko V S, Parmon V N, Khromova S A *Atmos. Ocean. Phys.* **20** 486 (2007); *Opt. Atmos. Okeana* **20** (6) 531 (2007)
190. Voronova G A et al. *Russ. J. Appl. Chem.* **82** 1351 (2009); *Zh. Priklad. Khim.* **82** 1256 (2009)
191. Voronova G A *Izv. Tomskogo Politekh. Univ.* **314** (3) 41 (2009)
192. Kubaschewski O, Hopkins B E *Oxidation of Metals and Alloys* (London: Butterworths, 1962); Translated into Russian: *Okislenie Metallov i Splavov* (Moscow: Metallurgiya, 1965)
193. Levinskii Yu V *p–T–x Diagrammy Sostoyaniya Dvoinykh Metallicheskikh Sistems* (p–T–x Diagrams of States of Binary Metal Systems) Book 2 (Moscow: Metallurgiya, 1990)
194. Sakovich G, Vorozhtsov A, Bondarchuk S, in *Energetic Materials: Characterization and Performance of Advanced Systems, 38th Intern. Annual Conf. of ICT, Karlsruhe, Germany, 2007*, p. 17